Aims and Scope

The International Journal of Advances in Telecommunications, Electronics, Signals and Systems (IJATES[2]) is an all-electronic international scientific journal with the aim to bring the most recent and unpublished research and development results in the area of electronics to the scientific and technical societies, and is supported by the ISES (International Science and Engineering Society, o.s.). The journal's scope covers all the aspects of telecommunication, signal processing, theory and design of circuits and systems for electronics.

The IJATES[2] is ready to publish experimental and theoretical full papers and letters submitted by prospective authors. Paper submitted for publication must be written in English and must follow a prescribed format. All papers are subjected to a critical peer-review prior to publication.

The IJATES[2] is an open access journal which means that all content is freely available without charge to the user or his/her institution. Users are allowed to read, download, copy, distribute, print, search, or link to the full texts of the articles in this journal without asking prior permission from the publisher or the author. This journal provides immediate open access to its content on the principle that making research freely available to the public supports a greater global exchange of knowledge.

www.ijates.org

CONTENTS

Vector Stochastic Differential Equations Used to Electrical Networks with Random Parameters

Edita Kolářová and Lubomír Brančík

***Abstract*—In this paper we present an application of the Itô stochastic calculus to the problem of modelling RLC electrical circuits. The deterministic model of the circuit is replaced by a stochastic model by adding a noise term to various parameters of the circuit. The analytic solutions of the resulting stochastic integral equations are found using the multidimensional Itô formula. For the numerical simulations in the examples we used MATLAB®. The SDE approach has its perspectives in the simulation even higher-order circuits representing more complex physical systems, as their real implementations are often subject to a number of random effects. An example for a transmission line lumped-parameter model is provided.**

***Keywords*—Stochastic differential equations, Wiener process, Itô formula, electrical network, transmission line model.**

I. Introduction

Stochastic differential equations (SDEs) describe systems including some random effects. In this paper we deal with vector Itô stochastic differential equations and refer to some utilization in electrical engineering simulations. Using the Itô formula we find the analytic solution of the equations containing one stochastic parameter. Then we apply the theory to the stochastic model of an RLC electrical network that we get by replacing one of its parameters in the deterministic model by a random process. The theory of SDEs can find its place in various fields of the science and engineering, when random effects are to be considered [1]-[4]. In field of the electrical engineering it can cover a number of random processes occurring in electrical systems, see e.g. [5]-[7] to mention at least a few application areas. Some attention is still paid to the first-order RL or RC circuits, see e.g. [8]-[11], where suitable numerical techniques and different noise types have been studied. From practical point of view, however, the second-order RLC or RLGC circuits are of major importance as they serve as building blocks of more complex physical models. In this paper we want to prepare a bases for the solution of interconnects under stochastically varied parameters, modelled by a cascade connection of just the 2nd-order networks [12], [13] and do first verifications. Whilst for the 1st-order models a scalar SDEs theory is commonly used, see [9], in case of higher-order models the vector SDEs are needed to be applied.

Edita Kolářová is with Brno University of Technology, Department of Mathematics, Technicka 8, Brno, Czech Republic. (e-mail: kolara@feec.vutbr.cz).

Lubomír Brančík is with Brno University of Technology, Department of Radio Electronics, Purkynova 118, Brno, Czech Republic. (e-mail: brancik@feec.vutbr.cz).

II. Stochastic Differential Equations

A. Vector Stochastic Differential Equations

In the theory of stochastic differential equations the Wiener process plays a very important role, because it represents the integral of the so called Gaussian white noise, that describes the randomness in stochastic models of physical events.

A real-valued Wiener process $W(t)$ is a continuous stochastic process with independent increments, $W(0) = 0$ and $W(t) - W(s)$ distributed $N(0, t - s)$, $0 \leq s < t$. Notice in particular that $E[W(t)] = 0$, $E[W^2(t)] = t$, $t \geq 0$.

We can define an N-dimensional SDE in vector form as

$$d\mathbf{X}(t) = \widetilde{\mathbf{A}}(t, \mathbf{X}(t))\, dt + \sum_{j=1}^{M} \widetilde{\mathbf{B}^j}(t, \mathbf{X}(t))\, dW^j(t), \quad (1)$$

where $\widetilde{\mathbf{A}} : \langle 0, T \rangle \times \mathbb{R}^N \to \mathbb{R}^N$ is a vector function, $\widetilde{\mathbf{B}^j}$ represents the $j-$th column of the matrix function $\widetilde{\mathbf{B}} : \langle 0, T \rangle \times \mathbb{R}^N \to \mathbb{R}^{N \times M}$ and $d\mathbf{W}(t) = (dW^1(t), \ldots, dW^M(t))$ is a column vector, where $W^1(t), \ldots, W^M(t)$ are independent Wiener processes representing the noise. The solution is a stochastic vector process $\mathbf{X}(t) = (X^1(t), \ldots, X^N(t))$. By an SDE we understand in fact an integral equation

$$\mathbf{X}(t) = \mathbf{X}_0 + \int_{t_0}^{t} \widetilde{\mathbf{A}}(s, \mathbf{X}(s))\, ds + \sum_{j=1}^{M} \int_{t_0}^{t} \widetilde{\mathbf{B}^j}(s, \mathbf{X}(s))\, dW^j(s), \quad (2)$$

where the integral with respect to ds is the Lebesgue integral and the integrals with respect to $dW^j(s)$ are stochastic integrals, called the Itô integrals (see [2]).

Although the Itô integral has some very convenient properties, the usual chain rule of classical calculus doesn't hold. The appropriate stochastic chain rule is known as the Itô formula.

B. The Multidimensional Itô Formula

Let the stochastic process $\mathbf{X}(t)$ be a solution of the vector stochastic differential equation (1) for some suitable functions $\mathbf{A}, \mathbf{B}$ (see [2], p.48). Let $\mathbf{g}(t, \mathbf{X}) : (0, \infty) \times \mathbf{R}^N \to \mathbf{R}^P$ be a twice continuously differentiable function. Then

$$\mathbf{Y}(t) = \mathbf{g}(t, \mathbf{X}(t)) = (g_1(t, \mathbf{X}), \ldots, g_P(t, \mathbf{X})) \quad (3)$$

is a stochastic process, whose $k-$th component is given by

$$dY^k = \frac{\partial g_k}{\partial t}(t, \mathbf{X})\, dt + \sum_i \frac{\partial g_k}{\partial x_i}(t, \mathbf{X})\, dX^i + \quad (4)$$

$$+ \frac{1}{2} \sum_{i,j} \frac{\partial^2 g_k}{\partial x_i \partial x_j}(t, \mathbf{X})(\, dX^i)(\, dX^j),$$

where $dX^i \cdot dX^j$ is computed according to the rules $dt \cdot dt = dt \cdot dW^i = dW^i \cdot dt = 0$ and $dW^i \cdot dW^j = \delta_{i,j}\, dt$.

C. Vector Linear Itô Stochastic Differential Equations

The stochastic differential equation (1) is called linear, provided the coefficients have the form

$$\widetilde{\mathbf{A}}(t, \mathbf{X}(t)) = \mathbf{A}(t)\mathbf{X}(t) + \mathbf{a}(t), \tag{5}$$

and

$$\widetilde{\mathbf{B}^j}(t, \mathbf{X}(t)) = \mathbf{B}^j(t)\,\mathbf{X}(t) + \mathbf{b}^j(t), \quad j = 1 \ldots M \tag{6}$$

for $\mathbf{A}, \mathbf{B}^j : \langle 0, T \rangle \to \mathbb{R}^{N \times N}$ and $\mathbf{a}, \mathbf{b}^j : \langle 0, T \rangle \to \mathbb{R}^N$.

For the applications to the RLC(G) circuit we need only a 2 dimensional vector linear equation with a one dimensional Wiener process, which has the form

$$\mathrm{d}\mathbf{X}(t) = \big(\mathbf{A}\,\mathbf{X}(t) + \mathbf{a}(t)\big)\,\mathrm{d}t + \big(\mathbf{B}\,\mathbf{X}(t) + \mathbf{b}(t)\big)\,\mathrm{d}W(t), \tag{7}$$

where $\mathbf{A}$ and $\mathbf{B}$ are 2×2 matrices, $\mathbf{a} : \langle 0, T \rangle \to \mathbb{R}^2$ and similarly $\mathbf{b} : \langle 0, T \rangle \to \mathbb{R}^2$ are vector functions, $W(t)$ is the Wiener process.

D. Solution with Additive Noise

First we solve the equation (7) with additive noise, which is the case when $\mathbf{B} \equiv 0$. To find the analytic solution of the equation

$$\mathrm{d}\mathbf{X}(t) = \big(\mathbf{A}\,\mathbf{X}(t) + \mathbf{a}(t)\big)\,\mathrm{d}t + \mathbf{b}(t)\,\mathrm{d}W(t), \tag{8}$$

we use the multidimensional Itô formula and find the derivative of the function $g(t, \mathbf{X}(t)) = \mathrm{e}^{-\mathbf{A}t}\mathbf{X}(t) : \langle 0, T \rangle \times \mathbb{R}^2 \to \mathbb{R}^2$:

$$\mathrm{d}g(t, \mathbf{X}(t)) = \mathrm{d}\left(\mathrm{e}^{-\mathbf{A}\,t} \cdot \mathbf{X}(t)\right) =$$

$$= -\mathbf{A}\mathrm{e}^{-\mathbf{A}\,t} \cdot \mathbf{X}(t)\,\mathrm{d}t + \mathrm{e}^{-\mathbf{A}\,t} \cdot \mathrm{d}\mathbf{X}(t) - 0 \cdot (\,\mathrm{d}\mathbf{X}(t))^2 =$$

$$= -\mathbf{A}\mathrm{e}^{-\mathbf{A}\,t}\mathbf{X}(t)\,\mathrm{d}t + \mathrm{e}^{-\mathbf{A}\,t}\mathbf{A}\mathbf{X}(t)\,\mathrm{d}t +$$

$$+ \mathrm{e}^{-\mathbf{A}t}\mathbf{a}(t)\,\mathrm{d}t + \mathrm{e}^{-\mathbf{A}t}\mathbf{b}(t)\,\mathrm{d}W(t).$$

We have

$$\mathrm{d}\left(\mathrm{e}^{-\mathbf{A}\,t} \cdot \mathbf{X}(t)\right) = \mathrm{e}^{-\mathbf{A}t}\left(\mathbf{a}(t)\,\mathrm{d}t + \mathbf{b}(t)\,\mathrm{d}W(t)\right).$$

Integrating the last equation we get

$$\mathrm{e}^{-\mathbf{A}\,t} \cdot \mathbf{X}(t) - \mathbf{X}(0) = \int_0^t \mathrm{e}^{-\mathbf{A}s}\,\mathbf{a}(s)\,\mathrm{d}s + \int_0^t \mathrm{e}^{-\mathbf{A}s}\,\mathbf{b}(s)\,\mathrm{d}W(s).$$

From this we can easily get the solution

$$\mathbf{X}(t) = \mathrm{e}^{\mathbf{A}t}\mathbf{X}(0) + \int_0^t \mathrm{e}^{\mathbf{A}(t-s)}\,\mathbf{a}(s)\,\mathrm{d}s + \int_0^t \mathrm{e}^{\mathbf{A}(t-s)}\,\mathbf{b}(s)\,\mathrm{d}W(s). \tag{9}$$

The solution $\mathbf{X}(t)$ is a random process and for its expectation we have for every $t > 0$

$$E[\mathbf{X}(t)] = \mathrm{e}^{\mathbf{A}\,t} \cdot E[\mathbf{X}(0)] + \int_0^t \mathrm{e}^{\mathbf{A}(t-s)}\,\mathbf{a}(s)\,\mathrm{d}s, \tag{10}$$

while the expectation of the Itô integral is zero. We can see, that for constant initial value $\mathbf{X}(0)$, which is usually the case, the expectation of the stochastic solution coincides with the deterministic solution of the equation (8). By the deterministic solution we mean the analytic solution of the ordinary differential equation

$$\mathrm{d}\mathbf{X}(t) = \big(\mathbf{A}\,\mathbf{X}(t) + \mathbf{a}(t)\big)\,\mathrm{d}t. \tag{11}$$

E. Solution with Multiplicative Noise

We will solve the linear stochastic equation :

$$\mathrm{d}\mathbf{X}(t) = \big(\mathbf{A}\,\mathbf{X}(t) + \mathbf{a}(t)\big)\,\mathrm{d}t + \mathbf{B}\,\mathbf{X}(t)\,\mathrm{d}W(t), \tag{12}$$

where $\mathbf{A}$ and $\mathbf{B}$ are 2×2 matrices and $\mathbf{a}(t) : \langle 0, T \rangle \to \mathbb{R}^2$ is a vector function.

We define a function $g(t, x_1, x_2, y) : \langle 0, T \rangle \times \mathbb{R}^3 \to \mathbb{R}^2$ by

$$g(t, x_1, x_2, y) = \mathrm{e}^{(\frac{1}{2}\mathbf{B}^2 - \mathbf{A})t - \mathbf{B}y}\begin{pmatrix} x_1 \\ x_2 \end{pmatrix} \tag{13}$$

and compute the derivative of $g(t, \mathbf{X}(t), W(t))$ by the Itô formula.

$$\mathrm{d}\left(\mathrm{e}^{(\frac{1}{2}\mathbf{B}^2 - \mathbf{A})t - \mathbf{B}W(t)}\mathbf{X}(t)\right) =$$

$$= \mathrm{e}^{(\frac{1}{2}\mathbf{B}^2 - \mathbf{A})t - \mathbf{B}W(t)}\left(\frac{1}{2}\mathbf{B}^2 - \mathbf{A}\right)\mathbf{X}(t)\,\mathrm{d}t +$$

$$+ \mathrm{e}^{(\frac{1}{2}\mathbf{B}^2 - \mathbf{A})t - \mathbf{B}W(t)}(-\mathbf{B})\mathbf{X}(t)\,\mathrm{d}W(t) +$$

$$+ \mathrm{e}^{(\frac{1}{2}\mathbf{B}^2 - \mathbf{A})t - \mathbf{B}W(t)}\,\mathrm{d}\mathbf{X}(t) +$$

$$+ \frac{1}{2}\mathrm{e}^{(\frac{1}{2}\mathbf{B}^2 - \mathbf{A})t - \mathbf{B}W(t)}(-\mathbf{B})(-\mathbf{B})\,\mathrm{d}^2W(t) +$$

$$+ \frac{1}{2}\mathrm{e}^{(\frac{1}{2}\mathbf{B}^2 - \mathbf{A})t - \mathbf{B}W(t)}(-\mathbf{B})\big(\,\mathrm{d}\mathbf{X}(t) \cdot \,\mathrm{d}W(t)\big) +$$

$$+ \frac{1}{2}\mathrm{e}^{(\frac{1}{2}\mathbf{B}^2 - \mathbf{A})t - \mathbf{B}W(t)}(-\mathbf{B})\big(\,\mathrm{d}W(t) \cdot \,\mathrm{d}\mathbf{X}(t)\big) =$$

$$= \mathrm{e}^{(\frac{1}{2}\mathbf{B}^2 - \mathbf{A})t - \mathbf{B}W(t)}\Big(\frac{1}{2}\mathbf{B}^2\mathbf{X}(t)\,\mathrm{d}t - \mathbf{A}\mathbf{X}(t)\,\mathrm{d}t - \mathbf{B}\mathbf{X}(t)\,\mathrm{d}W(t) +$$

$$+ \mathbf{A}\mathbf{X}(t)\,\mathrm{d}t + \mathbf{a}(t)\,\mathrm{d}t + \mathbf{B}\mathbf{X}(t)\,\mathrm{d}W(t) + \frac{1}{2}\mathbf{B}^2\mathbf{X}(t)\,\mathrm{d}t +$$

$$+ \frac{1}{2}(-\mathbf{B})\mathbf{B}\mathbf{X}(t)\,\mathrm{d}t + \frac{1}{2}(-\mathbf{B})\mathbf{B}\mathbf{X}(t)\,\mathrm{d}t\Big) =$$

$$= \mathrm{e}^{(\frac{1}{2}\mathbf{B}^2 - \mathbf{A})t - \mathbf{B}W(t)}\mathbf{a}(t)\,\mathrm{d}t.$$

We get

$$\mathrm{d}\left(\mathrm{e}^{(\frac{1}{2}\mathbf{B}^2 - \mathbf{A})t - \mathbf{B}W(t)}\mathbf{X}(t)\right) = \mathrm{e}^{(\frac{1}{2}\mathbf{B}^2 - \mathbf{A})t - \mathbf{B}W(t)}\mathbf{a}(t)\,\mathrm{d}t. \tag{14}$$

After the integration and some computation as in section D, we get the solution

$$\mathbf{X}(t) = \mathrm{e}^{(\mathbf{A} - \frac{1}{2}\mathbf{B}^2)t + \mathbf{B}W(t)}\mathbf{X}(0) +$$

$$\int_0^t \mathrm{e}^{(\mathbf{A} - \frac{1}{2}\mathbf{B}^2)(t-s) + \mathbf{B}(W(t) - W(s))}\mathbf{a}(s)\,\mathrm{d}s. \tag{15}$$

If $\mathbf{X}(0)$ is constant, the expectation of the solution, $E[\mathbf{X}(t)]$ for $t \in \langle 0, T \rangle$ is the unique solution of the ordinary differential equation, (see [1])

$$\mathrm{d}E[\mathbf{X}(t)] = \big(\mathbf{A}\,E[\mathbf{X}(t)] + \mathbf{a}(t)\big)\,\mathrm{d}t. \tag{16}$$

III. RLC Electric Circuit

A. Deterministic Model

Let $Q(t)$ be the charge at time t at a fixed point in an electric circuit, and let L be the inductance, R the resistance and $U(t)$ the potential source at time t. The charge $Q(t)$ satisfies the differential equation

$$LQ''(t) + RQ'(t) + \frac{1}{C}Q(t) = U(t), \qquad (17)$$

with initial conditions $Q(0) = Q_0$, $Q'(0) = I_0$. We can transform this equation by introducing the vector

$$\mathbf{X}(t) = \left(\begin{array}{c} X_1(t) \\ X_2(t) \end{array} \right) = \left(\begin{array}{c} Q(t) \\ Q'(t) \end{array} \right)$$

to the system

$$\begin{array}{rcl} X_1' & = & X_2 \\ X_2' & = & -\frac{1}{CL}X_1 - \frac{R}{L}X_2 + \frac{U(t)}{L}. \end{array} \qquad (18)$$

This in matrix notation gives

$$\frac{d\mathbf{X}(t)}{dt} = \mathbf{A} \cdot \mathbf{X}(t) + \mathbf{a}(t), \quad \mathbf{X}(0) = \mathbf{X}_0 \qquad (19)$$

where

$$\mathbf{A} = \left(\begin{array}{cc} 0 & 1 \\ -\frac{1}{LC} & -\frac{R}{L} \end{array} \right), \quad \mathbf{a}(t) = \left(\begin{array}{c} 0 \\ \frac{U(t)}{L} \end{array} \right), \quad \mathbf{X}_0 = \left(\begin{array}{c} Q_0 \\ I_0 \end{array} \right).$$

The equation (19) has the analytic solution

$$\mathbf{X}(t) = e^{\mathbf{A}t}\mathbf{X}_0 + \int_0^t e^{\mathbf{A}(t-s)}\mathbf{a}(s)\, ds. \qquad (20)$$

B. RLC Circuit with Stochastic Source

We will consider the source influenced by random effects. Instead of $U(t)$ we consider the non deterministic version of this function:

$$U^*(t) = U(t) + \text{``noise''}. \qquad (21)$$

To be able to substitute this into the equation (17) we have to describe mathematically the "noise". It is reasonable to look at it as a stochastic process called the "white noise process", denoted by $\xi(t)$. We get the following equation (α is a constant)

$$\frac{d\mathbf{X}(t)}{dt} = \mathbf{A} \cdot \mathbf{X}(t) + \mathbf{a}(t) + \left(\begin{array}{c} 0 \\ \frac{\alpha}{L}\xi(t) \end{array} \right). \qquad (22)$$

We multiply (22) by dt and then replace $\xi(t)\, dt$ by $dW(t)$; $W(t)$ is the Wiener process. Formally the "white noise" is the time derivative of the Wiener process $W(t)$. We get

$$d\mathbf{X}(t) = \left(\mathbf{A} \cdot \mathbf{X}(t) + \mathbf{a}(t) \right) dt + \left(\begin{array}{c} 0 \\ \frac{\alpha}{L}\, dW(t) \end{array} \right).$$

We got the equation of the form(8)

$$d\mathbf{X}(t) = \left(\mathbf{A}\cdot\mathbf{X}(t)+\mathbf{a}(t) \right) dt + \mathbf{b}\, dW(t), \text{ where } \mathbf{b} = \left(\begin{array}{c} 0 \\ \frac{\alpha}{L} \end{array} \right),$$

with the solution

$$\mathbf{X}(t) = e^{\mathbf{A}t}\mathbf{X}(0) + \int_0^t e^{\mathbf{A}(t-s)}\mathbf{a}(s)\, ds + \mathbf{b}\int_0^t e^{\mathbf{A}(t-s)}\, dW(s). \qquad (23)$$

and the expectation equal (20).

C. RLC Circuit with Stochastic Resistance

We consider now the resistance influenced by random effects. Instead of R we have:

$$R^* = R + \text{``noise''} = R + \alpha\xi(t), \qquad (24)$$

where $\xi(t)$ denotes the "white noise process", α is a constant. We put this to the form(17) and rewrite the second order equation as a system of two equations, then multiply both equations by dt and replace $\xi(t)\, dt$ by $dW(t)$. We get the stochastic vector equation (12)

$$d\mathbf{X}(t) = \left(\mathbf{A}\,\mathbf{X}(t) + \mathbf{a}(t) \right) dt + \mathbf{B}\,\mathbf{X}(t)\, dW(t),$$

where $\mathbf{B} = \left(\begin{array}{cc} 0 & 0 \\ 0 & -\frac{\alpha}{L} \end{array} \right)$, $\mathbf{A}$ and $\mathbf{a}(t)$ are as in (19), with the solution (15).

The expectation of $\mathbf{X}(t)$ solves the equation (19), so the expectation $E[\mathbf{X}(t)]$ is equal to the deterministic solution (20).

D. SDE Numerical Methods Applied

For practical use of stochastic differential equations we have to simulate the stochastic solution by numerical techniques. The simplest numerical scheme, the stochastic Euler scheme, is based on the Euler numerical scheme for ordinary differential equations.

Let us consider an equidistant discretisation of the time interval $\langle 0, T \rangle$, namely

$$t_k = kh, \text{ where } h = \frac{T}{K} = t_{k+1} - t_k = \int_{t_k}^{t_{k+1}} dt,$$

$K \in \mathbb{N}$, $k = 0, \ldots, K-1$ and the corresponding discretisation of the $j-$th component of the Wiener process,

$$\Delta W_k^j = W^j(t_{k+1}) - W^j(t_k) = \int_{t_k}^{t_{k+1}} dW^j(s).$$

To be able to apply a stochastic numerical scheme, first we have to generate, for all j, the random increments of W^j as independent Gauss random variables with mean $E[\Delta W_k^j] = 0$ and $E[(\Delta W_k^j)^2] = h$.

The explicit Euler scheme for the $i-$th component of the N dimensional stochastic differential equation (1) has the form

$$X_{k+1}^i = X_k^i + A^i(t_k, \mathbf{X}_k)h + \sum_{j=1}^{M} B^{i,j}(t_k, \mathbf{X}_k)\Delta W_k^j. \qquad (25)$$

For measuring the accuracy of a numerical solution to an SDE we use the strong order of convergence. The Euler scheme converges with strong order $\frac{1}{2}$ (see [3]).
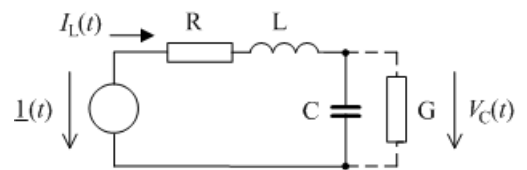

Fig. 1. RLC(G) circuit with unit-step voltage source.

IV. Examples

A. Example 1

First we consider the RLC circuit, see Fig. 1, excited from a unit-step voltage source influenced by a noise,

$$\underline{1}^*(t) = \underline{1}(t) + \alpha\xi(t),$$

with remaining circuit parameters deterministic.

The values of all the parameters are unit which corresponds to an underdamped behavior of the circuit. Hereafter we consider the capacitor voltage $V_C(t) = Q(t)/C$ and the inductor current $I_L(t) = Q'(t)$ as state variables in the circuit instead of the charge-based notations in (17)-(19), which will be useful for further considerations. Also zero initial conditions are considered in this example.

Current and voltage responses, namely their 100 realizations, including their sample means accompanied by 99% confidence intervals highlighted, are presented in Fig. 2. Deterministic solutions based on (20) lead to formulae

$$i_L(t) = \frac{1}{\omega L}\mathrm{e}^{-\beta t}\sin\omega t \tag{26}$$

$$v_C(t) = 1 - \mathrm{e}^{-\beta t}\left(\frac{\beta}{\omega}\sin\omega t + \cos\omega t\right) \tag{27}$$

with

$$\beta = \frac{R}{2L} \quad\text{and}\quad \omega = \sqrt{\frac{1}{LC} - \beta^2}.$$
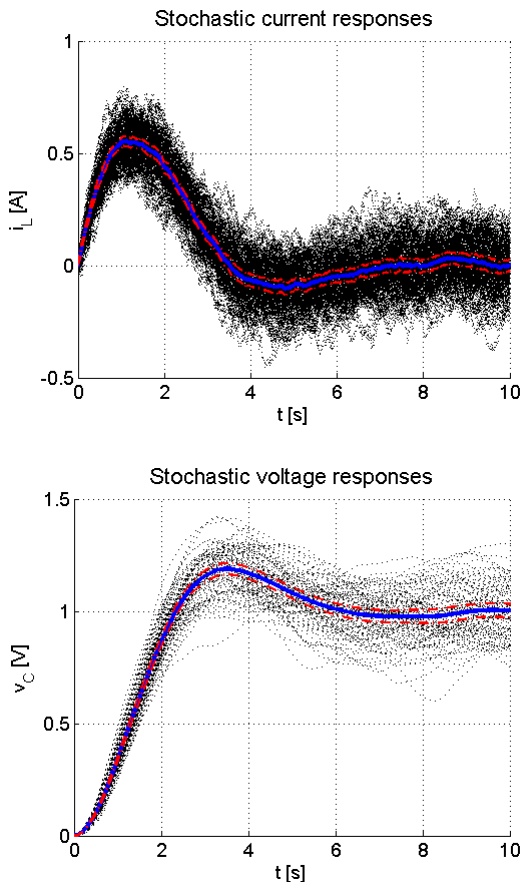

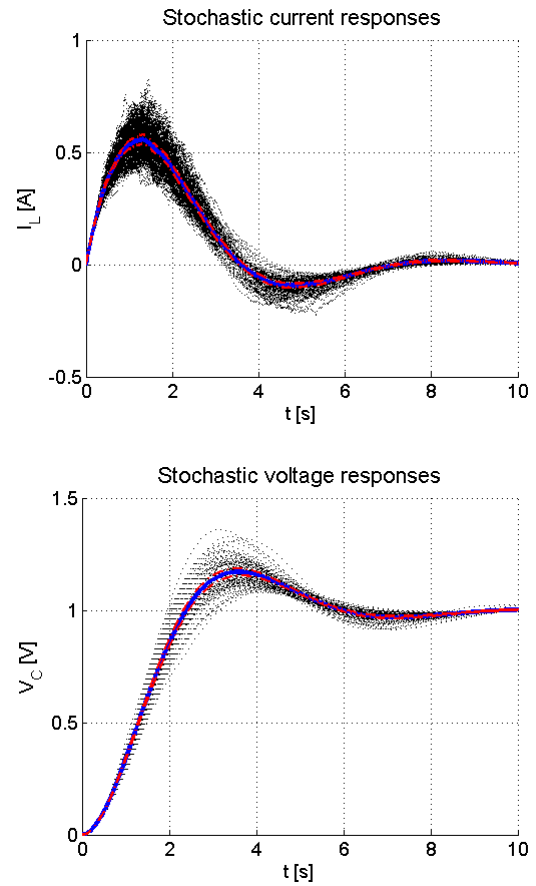Fig. 2.   RLC circuit stochastic responses ($\alpha = 0.15$, noisy source).

Fig. 3.   RLC circuit stochastic responses ($\alpha = 0.15$, noisy resistor).

It can easily be confirmed correspondences between the sample means in Fig. 2 and waveforms based on (26) and (27).

Some dissimilarities in the above stochastic processes can be observed, "smoother" character of the voltages is likely caused by a filtering effect of the low-pass filter formed by this network.

B. Example 2

The second example considers the RLC circuit excited from a deterministic unit-step voltage source $\underline{1}(t)$, with L and C deterministic as well, but with R influenced by a noise, i.e. its resistance is equal $R^*(t) = R + \alpha\xi(t)$.

The current and voltage responses (their 100 realizations), including their sample means with 99% confidence intervals highlighted, are depicted in Fig. 3. The voltage stochastic waveforms look again "smoother" than the current ones, even more when comparing with Fig. 2, and with less dispersions for the same noise intensity factor α.

C. Example 3

The third example considers an RLCG circuit, or the RLC circuit terminated by a resistive load . The conductance G can also model nonideal properties of a real electrical condenser, namely its nonzero leakage. In this case the matrix $\mathbf{A}$ defined in (19) changes as

$$\mathbf{A} = \begin{pmatrix} -\frac{G}{C} & 1 \\ -\frac{1}{LC} & -\frac{R}{L} \end{pmatrix},$$
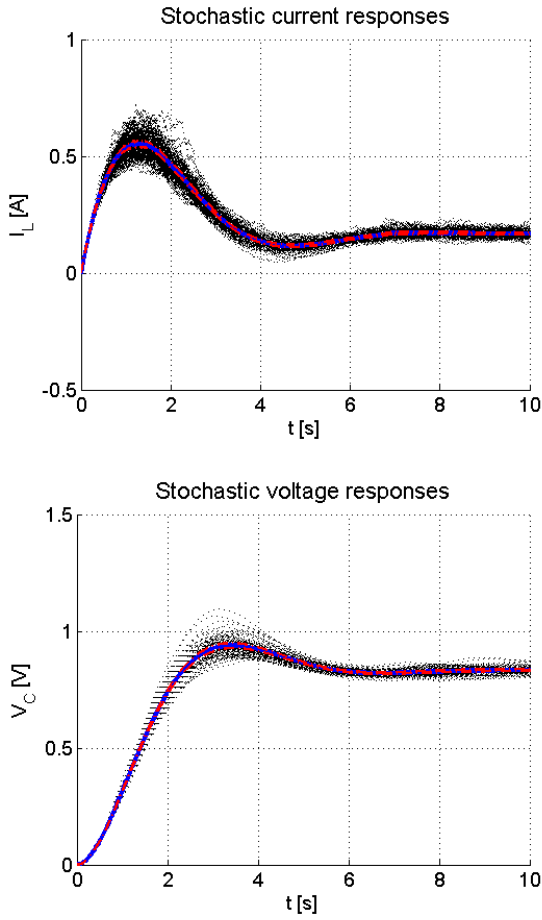
4

Fig. 4.   RLCG circuit stochastic responses ($\alpha = 0.15$, noisy resistor).

remaining matrices keep their forms. When a conductance is chosen e.g. as $G = 0.2S$, the circuit stays underdamped, with analytical solutions presented e.g. in [14]. Numerical solutions for stochastic exciting voltage source are, from qualitative viewpoint, very similar to those in Fig. 2. In case of stochastic resistance R, however, the results are presented in Fig. 4. Here it is obvious that due to a permanent current flowing through the resistor R, stochastic responses do not tend to be damped down to zero, unlike the RLC circuit in Fig. 3.

V. UNIFORM TRANSMISSION LINE MODELLING

Here a uniform transmission line (TL) lumped-parameter model will be considered and its responses simulated, see Fig. 5. If we denote l as a TL length and L_0, R_0, C_0 and G_0 as its per-unit-length parameters the lumped parameters of the model are defined by $L_d = L_0 l/m, R_d = R_0 l/m, C_d =$
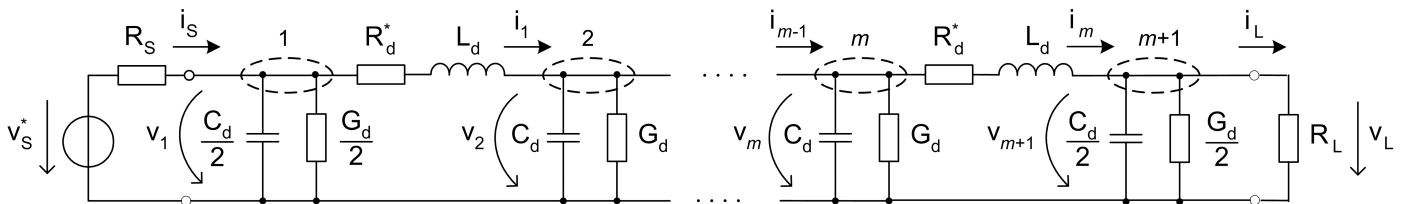
$C_0 l/m$, and $G_d = G_0 l/m$, where m is a number of Π sections in cascade. For the Thévenin resistances of terminal circuits supposed as nonzero, the terminal currents are given by $i_S = (v_S - v_1)/R_S$, and $i_L = v_L/R_L = v_{m+1}/R_L$. The asterisks at an exciting voltage, v_S^*, and series resistances, R_d^*, mean that respective quantity is considered as stochastically varying.

A. Deterministic Model

As is shown e.g. in [16] a uniform TL m-sectional model can be described by a state-variable method leading to a vector ordinary differential equation

$$\frac{\mathrm{d}\mathbf{x}(t)}{\mathrm{d}t} = \mathbf{A}\mathbf{x}(t) + \mathbf{B}\mathbf{u}(t) \tag{28}$$

with a well-known analytical solution

$$\mathbf{x}(t) = \mathrm{e}^{\mathbf{A}t}\mathbf{x}_0 + \int_0^t \mathrm{e}^{\mathbf{A}(t-s)}\mathbf{B}\mathbf{u}(s)\,\mathrm{d}s \tag{29}$$

Formal similarities with (19) and (20) suggest us to proceed with stochastic solutions by similar way, see next chapters. The individual terms in (28) will be formulated as follows. The matrices $\mathbf{A} = -\mathbf{M}^{-1}(\mathbf{H} + \mathbf{P})$, and $\mathbf{B} = \mathbf{M}^{-1}\mathbf{P}$, where

$$\mathbf{M} = \begin{pmatrix} \mathbf{C} & \mathbf{0} \\ \mathbf{0} & \mathbf{L} \end{pmatrix}, \ \mathbf{H} = \begin{pmatrix} \mathbf{G} & \mathbf{E} \\ \mathbf{-E^T} & \mathbf{R} \end{pmatrix}, \ \mathbf{P} = \begin{pmatrix} \mathbf{Y_E} & \mathbf{0} \\ \mathbf{0} & \mathbf{0} \end{pmatrix}, \tag{30}$$

with $\mathbf{C} = C_d \mathbf{I}_{m+1}, \mathbf{L} = L_d \mathbf{I}_m, \mathbf{G} = G_d \mathbf{I}_{m+1}$, and $\mathbf{R} = R_d \mathbf{I}_m$, as diagonal matrices (there are exceptions in $\mathbf{C}$ and $\mathbf{G}$ related to boundary elements, when $C_d/2$ and $G_d/2$ are used), $\mathbf{I}$ identity matrices of indexed orders, and $\mathbf{0}$ corresponding zero matrix. The $\mathbf{E}$ is a special $(m + 1) \times m$ bidiagonal matrix containing ± 1 and zeros, see [16] for more details, and the $(m + 1)$-order matrix $\mathbf{Y}_E = \mathrm{diag}(G_S, 0, ..., 0, G_L)$ is dependent on the external circuits, where $G_S = R_S^{-1}$ and $G_L = R_L^{-1}$. The column vector $\mathbf{x}(t) = [\mathbf{v}_C^T(t), \mathbf{i}_L^T(t)]^T$ consists of the state variables required, namely of subvectors $\mathbf{v}_C(t)$ and $\mathbf{i}_L(t)$ holding $m+1$ capacitor voltages and m inductor currents, respectively. Finally, the column vector $\mathbf{u}(t) = [\mathbf{v}_E^T(t), \mathbf{0}]^T$ contains the $(m + 1)$-order vector $\mathbf{v}_E(t) = [v_S(t), 0, ..., 0]^T$ acting as an excitation term.

B. Model with Stochastic Excitation

Here, instead of $v_S(t)$, a non-deterministic version is used

$$v_S^*(t) = v_S(t) + \alpha \xi(t). \tag{31}$$

while remaining parameters are deterministic.

Fig. 5.   Uniform transmission line m-sectional lumped-parameter model.

A noise term $\xi(t)$ is a stochastic process, namely a white noise, and with α a constant, expressing its intensity. After substitution (31) into (28) and doing arrangements keeping the SDE theory above we get a vector linear SDE with an additive noise

$$d\mathbf{X}(t) = (\mathbf{A}\mathbf{X}(t) + \mathbf{B}\mathbf{u}(t))\ dt + \mathbf{b}\ dW(t) \qquad (32)$$

with $\mathbf{b} = \mathbf{B}[\boldsymbol{\alpha_E^T}, \mathbf{0}]^T$, and $\alpha_E = [\alpha, 0, \ldots, 0]^T$ as a noise intensity vector of the order $m + 1$. The stochastic solution $\mathbf{X}(t)$ in (32) is marked by a capital letter to distinguish it from that deterministic in (29). After some modification of the theory from section two, considering the multidimensional Itô formula [1], [2], the formal analytical stochastic solution is

$$\mathbf{X}(t) = e^{\mathbf{A}t}\mathbf{X}_0 + \int_0^t e^{\mathbf{A}(t-s)}\mathbf{B}\mathbf{u}(s)\ ds + \int_0^t e^{\mathbf{A}(t-s)}\mathbf{b}\ dW(s), \qquad (33)$$

with the right term called as the Itô integral. The $\mathbf{X}(t)$ is a random process and for its expectation we have for $t > 0$

$$E[\mathbf{X}(t)] = e^{\mathbf{A}t}E[\mathbf{X}_0] + \int_0^t e^{\mathbf{A}(t-s)}\mathbf{B}\mathbf{u}(s)\ ds, \qquad (34)$$

when the expectation of the Itô integral is zero. It is evident that for an initial value $\mathbf{X}_0$ being constant, this expectation coincides with the deterministic solution (29).

C. Model with Stochastic Resistances

Herein the responses to a deterministic excitation $v_S(t)$ but under all m resistances R_d in the TL model influenced by random effects are considered. Instead of the original R_d, their non-deterministic versions are used as

$$R_{dk}^*(t) = R_d + \alpha_k\xi_k(t). \qquad (35)$$

$k = 1, \ldots, m$, where noise terms $\xi_k(t)$ are again considered as "white noise processes", and α_k as their intensities. Notice that the series resistances connected to different nodes are generally affected by different noise terms like it can occur on a real TL. After substitution (35) into (28), and keeping the SDE theory procedures, we get

$$d\mathbf{X}(t) = (\mathbf{A}\mathbf{X}(t) + \mathbf{B}\mathbf{u}(t))\ dt + \mathbf{D}_W(t)\mathbf{X}(t) \qquad (36)$$

with

$$\mathbf{D}_W = -\mathbf{M}^{-1}\begin{pmatrix} \mathbf{0} & \mathbf{0} \\ \mathbf{0} & \boldsymbol{\alpha_R}\ d\mathbf{W}_R(t) \end{pmatrix}, \qquad (37)$$

where the matrices $\boldsymbol{\alpha_R} = \mathrm{diag}(\alpha_1, \ldots, \alpha_m)$ and $d\mathbf{W}_R(t) = \mathrm{diag}(\ dW_1(t), \ldots,\ dW_m(t))$. This is a general vector linear SDE with a multiplicative noise, which is represented by a m-dimensional Wiener process. The solution in general doesn't have the normal distribution for X_0 constant see [1], but the expectation of the solution (36) is given again by (34), its exact analytical solution can be obtained by generalizing results shown e.g. in [17].

D. SDE Numerical Method Applied

As computer simulations revealed, the explicit Euler scheme (25) satisfies only for relatively low orders of electric models under consideration to get stable solutions. That is why, implicit Euler schemes will be used for all the practical simulations of the TL model. Then, based on [3] and considering (32) and (36), implicit stochastic Euler schemes can be formulated respectively as

$$\mathbf{X}^{n+1} = (\mathbf{I} - \mathbf{A}h)^{-1}\left(\mathbf{X}^n + \mathbf{B}\mathbf{u}^{n+1}h + \mathbf{b}\Delta W^n\right) \qquad (38)$$

for the SDE with an additive noise, and

$$\mathbf{X}^{n+1} = (\mathbf{I} - \mathbf{A}h)^{-1}\left(\mathbf{X}^n + \mathbf{B}\mathbf{u}^{n+1}h + \mathbf{D}_W^n\mathbf{X}^n\right) \qquad (39)$$

for the SDE with a multiplicative noise, where $\mathbf{I}$ is the identity matrix, being consistent with the Itô stochastic calculus.

E. Examples of TL Model Responses

Let us now consider a uniform TL with per-unit-length parameters $R_0 = 0.1\Omega/\mathrm{m}$, $L_0 = 494.6\mathrm{nH/m}$, $G_0 = 0.1\mathrm{S/m}$, and $C_0 = 62.8\mathrm{pF/m}$ [15]. The TL's length $l = 0.3\mathrm{m}$, the terminal resistances $R_S = 10\Omega$ and $R_L = 1\mathrm{k}\Omega$, the drive source is a sine-squared impuls, $v_S(t) = \sin^2(\pi t/2 \cdot 10^{-9})$ if $0 \le t \le 2 \cdot 10^{-9}\mathrm{s}$, and $v_S(t) = 0$ otherwise. To demonstrate overall state on the TL the deterministic solutions for voltage and current distributions are depicted in Fig. 6, computed through a continuous model in a Laplace domain to be more accurate for a comparison, and by using a numerical inversion of Laplace transforms [15].
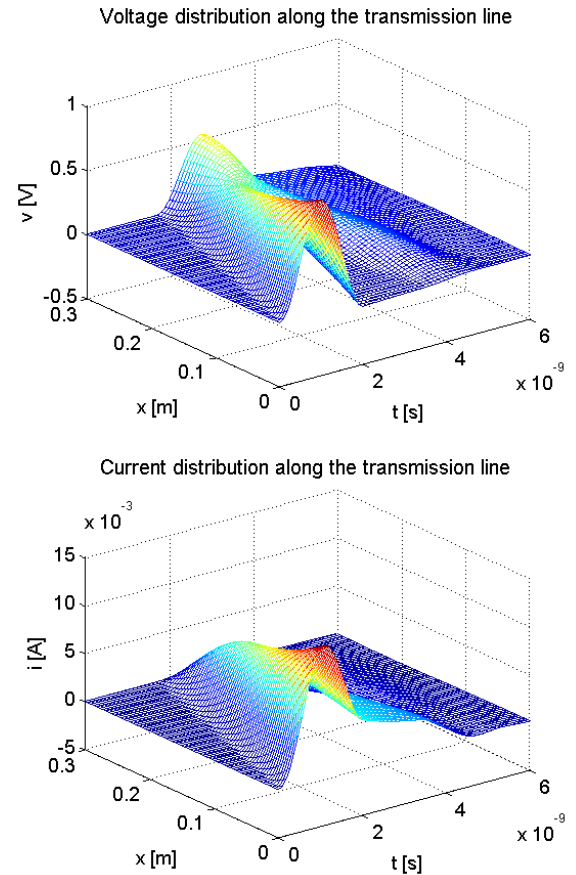

Fig. 6.   Voltage and current distributions along the uniform TL.
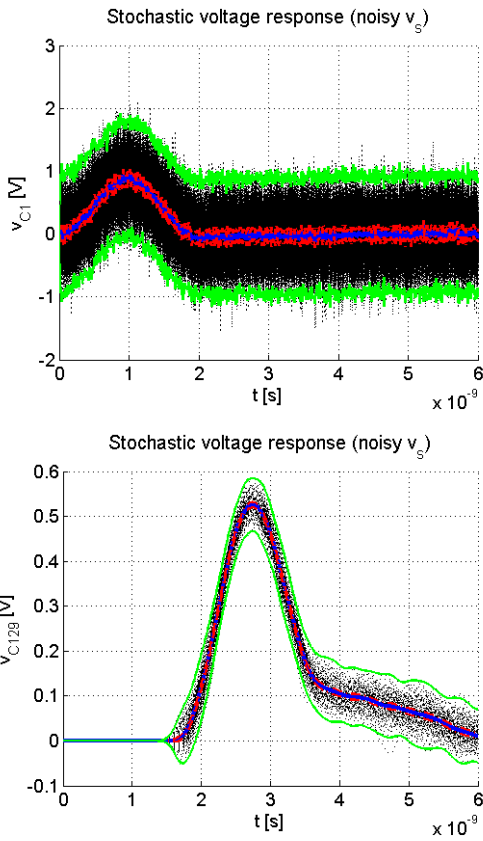
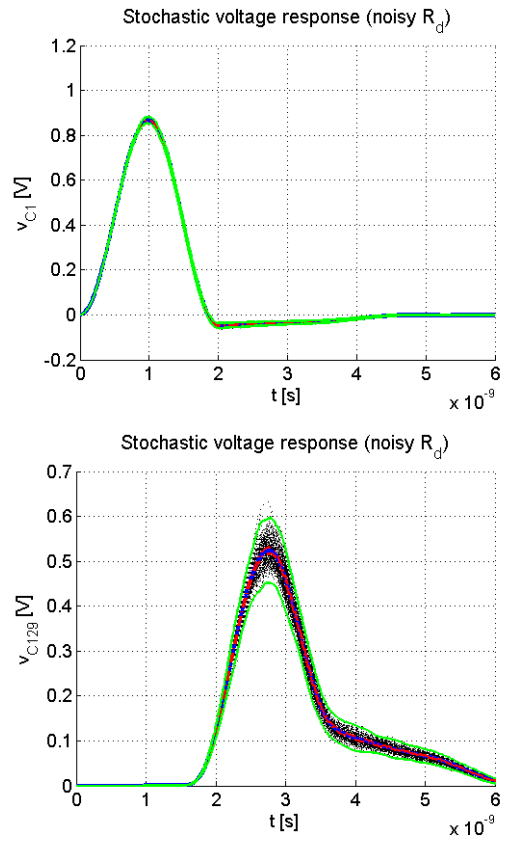Fig. 7.   Stochastic voltage responses for noisy excitation voltage.

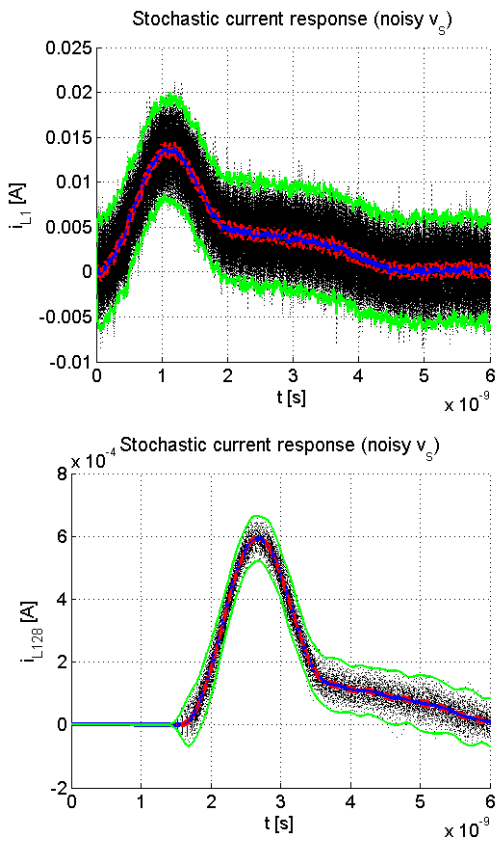Fig. 9.   Stochastic voltage responses for noisy series resistances.

Fig. 8.   Stochastic current responses for noisy excitation voltage.
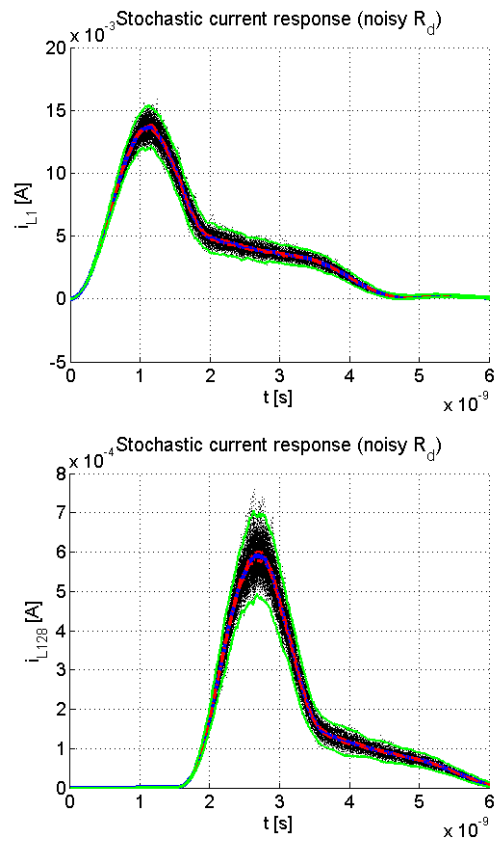
Fig. 10.   Stochastic current responses for noisy series resistances.

The Fig. 7 and 8 show a case of additive noises, Fig. 9 and 10 then a case of multiplicative ones. The computation was performed for $m = 128$ sections, which complies, with some margin, with rule of thumb the TL section delay is less then roughly a tenth of the rise/fall time of the impuls propagated ($m > 100$ would be good in our case, a choice 128 simplifies the usage of another comparative method, a 2D LT in conjunction with an FFT-based 2D-NILT algorithm).

The 99% confidence intervals (dashed red lines), marking uncertainies in determining the sample mean values (solid blue lines) are highlighted, together with the confidence intervals for individual samples (solid green lines), marking a measure of stochastic trajectories dispersion. In case of the additive noise the resultant stochastic processes keep their Gaussian distribution, and a student-t distribution can be directly applied. In case of the multiplicative noise, however, this is not valid, and the sample statistics are calculated via dividing the samples set into a number of batches while utilizing a central limit theorem, see [3] for more details. The noise intensities were chosen as $\alpha = 10^{-6}$ in case of the noisy source v_S^*, and $\alpha_k = 10^{-5}, \forall k$, in case of the noisy series resistances R_d^*. Distinct noise intensities for different noisy elements, which result in comparable dispersions of stochastic processes, can help to evaluate components of the TL model with significant noise effects. It should be noticed that stochastic processes $\mathrm{d}W_k(t)$, needed for all numerical solutions, are generated by the MATLAB$^{\circledR}$ function for normally distributed random numbers.

VI. Conclusion

Real implementations of the interconnects in high-speed electronic systems are being influenced by a number of physical effects [13]. The stochastic differential equations approach can therefore be an interesting alternative to other probabilistic approaches, how to process such the random effects. We can mention at least [18], where a stochastic Galerkin method for the solution of stochastic telegrapher's equations is used, [19], where a polynomial-chaos expansion method is adopted, or [20], where a method based on a classical Monte Carlo analysis is considered. In mentioned cases, however, the solutions are performed in the frequency domain, in contrast to our work, where the responses in the time domain are directly treated. Especially at the solution of signal integrity issues an overall dispersion in the time domain can help to evaluate whether digital signals delivered are treatable by receivers. However, the application of the SDE theory in the TLs modelling in the frequency domain is also enabled.

We will focus our further research on a few directions. From the point of view of theoretical studies the remaining RLCG circuit elements will be taken into account to produce stochastic effects, and also their simultaneous actions will be investigated. A SDEs approach will again be used to model higher-order systems, especially those with multiconductor transmission lines (MTL) [15], [21]. Finally, other higher-order numerical techniques consistent with the Itô stochastic calculus will further be considered to ensure even better stability and accuracy of the solutions.

References

[1] L. Arnold, *Stochastic Differential Equations: Theory and Applications*, New York: John Wiley & Sons, 1974.

[2] B. Øksendal, *Stochastic Differential Equations, An Introduction with Applications*, New York: Springer-Verlag, 2000.

[3] P. Kloeden, E. Platen, and H. Schurz, *Numerical Solution of SDE Through Computer Experiments*, New York: Springer-Verlag, 1997.

[4] S. Cyganowski, P. Kloeden, and J. Ombach, *From Elementary Probability to Stochastic Differential Equations with Maple*, New York: Springer-Verlag, 2000.

[5] D. Ham, and A. Hajimiri, "Complete Noise Analysis for CMOS Switching Mixers via Stochastic Differential Equations," in *Proc. IEEE 2000 Custom Integrated Circuits Conference*, Orlando, pp. 439-442., 2000.

[6] K. Wang, and M. L. Crow, "Numerical Simulation of Stochastic Differential Algebraic Equations for Power System Transient Stability with Random Loads," in *Proc. 2011 IEEE Power and Energy Society General Meeting*, San Diego, pp. 1-8, 2011.

[7] A. Zjajo, Q. Tang, M. Berkelaar, J. P. de Gyvez, A. Di Bucchianico,and N. van der Meijs, "Stochastic Analysis of Deep-Submicrometer CMOS Process for Reliable Circuits Designs," *IEEE Transactions on Circuits and Systems I: Regular Papers*, vol. 58, no. 1, pp. 164-175, 2011.

[8] E. Kolářová, "Modelling RL Electrical Circuits by Stochastic Diferential Equations," in *Proceedings of International Conference on Computer as a Tool,* Belgrade (Serbia and Montenegro): IEEE R8, pp. 1236-1238, 2005.

[9] E. Kolářová, "Statistical estimates of stochastic solutions of RL electrical circuits," in *Proc. of the IEEE International Conference on Industrial Technology ICIT06,* Mumbai, pp. 2546-2550, 2006.

[10] N. S. Patil, B. G. Gawalwad, and S. N. Sharma, "A random input-driven resistor-capacitor series circuit," in *Proc. 2011 International Conference on Recent Advancements in Electrical, Electronics and Control Engineering,* Sivakasi, pp. 100-103, 2011.

[11] F. Rahman, and N. Parisa, "A stochastic perspective of RL electrical circuit using different noise terms," *COMPEL: The International Journal for Computation and Mathematics in Electrical and Electronic Engineering*, vol. 30, no. 2, pp. 812-822, 2011.

[12] C. K. Cheng, J. Lillis, S. Lin, and N. Chang, *Interconnect Analysis and Synthesis*, New York: John Wiley & Sons, 2000.

[13] M. P. Li, *Jitter, Noise, and Signal Integrity at High-Speed*, Upper Saddle River: Prentice Hall, 2007.

[14] E. Kolářová, and L. Brančík, "Application of stochastic differential equations in second-order electrical circuits analysis," *Przeglad Elektrotechniczny*, vol. 88, no. 7a, 2012, pp. 103-107.

[15] L. Brančík, "Time and Laplace-domain methods for MTL transient and sensitivity analysis," *COMPEL: The International Journal for Computation and Mathematics in Electrical and Electronic Engineering*, vol. 30, no. 4, pp. 1205-1223, 2011.

[16] L. Brančík, and E. Kolářová, "Analysis of higher-order electrical circuits with noisy sources via stochastic differential equations approach," *in Proc. of 22nd Int. Conf. Radioelektronika'2012*, Brno, 2012, pp. 81-84.

[17] E. Kolářová, and L. Brančík, "Vector linear stochastic differential equations and their applications to electrical networks," *in Proc. of 35th Int. Conf. on Telecommunications and Signal Processing TSP2012*, Prague, 2012, pp. 311-315.

[18] D. V. Ginste, D. De Zutter, D. Deschrijver, T. Dhaene, P. Manfredi, and F. Canavero, "Stochastic Modeling-Based Variability Analysis of On-Chip Interconnects", *IEEE Trans. on Components, Packaging and Manuf. Technology*, vol. 2, no. 7, 2012, pp. 1182-1192.

[19] D. Spina, F. Ferranti, T. Dhaene, L. Knockaert, G. Antonini, and D. V. Ginste, "Variability analysis of multiport systems via polynomial-chaos expansion", *IEEE Trans. on MTT*, vol. 60, no. 8, 2012, pp. 2329-2338.

[20] D. V. Ginste, D. D. Zutter, D. Deschrijver, T. Dhaene, and F. Canavero, "Macromodeling based variability analysis of an inverted embedded microstrip line" *in Proc. IEEE 20th Int. Conf. Elect. Perform. Electron. Packag. Syst.*, San Jose, CA, 2011, pp. 153-156.

[21] L. Brančík, and E. Kolářová, "Stochastic differential equations approach in the analysis of MTLs with randomly varied parameters," *in Proc. of 19th IEEE International Conference on Electronics, Circuits, and Systems ICECS2012*, Sevilla, 2012, pp. 725-728.

A Framework for Smart Home Services with Secure and QoS-aware Communications

Markus Hager, Sebastian Schellenberg, Jochen Seitz, Sebastian Mann, Gunar Schorcht

Abstract—The scenario of smart home services will be discussed with regard to two important aspects: the quality of service problem for the in-house communication and the need for a security scheme for the whole system. We focus on an installation with smart computers in each flat interconnected using a switched Ethernet network. These smart devices are responsible for performing local services, user control and operate as a gateway for the different types of sensor and actor networks installed at each flat. We propose a QoS scheme to prevent congestion situation for the Ethernet network which is applicable to currently available cost-sensitive hardware. Furthermore, the whole system, all communication channels, user data and the access to the framework are secured by our proposed security architecture. Finally, we will present the latest improvements on Ethernet network standards, the ongoing work on this topics and our next steps for future work.

Keywords—smart home, quality of service, Ethernet, security

I. INTRODUCTION

Smart home services (SHS) are software modules that expand the concept of the home automation scenario. The idea is to do more than just switching the heating operation status, based on the available temperature sensor information. To create a smart home, the necessary basis are different sensor units collecting as many information as possible and actors to perform the desired actions. Due to the fact, that there is no base technology comprising sensors and actors for all of the comprehensive use cases, there is the need for a solution, that offers the possibility to integrate the different sensor and actor networks into one system. This was one of the main goals of the SHS research project [1]. There are also some products which are established in the market like the "ViciOne" home and building automation system [2]. For the rest of the paper we will use the HAM (home automation module) notation, used by [3] as name for their developed automation computer unit as a placeholder for similar technologies like this, allowing to realize the interconnection of different sensor and actor networks.

The advantage of such a solution is that all information about the state of the house or flat is now available at one central point. This offers the chance to combine the data of the installed technologies to realize better services, known as smart services. This means for example that the heating

M. Hager, S. Schellenberg, J. Seitz are with the Department of Electronic Engineering and Information Technology, Communication Networks Group, Ilmenau University of Technology, Germany,
e-mail: (see http://www.tu-ilmenau.de/kn)
S. Mann, G. Schorcht are with the Department of Applied Informatics Research Laboratory, Erfurt University of Applied Science, Germany,
e-mail: (see http://www.ai.fh-erfurt.de)

control is no longer just based on the temperature sensor, also the information if a window is opened, someone is inside the room and maybe also the weather forecast is taken into account to make a better decision for how the heating should be controlled. Also, the recorded history could be used to make a prediction which could be useful if the costs of a resource varies over time.

Such systems make it more comfortable to live in those houses and therefore the current focus in the already mentioned SHS research project is to adapt these concepts for housing associations. This cannot be done by a simple expansion of the system, because a larger network must be established, it must use standard low cost hardware and especially the control and the data of the system must be secured. As we know, the existing systems are either designed for private houses and/or have no special security and quality of service concept. Due to that, in this paper we present our solution offering a security and quality of service system for this scenario.

Fig. 1 shows an example of a typical SHS network. The mentioned HAM units are installed in each flat and are interconnected with Ethernet, because it is one of the main network standards and highly available, cost efficient and guarantees a simple installation. The HAM units have a touch screen to give the user the chance to interact with the system. Moreover, a NAT gateway with Internet connection gives the user the option to get Internet access based on the installed network. Further applications like VoIP phones or other multimedia devices could also use the network. Finally, the HAM units are controlled and administrated by a central server which could be part of the network or a computer from the Internet.

II. RELATED WORK

A. Security

There exists a variety of different home automation systems. All these systems have in common, that they are interchanging information and personal data via unsecured communication channels. If a malicious intruder has access to these data, he is able to obtain a complete picture of the regarding individual. It is possible to gather information of the private behavior, of the presence in the flat or of Internet usage. To prevent this leakage it is necessary to secure these data concerning information interchange, access, storage and processing. Furthermore, it is necessary to check the authentication of the participating entities and the integrity of each delivered message to ensure that the received message is sent by the claimed originator and is not altered.
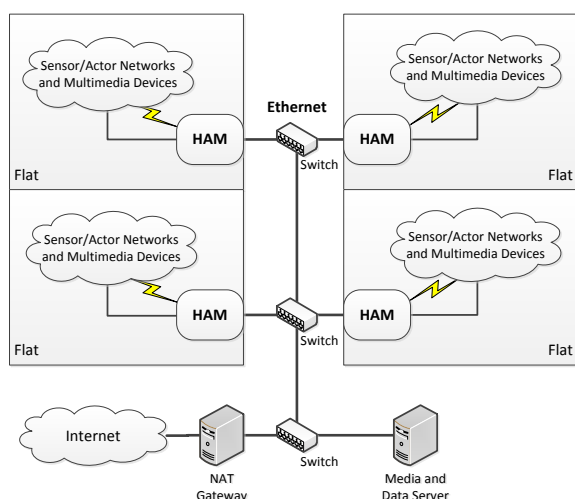
Fig. 1.   Structure of the SHS network.

There are many different ways to secure each of these aspects. To secure the storage or the data interchange it is possible to encrypt the data, so that an eavesdropper is not able to retrieve the data. But this leads to a new problem, the key exchange management. How to provide the encryption keys to the eligible entity?

Some exemplary home automation systems are "Smart Home", "Smarter Wohnen ®NRW", "SerCHo" and "ViciOne" (see [2, 4–6]). All of these existing security concepts for home automation systems are having one problem in common. All of them are providing some singular security features, but there is no comprehensive concept, which fits to all of the named aspects. Only "ViciOne" provides a comprehensive home automation system, with a security concept. This concept provides many security features, but some important features, like authentication of users and devices, are missing. All of them are isolated applications for each regarded system.

B. Quality of Service

Every quality of service solution is mainly designed based on the used hardware and due to the fact, that switched Ethernet is used for the SHS network, we will only focus on solutions based on this technology. Furthermore, quality of service is a collective term for many aspects classifying a connection. In the SHS scenario, the most important aspects are the available data rate for an end to end connection inside the SHS network and the delay and/or the jitter for this connection.

Moreover, a separation based on the different services running on the HAM units must be done, because on the one side we have applications with high priority, for example the message of a smoke detector or some administration commands and on the other side less important data streams like the heating control communication or the Internet session of a user. Ethernet offers a well-known scheme to mark each packet either in the type of service field of the IP header or in the QoS field of the Ethernet frame (see IEEE 802.1Q or IEEE

802.1p) to allow the network components to handle packets with a certain priority in a preferred way.

However, there is one main problem concerning these concepts: if there are more packets arriving at a switch than it can handle, some packets still get discarded due to buffer overflows. This could affect UDP streams because there is no flow control mechanism like TCP streams have. Therefore, a quality of service concept has to be developed based on traffic shaping, that avoids congestions at any point inside the smart home network.

AVB (audio/video bridging [7]) is one concept, to expand the behavior of standard Ethernet. The main idea is to use a similar mechanism as in the case of the RSVP (resource reservation protocol). Before establishing a new connection, every switch for this connection gets a request and checks whether or not the necessary resources are available. This is a suitable solution for some cases, but has also some disadvantages: special AVB switches are required and there is no scheme implemented, that adapts the different data streams, if the requested resources are not obtainable. Finally, the applications must support these requests.

Therefore we think, the access to the network must be managed based on the applications, the destination of each communication session and the current status on each link of the network for these data streams. [8] demonstrates how traffic shaping could be applied, but the presented solution is designed for virtual machines and the network topology is not taken into account. Besides, there are a lot of other publications, e.g. [9, 10], but after all we have not yet identified one concept that fulfills all our requirements:

- guaranteed and/or best effort data rate for individual applications
- consideration of the network topology
- avoidance of network congestion for end-to-end communication
- integration of standard off-the-shelf switches
- no changes to the network stack
- no special requirements for the behavior of the applications

In the following sections we will present our solution, first the security architecture and finally the quality of service scheme for the SHS network scenario.

III. CONTRIBUTION OF OUR WORK

The main contribution regarding the security architecture is the new combination of different approaches working co-operatively together to address the security aspects of the smart home scenario. This includes as starting point the collection of important threads and results, in combination with the role based access system, in a complete overview of the security problem. Our solution is designed in view of this analysis and evaluated with respect to the different hardware and software elements which are part of a smart home system. Furthermore, the QoS system realized by a middleware addresses the requirements pointed out in the previous subsection, whereas the most important requisites are a cost-sensitive installation and a framework without an

additional interface to the applications running on the HAM units. Finally, some alternative approaches regarding QoS will be separately discussed in section VI.

IV. Security Architecture

Regarding the problem, that there is no all in all security concept, we developed such a concept in the SHS research project. We propose a complete and comprehensive security system with features for each single application of the SHS system, by providing a new combination of commonly known security features (e.g. encryption, hashing) together with new, improved or adapted features (e.g. authentication, role-based access). This includes features for encrypting transferred and stored data, to authenticate each participant and for a role-based access-system to restrict access to all the data and functions of the system. We also performed threat modeling to identify the most common security threats to the system and developed solutions for these threats.

A. Threat Modeling

Threat modeling is a common method to identify and evaluate all potential threats of a system. The procedure is to identify the threats and visualize them in a threat matrix. The most dangerous of them are chosen to build threat trees to give an overview about the reason of the threat. Furthermore, all security assets and security leaks are identified and possible attack scenarios and corresponding countermeasures are shown.

Threats: Some of the identified threats of the provided system are:

- physical threats like vandalism, burglary, theft of devices
- theft of passwords
- intentional disclosure of administrator passwords
- hacking of accounts, passwords or ciphers
- phishing of information
- spoofing within authentication procedures
- intentional backdoors in external code
- denial-of-service attacks, remote control of devices
- computer viruses and the like
- misuse of administrative privileges
- denial of information

These threats are just the most common, of course there are more threats or attacks possible, but they are more unlikely or they do not harm that much. All of these threats were analyzed and rated, in order to compare threats. In our analysis, we identified phishing as the most likely and breaking a cipher as the most harmful threat. In the following we will exemplarily analyze the threat of breaking a cipher. Hacking of a cipher has an enormous damage potential. In the worst case the adversary gets all information, which are sent over the network. This contains user names and passwords as well as all necessary authentication information. So it is conceivable that the attacker gets root permission to the system. In the worst case, which means that there is no reissuing of keys and no random numbers are used (depending on the cipher), this attack is repeatable at any

time. Only highly skilled programmers could perform this attack and tools are only useful if the security architecture has some significant weaknesses. So the probability of this scenario has to be put on a medium level. Depending on the location of the attack, e.g. within a flat, at a NAT gateway or at a HAM, some single user might be affected up to all users and the provider. This attacking scenarios is usually discoverable by the leak of sensitive information. After a successful attack it is possible, that the users lose their trust in the system and in the worst case there is a possibility of legal consequences. Summarizing this, hacking a cipher is the most harmful threat with inestimable consequences. There are different vulnerabilities to perform this attack. The key length has to be chosen depending on the available resources and is hence not necessarily optimal to security. Another weakness is the key management, as in some cases it is possible that unauthorized persons could find out the keys. The most common way to break a cipher is the brute force attack, where every possible key is sequentially checked. An improvement is the dictionary attack. Other, more sophisticated, attacks are: man-in-the-middle attack, linear and differential cryptanalysis or other algebraic attacks. The most useful countermeasures are extending the key length (regarding the resources), the use of a key management system, like DHKE.

Security Assets – A main part of our research was to identify all security assets of the given building automation system. Assets define all system features, processed data and system functions which have to be protected against attacks. Those security assets are:

- confidentiality – all personal data in the system has to be confidential, i.e. data has to protected against unauthorized access and it has to be assured, that only the designated receiver can read the data.
- authenticity – it has to be assured that received data are originated by the claimed sender, i.e. the sender's authenticity has to be ensured.
- accountability – it must be possible to identify the responsible entity for each incident.
- integrity – unintended and intentional data altering have to be recognizable or preventable. Therefor it is necessary to identify the originator of data uniquely.
- availability – the system's inherent services and functions have to be available and have to work correctly.
- controlled access – only authorized entities are allowed to access services, functions and data.
- anonymity (pseudonymity) – personal data has to be pseudonymized. This means, that it is not possible to associate personal data to a single user, even if there is an unauthorized access.
- impossibility of finding linkage of intercepted data – all data, processed in the system, have to be encrypted in a way, that it is not possible to determine connections between the data and the system status. E.g. it should not be possible to create a presence profile based on intercepted radiator usage data.
- robustness – the system has to be robust against faults,

that means that the system has to work properly even if some instances have malfunctions.

- physical safety of devices – it is also important to ensure the physical safety of all devices, because all functionalities of the system depends on the correct behavior of the devices. However the physical safety is no part of the security architecture. For example the physical safety can be improved by using backups of the devices and servers.

B. Encryption Features

The proposed security architecture provides a combination of features for encrypting transferred and stored data, management of key exchange and to ensure message authentication, while being liable to severe restrictions of computing power, because most of the used devices are embedded systems with low resources. There is no security architecture, which combines security features for all kind of devices and all parts of a home automation system. Due to the ressource restrictions we can use neither asymmetric ciphers nor a complete public key infrastructure. We provide two different ciphers, which can be used within the system. Those ciphers are AES128 (Advanced Encryption Standard with 128 bit key length, see [11]) and RC4 (Ron's Code Nr. 4, see [12]). We recommend the use of RC4, because it is more secure and faster than AES128, but AES128 is a more widely spread standard. Of course there are many other encryption standards, but they all have crucial disadvantages like lack of security, high performance needs or they are not supported by most manufacturers.

Symmetric ciphers work with one key for both participants (sender and receiver). The main problem is how to provide this key to both parties. It is insecure to send the key in plain text over an insecure channel and it is impracticable to commit the keys personally. So there is a need for a key exchange management. We provide a common procedure for secure key exchange, the Diffie-Hellman Key Exchange (DHKE, see [13]). The DHKE establishes a shared secret, which can be used for secret communication.

The security of the DHKE is based on the discrete logarithm problem, which makes it hard to compute g^{ab} from given g^a, g^b. This key exchange is used to provide keys between parties, which communicate bidirectionally. This comprises user, operators, provider and all devices, that are able to communicate bidirectionally. To provide keys to unidirectionally communicating devices, the key is stored at the device during the manufacturing process and, after putting into operation manually, provided to other parties. In order to provide as much security as possible, a periodic key renewal is necessary. This is only applicable with bidirectionally communicating devices by using the key exchange method again.

As mentioned above we use AES-128 as encryption method, so we need symmetric keys of 128 bit length. Referring to [14] and [15] we need the public DH-parameters p (prime number) and g (primitive root) as well as the private DH-parameters a and b (private random numbers). The requirements to this parameters are shown in table I.

In [15] it is shown how to extract a 128 bit shared key. A symmetric key of 128 bit length is equivalent in strength to a 3072 bit asymmetric key, as claimed by RSA Security in 2003 (see [16]). An asymmetric key length of 3072 bit should be used if security is required beyond the year 2030.

Due to known problems of DHKE, e.g. the possibility of a man-in-the-middle attack (a man in the middle masquerades himself as Alice and Bob and performs two distinct DHKE, so he is able to decrypt and re-encrypt messages), it is necessary to provide advanced versions of the DHKE. A possible countermeasure for man-in-the-middle attacks is the use of an authenticated DHKE, or station-to-station protocol (STS, see [17]). The STS-protocol is based on the classic DHKE and its security is also based on the discrete logarithm problem. As distinct from DHKE, the STS-protocol uses an asymmetric key pair for each party to sign the key exchange process. This advancement results in a mutual authentication of each other, that means the originator of a message within the key exchange is the claimed one and there is no man in the middle. The disadvantage of the STS-protocol is the additional computational cost. Therefore, we provide both methods, the classic DHKE for devices with high resource restrictions and the STS-protocol for devices with more available resources .

Besides encryption and key exchange, we provide a feature to ensure message integrity. Therefore, we use special message authentication codes, so called cryptographic hash algorithms. We provide two different hash algorithms, the widely known SHA-1 (Secure Hash Algorithm Nr. 1, see [11]) and the RIPEMD128 algorithm (RACE Integrity Primitives Evaluation Message Digest, see [18]). Both algorithms generate a unique 128 bit hash based on the message. Each message can be identified by this hash. Comparing the hash of a message m, denoted by $h(m)$, which is sent and encrypted within the message, with a self computed hash of the received message m', $h(m')$, you can detect altering of a message, by $h(m) \neq h(m')$, which ensures the message integrity.

As mentioned in section "Conclusion and Future Work" of our previous work [19] there was an ongoing NIST (National Institute for Standardization and Technology) competition for the next secure hash algorithm. Just a few weeks ago, on Oktober 3rd, the NIST pronounced the hash algorithm KECCAK (see [20]) to be the next secure hash algorithm, called SHA-3 (see [21]). SHA-3 is not meant to replace the common SHA-2, since no significant attacks on SHA-2 are known. Due to given theoretical attacks on SHA-1, there was a need for an alternative, different hash function. Keccak is built on a so called sponge function. A sponge function has an finite internal state und uses an input stream of any length and produces an output stream of any desired length. SHA-3 is a family of hash function with the possible state sizes of $\{25, 50, 100, 200, 400, 800, 1600\}$ bit and possible hash sizes

TABLE I
REQUIREMENTS TO THE DHKE-PARAMETERS

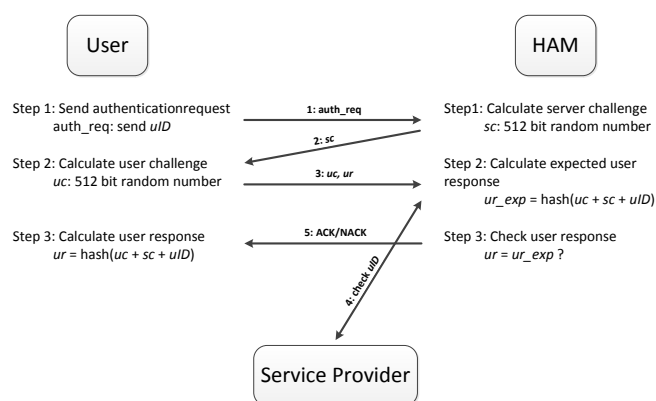| Value	Size
p	min. 512 bit (recommended 1024 bit)
g	$0 < g < p$
a	$0 \leq a \leq p - 1$
b	$0 \leq b \leq p - 1$

Fig. 2.   User Authentication Process.

of $\{224, 256, 384, 512\}$ bit.

Nevertheless we can not recommend the use of SHA-3 without testing it in the context of embedded systems. Keccak is a very simple and fast hash algorithm based on a different architecture than SHA-2. Even so an implementation for micro controller is needed and hast to be tested, before we can recommend a use within the building automation system.

C. Authentication

Authentication is the process of verifying a claim made by a subject that it should be allowed to act on behalf of a given entity (person, computer, process, etc.). There are many different ways generally known for authentication, e.g. two-factor authentication, login / password, ownership authentication or knowledge authentication. For authentication we propose an adapted challenge-response protocol. Challenge-response authentication is a family of protocols in which one party presents a question ("challenge") and another party must provide a valid answer ("response") to be authenticated. Since we support many different entities, we need different types of knowledge for every entity type. Electronic devices possess a unique identity number, which can be used for authentication. A user receives such a number during the registration process.

To clarify this authentication methods, we will describe the authentication process of an user exemplarily. Every user of the system needs to be registered by a service provider. Within this registration process the user is provided with a unique identifier. This identifier is used to authenticate the user at his first participation in the system. After this first authentication, the user chooses a nickname and a password for every further authentication due to usability reasons. In the following, we will describe this first authentication process.

The authentication starts after receiving the unique identifier. The user wants to take part in the system and sends an authentication request to the system. As shown in figure 2, the user and the system perform a challenge-response process. Due to this process, the system and only the system is able to check whether the user is allowed to participate in the system or not. If the process is exited successfully, the user chooses a unique nickname and a password for any further authentication and the system only needs to check the combination of nickname and password.

D. Role-Based-Access-System

A home automation system, like SHS, has a number of functions and a variety of different and partly personal data. Required by law, the provider of such a system has to secure the personal data itself as well as proper handling of the data. That means for example, that only eligible persons for an assigned purpose are allowed to access this data. Because of the nature of a home automation system, there are some functions whose wrong usage can affect dependability. For this reason, the restriction of those functions is essential to ensure functionality at any time.

To provide this feature, we developed a role-based access system for the SHS scenario. First of all, we identified all participating entities, i.e. all kinds of persons or electronic devices which take part in the system. After that, we defined some standard roles and possible profiles and assigned the access authority to the specific data and functions:

- administrator - non-personalized user profile, personalized user profile (e.g. flat administrator, parents, ...)
- limited user - limited user profile (limitations individually determinable by flat administrator, e.g. profile: children,...)
- maintenance user - non-personalized profile with limitations for the purpose of maintenance (remote profile, on site profile,...)
- guest user - non-personalized limited profile with optional non-critical authorizations
- system provider - provider of the SHS system
- property provider - provider of the property, lessor
- service provider - external service provider, who offers services to normal users

We further identified the complete system functions/data and for all of them we assigned useful authorizations for every role. There are roles, like the administrator, who has authorization to all functions and data. Other roles, like a maintenance user, own only task-specific authorizations with respect to users privacy. Every system function and every data has an access control and only authorized users are able to get access. For every access, the system checks the user profile attributes whether the access is allowed or not. Within the registration process of a new user, there is a form where the registrar has to check which parts of system have to be accessible by the new user. In table II we will show the role-based-access-rights for some selected data and functions of a single facility service of the SHS-system. The shown service, "wireless reading of consumption data", is an important and sensitive functionality of the SHS-system, so a restriction of access right is absolutely necessary.

E. Simulation Results

All provided algorithms work on embedded systems, which are supplied with battery and have only low resources. So it is necessary that each algorithm uses only a small amount of energy and time. So we measured duration and energy consumption of all cryptographic algorithms. The computations

TABLE II
ACCESS RIGHTS FOR SELECTED DATA AND FUNCTIONS OF "WIRELESS
READING OF CONSUMPTION DATA."

	Role	Yes	No
Consumption data	Admin (Inst.)	x	
	Admin (Flat)	x	
	limited user		x
	maint. user		x
	guest user		x
	serv./prop. prov.	x	
	serv. prov		x

	Role	Yes	No
Transmission of data	Admin (Inst.)	x	
	Admin (Flat)		x
	limited user		x
	maint. user	x	
	guest user		x
	serv./prop. prov.	x	
	serv. prov		x

were processed on two different micro-controllers, the HCS08 and the MSP430.

HCS08 - all computations were processed by 8 MHz of clock frequency, a voltage of 3 V and a maximum current of 5 mA. Due to compiler license restrictions, RIPEMD128 was not tested on this device. The measurement results are shown in table III.

MSP430 - the computations were processed by a clock frequency of 25 MHz, a maximum of 3.6 V and a maximum current of 8.9 mA. The results are shown in table IV.

The energetic consideration of the implemented algorithms shows, that the Diffie-Hellman key exchange consumes the most energy. For this reason, we recommend to perform the key exchange only once during the first authentication. Every further key should be transferred via the established secure channel. As an energetically convenient cipher, we recommend AES128. Furthermore, it is supported by almost every device. We recommend RIPEMD128 as an energetic-optimal hash algorithm, because it is obviously better than SHA-1.

The following scenario within a home automation system demonstrates how important a security system is. Let us assume a radiator remotely controlled via Internet, i.e. the user wants to turn on the radiator thirty minutes before he arrives at the flat. He uses his smart phone to connect to the system remotely and uses a system function to turn on the radiator. In this scenario, there are many security needs. The remote connection has to be secured, the remote device has to authenticate itself, the accessing user has to be authorized and it has to be checked if the user has the right to access. If one of those needs is not satisfied it is possible for a malicious person to turn on the radiator whenever he wants to. Furthermore, for

TABLE III
ANALYSIS OF THE HCS08 MICRO-CONTROLLER

Algorithm	Duration [ms]	Enery use
DHKE	5220	87.5 mWs
RC4	14	210 μWs
AES128	5.7	85.5 μWs
SHA1	191	2.87 mWs
RIPEMD128	-	-

TABLE IV
ANALYSIS OF THE MSP430 MICRO-CONTROLLER

Algorithm	Duration [ms]	Enery use
DHKE	464	14.9 mWs
RC4	4.98	159 μWs
AES128	2.00	64.1 μWs
SHA1	6.57	211 mWs
RIPEMD128	0.827	26.5 μWs

an intruder it would be possible to detect if the user is not at home, which means a high burglary risk. The proposed security architecture satisfies all of the named needs. We provide a secure Internet connection via SSL and the named encryption algorithms, our system is able to authenticate the accessing device and user and we can refuse the connection if an unauthorized access occurs.

V. QUALITY OF SERVICE SYSTEM

A. Theoretical Functionality

The fundamental idea of our quality of service solution is to control the access to the SHS network on each HAM unit and differ thereby between the applications based on a predefined priority scheme for each service. This means, that we allow each application to use only a defined data rate for communication. Furthermore, an adaptation of these settings is continuously made based on the state of the network. To perform this evaluation, first the network topology must be known and second, the current behavior of the applications must be obtained. For the first task, there exist diverse techniques to get this information automatically, but currently this is not a part of our application, we simply work with the predefined information of the network topology.

The second task is to measure and to shape the traffic caused by the services on the HAM unit. Both parts are highly related to the used operation system. To monitor the traffic, a packet analyzer, developed with the help of the "pcap" library, is used. This software offers the possibility to implement our system on Linux and on Windows machines, because this library is based on a portable framework. The shaping of the outgoing traffic is more challenging, but from a general point of view, Linux as well as Windows have a mechanism, that allows to take control of the data rate on the network interface card. The mechanism can be divided into two parts: a filter and a queue. The filter is used to assign specific packets to a queue, whereby several attributes could be used, e.g. a destination port range, a process ID of the sending process or the 802.1p flag settings of the packet. Each filter is assigned to a queue, but it is also possible to connect several filters to the same queue. If necessary, a serving strategy of the queue, like HTB (hierarchical token buffer) could be used, but in our case, a simple FIFO strategy is sufficient. The queue schedules the transmission of the packets, so that the defined data rate is guaranteed.

Our complete quality of service system works as follows: on each HAM unit a middleware is installed, that monitors and controls the outgoing network traffic with the help of the instruments recently described. A powerful HAM unit or
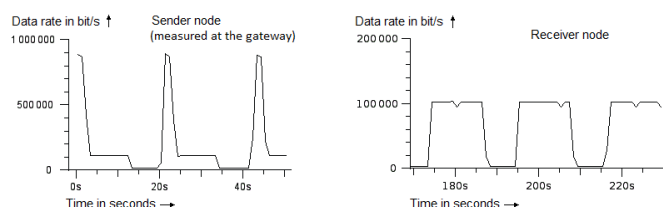
Fig. 3.   Shaped traffic caused by multimedia device.

an additional control server is used as control manager of the network. The middleware on each HAM unit reports the communication status frequently in a certain time interval, e.g. 200 ms, to the control server. With this information, the server checks the network status on each link and sends adaptation messages to the middlewares, if one or more applications cause more traffic than suitable for the network. The adaptation process guarantees, that the high priority services of the SHS system can use their desired data rate for communication and prevents congestion situations inside the network.

B. Simulation and Evaluation

To test the quality of service system, we used a virtual network to check the functionality of the system and as well a real network to get reliable measurement data to prove the correct system behavior.

As mention in the introduction, the HAM unit is not only used as gateway for the sensor network, it is also used by some multimedia devices like a VoIP phone or a smart phone to allow them to communicate with each other and to give them access to the Internet via the installed SHS network. Therefore, by the virtual setup, we first checked the behavior of such devices and how the traffic shaping could be applied to control the traffic caused by such devices. Because the HAM unit acts as gateway in this case, the only way to assign this traffic to a filter is to use the second network interface as specific attribute for this packet and the MAC-address of the devices, to handle them individually.

Fig. 3 presents the measured results. The axis of abscissas shows the time in seconds, but the time axises of the two plots are not synchronized and the axis of ordinates is scaled in bits per second. The multimedia device sends three data packets in a row separated by a short time interval. The adaptation of the traffic class due to the reached data rate limit is not visualized in the diagrams.

The left plot shows the data received on the gateway sent by the multimedia device and the right plot shows the data received at the addressed destination. It illustrates that the traffic is limited to 100 kbit/s which was the default setting by our setup for this traffic class. Noticeable is the fact, that the gateway gets a short packet burst from the multimedia device at the startup, but the received traffic at the destination shows that the shaping works well when the gateway forwards the traffic to the SHS network.

Next, we used a real network for the evaluation of the system. To reduce the complexity, only two PCs, acting as HAM unit, are sending data to one destination and according
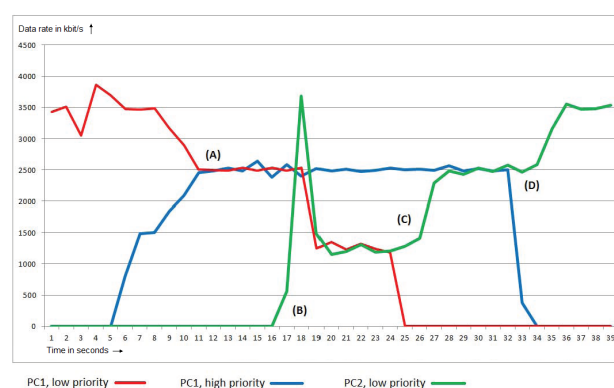

Fig. 4.   Shaped traffic of some SHS services.

to that, there is one unique bottleneck link inside the network. Fig. 4 illustrates the traffic on that link. To eliminate the influence of the network devices and the system performance of each unit, we modeled each link inside the network to support only a maximum data rate of 5 Mbit/s. Finally we used only two priority classes and reduced the system reaction time to one second, which means that the middleware sends the current status each second to the control server. As above, the abscissa represents the time in seconds, but the data is reduced to the situations, where some changes happened. The ordinate dimension is in kbit/s.

Initially, PC1 sends a data stream with low priority and a data rate of 3.5 Mbit/s. Next, after a few seconds, this PC initializes a data stream with 2.5 Mbit/s but high priority. Due to the adaptation strategy, both streams are reduced to 2.5 Mbit/s (point A), because the link supports only 5 Mbit/s, but any other user defined partitioning would also be possible. This behavior is described in the system configuration, which could be changed by administrator.

After a few seconds, PC2 starts a data stream with low priority and a desired data rate of 3.5 Mbit/s (point B). In this case the adaptation of the data streams is different because we have two data streams coming from different PCs with different priority at the same time on the link. The reaction is, that both data streams with low priority in summary and the high priority data stream will get an equal data rate. This means, that the high priority data stream of PC1 is unchanged but the two low priority data streams are reduced to 2.5 Mbit/s in total.

Next, after the situation is stable, the low priority data stream from PC1 is stopped (point C) and so the low priority data stream of PC2 reaches the maximum of 2.5 Mbit/s, because there is still the high priority data stream of PC1. Finally this high priority stream is canceled (point D) and due to that, the data rate of the last stream inside the network can increase the date rate to the desired value of 3.5 Mbit/s.

VI. FURTHER CONSIDERATIONS FOR ETHERNET

As pointed out in the previous section, our proposed QoS system is based on an admission control scheme with a continuous evaluation and adaption of the network QoS settings made by a central control server. Nevertheless, this approach

solves the addressed problem under some practical constraints and can be realized with currently available hardware, it also introduces two critical problems. First, the single point of failure of the control server and second, the scaling problem conditional to these control servers if the size of the network is increased.

Due to the fact that each node of the network managed by the control server could also be a gateway to other networks or subnetworks, it is possible to split large networks into smaller sections and apply a control server to each of these network sections. This would mitigate the scaling problem and as well the single point of failure aspect. However, we still have to rely on these control servers, either for the complete network or at least for each section of the network. Therefore, a better alternative is to use distributed mechanisms to overcome these problems.

A. Distributed Approaches

The challenge of distributed algorithms is to reach a global objective for a large system consisting of several elements by controlling the system behavior only at each element. For example, the shortest path problem could be globally solved by the Dijkstra or Bellman-Ford algorithm but this is also a typical example for the ant colony optimization approach [22] and demonstrates how a simple idea could be used to solve problems based on a distributed technique.

In the case of an Ethernet network, the problem is more complex and therefore it is difficult to find adequate solutions solving the quality of service problem with a decentralized scheme. Nevertheless, many approaches have been investigated and collected under the term 'data center bridging' (DCB) based on several IEEE projects, see e.g. [23].

- congestion notification, IEEE 802.1Qau
- priority-based flow control, IEEE 802.1Qbb
- enhanced transmission control, IEEE 802.1Qaz

And the IEEE 802.1aq shortest path bridging standard, but we will discuss this together with an alternative in the next subsection in more detail.

Using these techniques, it should be possible to improve the performance and effectiveness of Ethernet networks and to integrate some QoS-aware behavior. The standards are mainly completed, but the corresponding hardware supporting these features is currently not available as well as comprehensive simulation studies showing how powerful all these ideas can work together related to the requirements of a QoS-aware network, whereas some other publications have already proposed some modification of these ideas to improve the standard.

The IEEE 802.1Qau congestion notification standard addresses the already mentioned overflow problem which occurs if a switch receives more data packets than it can transmit. As known, a point-to-point based congestion handling is not selective enough and could dramatically decrease the network performance especially in the case of large networks [24]. This standards attempts to overcome the problem by extracting the causing node of the congestion at the edge of the network. Each switch of the network detecting a congestion

situation generates a congestion notification message which is sent over other switches to the causing node. Based on the received congestion notification, a rate limiter adjusts the injection rate for the services whereas the signaling contains enough information to selectively decrease only traffic, that is responsible for the occurred congestion situation. Evaluations and improvements of this standard can be found in [25] or [26].

Besides the Xon/Xoff signaling (PAUSE frame), the IEEE 802.1Qbb standards defines an enhanced mechanism of this idea. Similar to the situation described in the last paragraph, the Xon/Xoff signaling controls the incoming traffic to a switch to prevent buffer overflows. However, this regulation affects the complete traffic without evaluating the priority of the data packets. Because this is also part of the network interface card, the nodes of the network are affected by this mechanism, too. A more detailed discussion and performance evaluation can be found in [27]. The challenge how the controlling based on these priority classes should be done is addressed by the IEEE 802.1Qaz standard.

All these techniques are able to improve the performance, efficiency and the QoS-aware behavior of Ethernet networks. But it still must be evaluated how well these standards are able to enhance the network functionality with regard to specific requirements of different use cases, especially because these standards are not able to provide hard QoS as AVB ([7], II-B) does.

B. Bridging Strategies

The standards described in the section above are responsible for link control like traffic engineering, congestion management and the handling of traffic classes. Here, we will discuss a more fundamental aspect of an Ethernet network, the layer two topology. As presented in [28], Ethernet networks are typically based on the spanning tree protocol or some derivations of it. The main purpose for these protocols was to simplify the forwarding strategy for switches. Due to the deactivation of redundant paths in an Ethernet network, each switch could be sure, that sending out data packets with a destination MAC-address at that port where a packets was received with the corresponding source MAC-address before, is sufficient. The problems of circling data packets or packet duplicates did not have to be considered, either. Besides these advantages, the reduction of the network topology to a spanning tree goes around with a negative effect, too: redundancy is the basis for high performance, reliability and effectiveness and therefore not applicable in those networks.

Nevertheless, the IEEE 802.1aq shortest path bridging standard and TRILL (transparent interconnection of lots of links, RFC 6325) propose a bridging strategy for Ethernet networks where the setup of a unique spanning tree is no longer necessary and where the redundant paths are used to improve the network. The goal is to fully utilize equal cost paths in a mesh network topology to open the area where Ethernet could be applied, especially in view of data center networks and metropolitan area networks. Compared to the classical hierarchical separation of networks into core/aggregation/access

layer, these technologies permit the chance to unify the access and aggregation network technology.

Both techniques, shortest path bridging and transparent interconnection of lots of links, have been evaluated based on various conditions and even some improvements have been discussed [29–31]. However, as we think, the challenge here is to define a suitable and reproducible network scenario allowing to fairly evaluate the performance of both techniques. Furthermore, the evaluation and comparison must be based on exactly defined and convincing performance metrics like throughput, adaption time, link utilization or how good specific requirements are fulfilled. To perform an evaluation of a network or even more a comparison of different network techniques, it is very important to spend effort on the definition of usable metrics for this case. In our view, this was not the main focus of many publications on this topic, hence, it is hard to compare these results. Therefore, our future work is to define these metrics to determine under which conditions IEEE802.1aq and TRILL perform best.

VII. Conclusion and Future Work

In this paper we provided a complete communication architecture for the smart home scenario which offers both, an adequate security system and a quality of service scheme. The comprehensive security architecture addresses all needs of modern building automation systems. We performed threat modeling and identified all possible threats and all security assets of the system. We provide security features and functions for all needs, comprising encryption features, hash algorithms, authentication methods and a role-based-access-system. The proposed security architecture satisfies all actual legal requirements regarding the German federal data security law. In the near future, updates of this law in relation to smart metering systems are expectable. Nevertheless, the proposed architecture will also fulfill these requirements, but the actual certification has to be considered. Moreover, the evaluation of the quality of service strategy demonstrated, that the main parts of that solution can cooperate to avoid network congestion inside the home network. As described, there are interesting alternative approaches for Ethernet and our main focus for the future work is to compare and evaluate this techniques with respect to the QoS aspects of the SHS scenario.

Acknowledgment

References

[1] Smart Home Services Research Project. (2011). [Online]. Available: http://www.smart-home-services.de/

[2] ACX GmbH. (2011) ViciOne Home and Building Automation. [Online]. Available: http://www.acx-gmbh.de/de/home-building-automation/index.html

[3] M. A. Zamora-Izquierdo, J. Santa, and A. F. Gomez-Skarmeta, "An Integral and Networked Home Automation Solution for Indoor Ambient Intelligence," *IEEE Pervasive Computing*, vol. 9, pp. 66–77, October 2010. [Online]. Available: http://dx.doi.org/10.1109/MPRV.2010.20

[4] Smart Home der Bundeswehr Universitaet Muenchen. (2011). [Online]. Available: http://www.unibw.de/eit8_2/forschung/projekte/shfilm/

[5] Smarter Wohnen ®NRW, Fraunhofer IMS, Fraunhofer ISST, HGW. (2011). [Online]. Available: http://www.smarterwohnennrw.de

[6] Service Centric Home. (2011). [Online]. Available: http://www.sercho.de

[7] IEEE 802.1 Audio/Video Bridging Task Group Home Page. (2011). [Online]. Available: http://www.ieee802.org/1/pages/avbridges.html

[8] Bannazadeh H. and Leon-Garcia A., "A Distributed Ethernet Traffic Shaping System," *Local and Metropolitan Area Networks (LANMAN), 2010 17th IEEE Workshop on*, May 2010.

[9] Y. Zhang, R. Yu, S. Xie, W. Yao, Y. Xiao, and M. Guizani, "Home M2M Networks: Architectures, Standards, and QoS Improvement," *Communications Magazine, IEEE*, vol. 49, no. 4, April 2011.

[10] G. McAlpine, "Congestion Control for Switched Ethernet," *High Performance Interconnects for Distributed Computing*, 2005.

[11] N. Ferguson and B. Schneier, "Practical Cryptography," *Wiley Publishing, Indianapolis, ISBN 0-471-22357-3*, 2003.

[12] N. W. Group, "A Stream Cipher Encryption Algorithm 'Arcfour'," *Internet Engineering Task Force*, 1997.

[13] W. Diffie and M. E. Hellman, "New Directions in Cryptography," *In IEEE Transactions on Information Theory. 22, Nr. 6*, 1976.

[14] RSA Security. (1991) Public Key Cryptography Standards Number 3: Diffie Hellman Key Agreement Standard. [Online]. Available: http://www.rsa.com/rsalabs/node.asp?id=2126

[15] N. W. Group, "RFC 2631: Diffie-Hellman Key Agreement Method," *Internet Engineering Task Force*, 1999.

[16] B. Kaliski, RSA Security. (2003) TWIRL and RSA Key Size. [Online]. Available: http://www.rsa.com/rsalabs/node.asp?id=2004

[17] W. Diffie, P. C. V. Oorschot, and M. J. Wiener, "Authentication and Authenticated Key Exchanges," *Designs, Codes and Cryptography*, vol. 2, no. 2, pp. 107 – 125, 1992.

[18] H. D. B. Preneel, A. Bosselaers, "The Cryptographic Hash Function RIPEMD-160," *CryptoBytes, Vol. 3, Nr. 2*, 1997.

[19] M. Hager, S. Schellenberg, J. Seitz, S. Mann, and G. Schorcht, "Secure and QoS-aware Communications for Smart Home Services," in *Telecommunications and Signal Processing (TSP), 2012 35th International Conference on*, july 2012.

[20] G. Bertoni, J. Daemen, M. Peeters, and G. V. Assche, "The keccak reference," Submission to NIST (Round 3), 2011. [Online]. Available: http://keccak.noekeon.org/Keccak-reference-3.0.pdf

[21] N. I. for Standards and Technology, "Winner of the cryptographic hash algorithm competition for sha-3," 2012. [Online]. Available: http://www.nist.gov/itl/csd/sha-100212.cfm

[22] Jayadeva, S. Shah, R. Kothari, and S. Chandra, "Debugging ants: How ants find the shortest route," in *Information, Communications and Signal Processing (ICICS) 2011 8th International Conference on*, dec. 2011.

[23] S. Reinemo, T. Skeie, and M. Wadekar, "Ethernet for high-performance data centers: On the new ieee datacenter bridging standards," *Micro, IEEE*, vol. 30, no. 4, pp. 42 –51, july-aug. 2010.

[24] W. Noureddine, F. Tobagi, W. Noureddine, and F. Tobagi, "Selective back-pressure in switched ethernet lans," in *Proceedings of IEEE GLOBECOM*, 1999, pp. 1256–1263.

[25] M. e. a. Alizadeh, "Data center transport mechanisms: Congestion control theory and ieee standardization," in *Communication, Control, and Computing, 2008 46th Annual Allerton Conference on*, sept. 2008.

[26] W. Jiang, F. Ren, C. Lin, and I. Stojmenovic, "Analysis of backward congestion notification with delay for enhanced ethernet networks," in *INFOCOM, 2012 Proceedings IEEE*, march 2012, pp. 2961 –2965.

[27] M. Hagen and R. Zarick, "Performance evaluation of dcb's priority-based flow control," in *Network Computing and Applications (NCA), 2011 10th IEEE International Symposium on*, aug. 2011, pp. 328 –333.

[28] R. Sofia, "A survey of advanced ethernet forwarding approaches," *Communications Surveys Tutorials, IEEE*, vol. 11, no. 1, quarter 2009.

[29] R. Perlman, "Challenges and Opportunities in the Design of TRILL: A Routed Layer 2 Technology," in *GLOBECOM Workshops, IEEE*, 2009.

[30] K. Miyazaki, K. Nishimura, J. Tanaka, and S. Kotabe, "First-Come First-Served Routing for the Data Center Network: Low Latency Loop-Free Routing," in *World Telecommunications Congress (WTC),*, march 2012.

[31] D. Allan, J. Farkas, and S. Mansfield, "Intelligent load balancing for shortest path bridging," *Communications Magazine, IEEE*, july 2012.

Portable Heart Rate Detector Based on Photoplethysmography with Android Programmable Devices for Ubiquitous Health Monitoring System

Chi Kin Lao, U Kin Che, Wei Chen, Sio Hang Pun, Peng Un Mak, Feng Wan, and Mang I Vai

Abstract—In this paper, a miniature portable heart rate detector system is implemented by modern hardware ICs and simple sensor circuit with software executable on both PC and Android platform. The biosignal is first extracted via photoplethysmography (PPG) principle into electric signal. Then a microprocessor is used to covert biosignal from analog to digital format, suitably for feeding into an RF module (nRF24L01 for RF transmission). On the receiver end, the computer and/or smart phone can analyze the data using a robust algorithm that can detect peaks of the PPG waveform, hence to calculate the heart rate. Some application software running on Windows and Android phone have been developed to display heart rate information and time domain waveform to users for health care monitoring. In the future, pure Bluetooth technology will be used for wireless personal communications instead of RF modules. At the same time, the data can be sent to computer console using existing available networks (3G, 4G, WiFi, etc.) for health database logging purpose.

Keywords—Heart rate detector, Android application, healthcare monitoring, Photoplethysmography (PPG), peak detection algorithm, wearable/portable device.

I. Introduction

Because of the rapid medical development of our modern societies, the health care system becomes much more mature and professional. Migrating regular mature in-clinic/in-hospital health system to individual wearable monitoring systems for chronic disease becomes popular. This trend will go on in forthcoming years as the average number of elderly has continued to occupy large portions worldwide. In order to decentralize the current burden of public health system and promote the popularity of routine health self-check, many techniques in Biomedical Engineering have been developed for making faster and more accurate pre-diagnoses with ease-of-use.

The traditional devices are quite bulky, so the patients usually need to go hospital/clinic every time whenever health checks are conducted even for slight discomfort. This is quite inconvenient, especially for the patients with chronic diseases and/or with moving difficulty. Although some small mobile devices [1][2] have been developed recently, they are still equipped with some unwieldy cables, which lead to some inconvenience. Lately, biomedical devices using wireless techniques are developed, and their sizes become much smaller than those before.

To address the health problem mostly related to the general public, small devices for the cardiovascular diseases (CVDs) can provide timely & immediately supports for the most patients at home. In according to the World Health Organization, CVDs are the first cause of death, equivalently 30% of global deaths in 2008. This figure is estimated to rise up to about 25 million of deaths by 2030 [3]. Despite of devoting efforts in prevention of CVDs, we should also prepare for easing the increasing pressure for the public health system.

Electrocardiography (ECG) monitoring has been a standard norm procedure for CVDs diagnosis and the need to develop a miniaturized device for self-assessment and monitoring of the CVDs patient is important. By measuring the Heart Rate Variability (HRV), the status of the heart activities can be estimated. However, measuring the ECG of the patient is not easy for untrained personnel, not mentioning long-term monitoring without significant interference in the daily life. Although it is less prominent than that from ECG [4], HRV from PPG can be still an acceptable compromise for non-professional and daily monitoring. PPG would be more acceptable for general public because of single detection location (usually at fingertip or ear lobe) and no gel electrode needed. It is one of non-invasive methods for measuring the amount of the blood volume changes inside the blood vessel [5]. In general, PPG sensing device is easy to position for long term monitoring purpose and can monitor several CVD related parameters such as heart rate, blood oxygen level, respiration, etc.

In this paper, a portable biomedical detector prototype that monitors heart rate and potentially measures blood oxygen level in the future using PPG is designed and implemented, as well as a robust PPG waveform detection algorithm is proposed. To minimize the size of the system, hardware devices were carefully chosen with multiple functions on the same chip. Also wireless communication is realized by small size RF modules and leave further analyses for computers/PDAs. The next Section gives the system overview. Section III introduces various subsystems/building blocks & prototype results for our implementation. Section IV explains the technical

All authors are with Department of Electrical and Computer Engineering, Faculty of Science and Technology, University of Macau, Macau SAR, China (phone: 853-8397-4276; fax: 853-8397-4275; Corresponding email: fstpum@umac.mo). Mang I Vai and Sio Hang Pun are also with the State Key Laboratory of Analog and Mixed-Signal VLSI, University of Macau, Macau SAR, China) and Peng Un Mak is currently on leave to the Anschutz Medical Campus, University of Colorado, USA

details about the adopted peak detection algorithm. Prototype results and conclusions are given in Section V and future improvement suggestion can be found in the end.

II. SYSTEM OVERVIEW

The overall design block diagram of our PPG heart rate detector is shown in Fig. 1. In the current design, the system is divided into two main parts: PPG detector and Human Interface. The PPG detector, as shown in the upper portion of Fig. 1, consists of a battery-powered standalone device consisting of a special designed optical sensor for PPG detection, a conditioning circuit for noise reduction & anti-aliasing, a MCU for digitizing the PPG signal & preparing the data for transmission, and a RF transmitter for connection to the server computer.

The block diagram of the Human Interface, as shown in the lower part of Fig. 1, consists of a RF receiver, a server computer and an Android ready mobile phone. The server computer communicates with the PPG detector via the RF receiver. In the same time, the PPG data is stored for in-depth analysis for the purposes of diagnosis and treatment planning in the future. In the meanwhile, related information is sent to a smartphone for user's concern wirelessly. In the next Section, the function of each component will be briefly discussed.
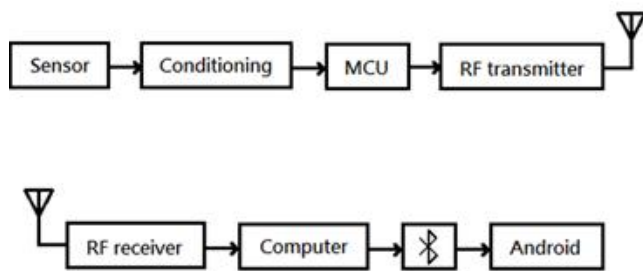
Fig. 1.   Block diagram of the PPG heart rate detector and Human interface

III. FUNCTIONAL PARTS & PROTOTYPE RESULT

In this section, the role and characteristics of the each module within the system are introduced and described.

A. Wearable Sensor

To facilitate plethysmography measurement, three sensing mechanisms are commonly used, namely, volume displacement plethysmography, impedance plethysmography, and photoplethysmography [6]. The photoplethysmography is preferred in our design because measurement can be performed on fingertip without precise positioning. Additionally, the design can easily upgrade to blood oxygen saturation measurement. Photoplethysmography (PPG) is based on plethysmography and photovoltaic technique, as displayed in Fig. 2(a). Every time when blood pumps to periphery (ejection phase), blood vessels expand due to the blood pressure from the heart, a pulse will be generated. And every time when the blood flows back (diastolic filling phase), another pulse follows. So the PPG signal will be the superposition of the pumping pulse
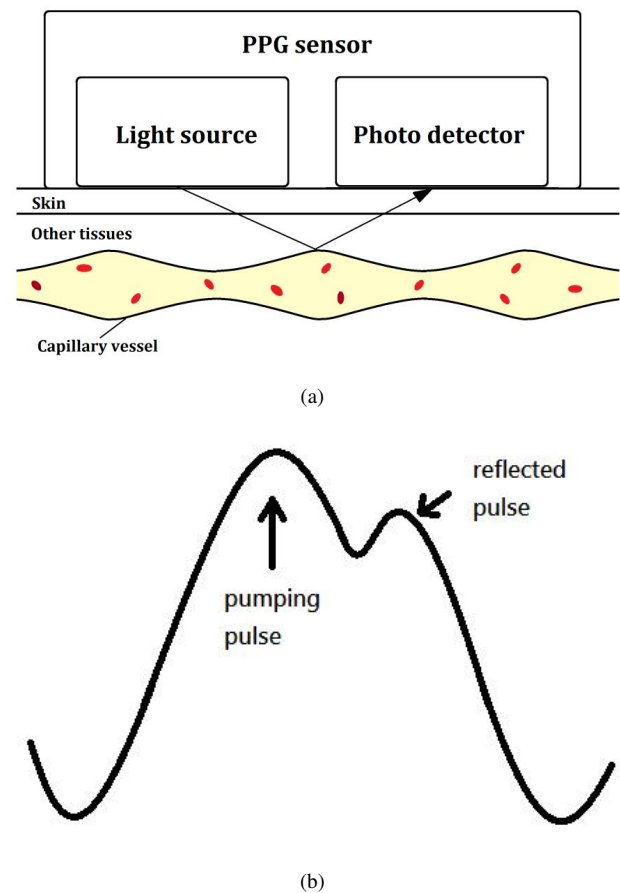

(a)

(b)

Fig. 2.   (a) Basic PPG technique; (b) Sample PPG waveform
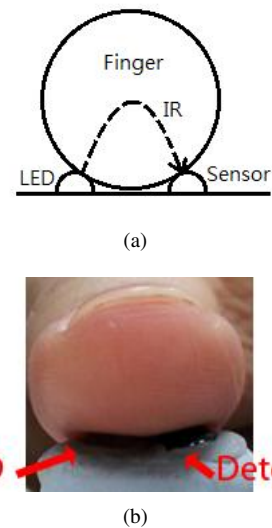

(a)

(b)

Fig. 3.   (a) Illustration of PPG sensor schematic; (b) physical case during signal extraction

and the reflected wave, as shown in Fig. 2(b).

Fig. 3 depicts our conceptual diagram of PPG measurement on fingertip. An infra-red LED and a detector were placed beneath the fingertip of the patient for measuring the change of blood volume by the activities of the heart. The volume change of the blood within the artery will directly affect the scattering light

received by the photo-detector and thus, a simple circuitry, as shown in Fig. 4, is used to generate the electric pulsation related to the plethysmography. A sample output of the sensor in both time and frequency domains is shown in Fig. 5. One can observe the heart rate is located around 1-2 Hz while the power line 50 Hz is strongly presented.
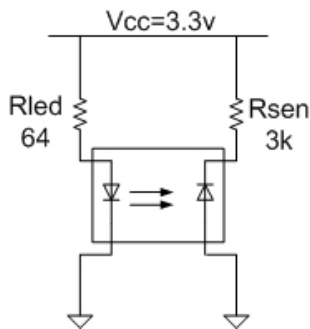

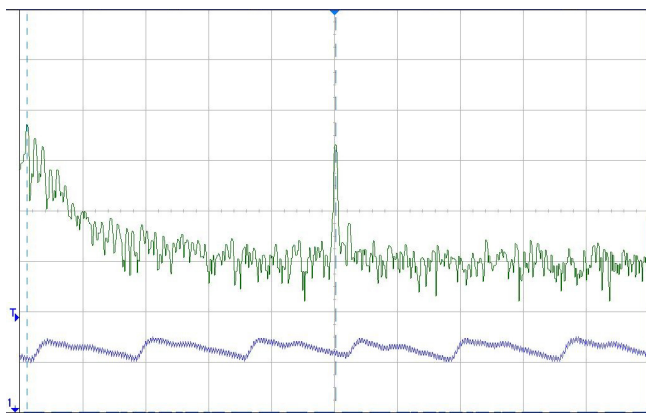Fig. 4.   Block diagram of the PPG heart rate detector

Fig. 5.   Acquired Electric pulsation of the plethysmography from sensor (Purple colour: Time domain & its FFT in green colour)

B. Signal Conditioner

As one can observe the PPG signal in Fig. 5, the raw signal from the sensor is quite weak (8 mVp-p) and is contaminated with noise (especially 50 Hz power-line) on top of a DC component. Therefore, a high pass filter with stop corner frequency of 0.5 Hz, as shown in Fig. 6, is applied.

Additionally, an operation amplifier (AD626), which has
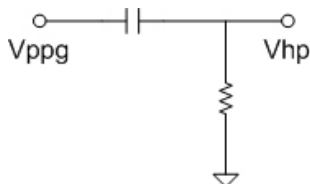
Fig. 6.   Circuit to filter out the DC components of the PPG signal

maximum 100 V/V voltages gain and intrinsic structure for adding low pass filter (corner frequency set to 34 Hz), was used to eliminate the noise component in the signal and

boosted the signal for the A/D converter in the next stage. The schematic of the pre-amplifier can be found in Fig. 7(a) while its frequency response is shown in Fig. 7(b). The corner frequencies of high pass and low pass filters in this signal conditioning block setting satisfied the ordinary PPG signal with frequency in several Hz [7], and its bandwidth of the PPG signal is 0 - 30 Hz [8].

Fig. 8 displays the processed PPG signal before entering
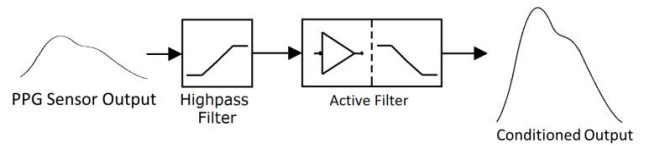
(a)
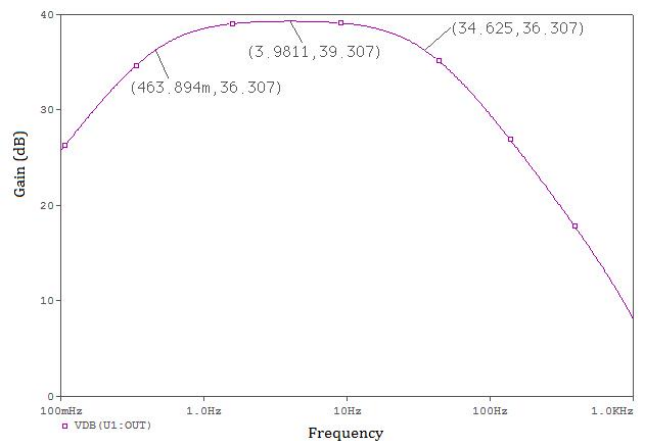
(b)

Fig. 7.   (a) Schematic of the pre-conditioning module; (b) Its frequency response

the next stage of microprocessor. The PPG signal and its characteristics can be clearly identified.
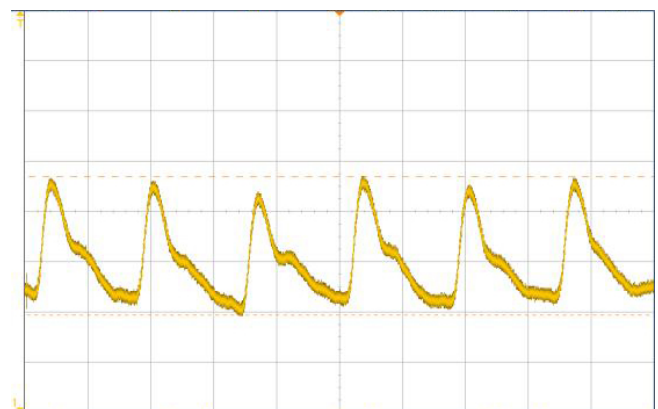

Fig. 8.   Sample Conditioned PPG signal

C. Microprocessor

To build a wearable PPG device with extended battery life, we select the C8051F930, which belongs to an 8051 family microprocessor with built-in 10-bit ADC, 90 μA supply

current, and small form factor 9 x 9 x 1.6 mm^3. The sampling frequency of the ADC is set to be 250 Hz.

D. RF Transceiver

nRF24L01 [9] is used to wirelessly transmit the PPG signal to the server computer or equivalent. It is chosen because of its small size of around 4 x 4 mm^2 and can be operated through a standard Serial Peripheral Interface (SPI). The carrier frequency is ISM frequency band around 2.4 GHz and operates up to 1 Mbps data rate. The supply voltage is 3.3V from lithium ion battery of 70 mAh capacity.

E. Finger Clip Housing

In order to accommodate all the hardware of aforementioned subsystems, we use a 3-D printer, Fortus 400mc model [10] to print our finger chip housing. This can allow us to flexibly minimize the mechanical housing of our clip in ergonomic consideration; and at the same time, to provide hidden room for various electronic building blocks. Fig. 9(a) shows our home-made finger clip housing outlook while Fig. 9(b) & 9(c) display various electronics components in assembly. The initial prototype size is around 40 x 30 x 20 mm^3 and could be smaller in later version.

F. Windows Application

As Android phones and iPhones are the most popular phones nowadays and possibly in near future, we would like to select one of them to develop our PPG application. Finally we choose Android because development on iOS has much more limitations in comparison to those on Android, which belongs to Open-Source. However, apps that are not from the Apple Apps Store cannot be installed to a standard iPhone. For an Android phone, we just need to develop our app to be a signed app, then our app can be installed on the phone and start the testing. A Windows application written in Visual Basic is developed as a server for processing the PPG signal. In this stage, a new peak detection algorithm for heart rate calculation is designed, which is fast enough to satisfy the real-time application on the smartphone and somewhat adaptive and predictive to achieve its robustness. The algorithm will be discussed in details in the next section.

The whole digital processing including the peak detection and procedure of heart rate calculation is shown in Fig. 10. The mini-system continuously receives the PPG from the wearable sensors wirelessly, processes the raw PPG signal, stores for future reference, and retransmits the PPG signal & information to a smartphone app via Bluetooth. In addition to these basic functions, the server computer can also display the PPG signal in real time (as shown in Fig. 11). One can observe that Fig. 11 basically retains most information carried by Fig. 8. Hence, Heart Rate can be readily obtained.
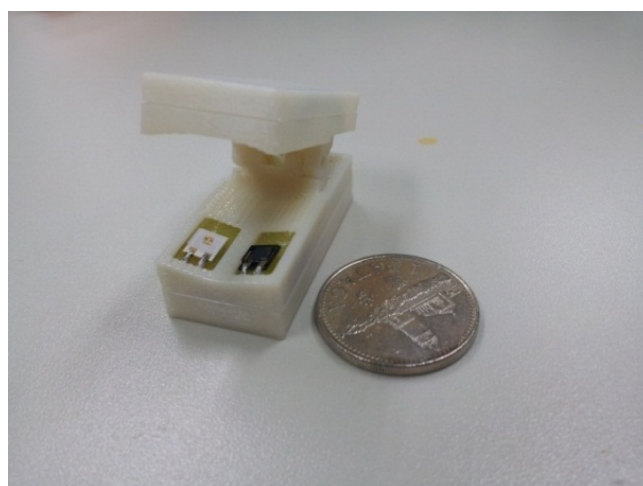
G. Android App

In order to display the PPG signal in smartphone devices, an Android apps was developed. The Bluetooth APIs of Android
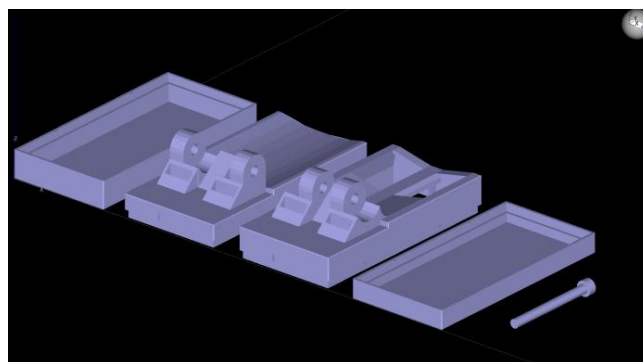
(a)
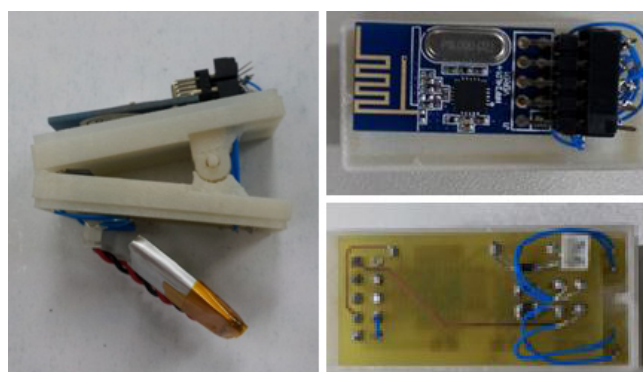
(b)

(c)

Fig. 9.   (a) Finger clip housing; (b) microprocessor, and RF module; (c) Sensor circuit with 1 Macau Pataca Coin

supports the cable replacement protocol RFCOMM which provides serial port (RS-232) emulation. By using the serial port emulation mode, the PPG data with necessary information can be easily delivered to the smartphone apps without excess computing consumption. The main technique of this kind of communication is to establish a virtual serial port while pairing with the Android phone using Fig. 10 algorithm. Finally, an open source pure Java API, AndroidPlot, was used to create dynamic PPG chart. Its library was added to our Android application, then the plot view can be added to the layout main file and the corresponding program which is based on
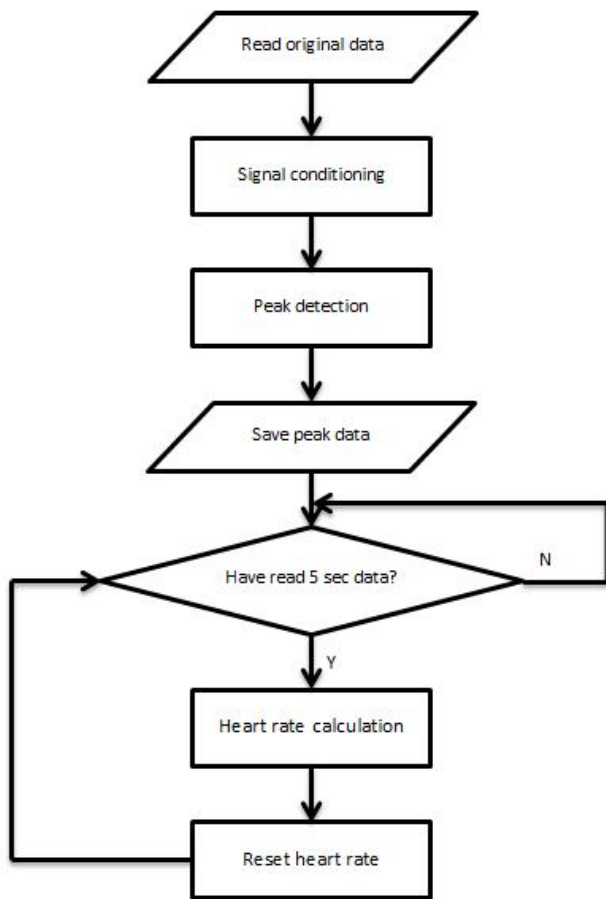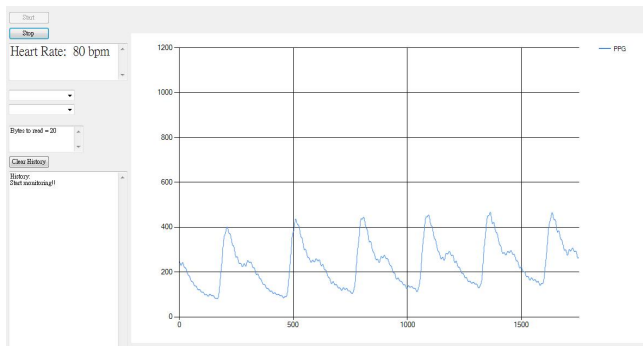
Fig. 10.　Flowchart of our digital processing

Fig. 11.　Sample PPG plot from the server computer

the AndroidPlot example "Orientation Sensor" is added to the main activity file. When there is new PPG data reading, the PPG plot will be updated, as shown in Fig. 12 below.

IV. PPG SIGNAL PROCESSING ALGORITHM DESIGN

Admittedly, PPG waveform has a lesser complicated morphology than other physiological signals, such as EEG and ECG and etc. However, there always exist high-frequency noises as well as the low-frequency baseline drift, derived from either the measurement itself or respiration and motion artifacts. Recently, there are several PPG signal processing algorithms proposed in the recent years, including adaptive
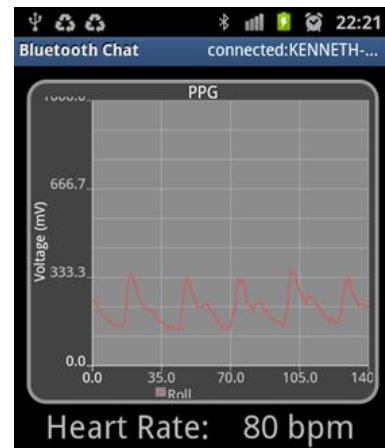

Fig. 12.　Sample PPG plot in a Smart Phone

threshold method [11], cubic spline interpolation [12], local maxima method [13][14]. They almost contain two parts, namely the signal pre-processing/conditioning and peak detection or feature extraction.

Likewise, our algorithm for PPG signal processing also primarily consists of two parts: signal conditioning [13] and peak detection [11]. The algorithm was previously implemented in MATLAB R2011a (The Mathworks, Inc.), and then transformed into Visual Basic 2010 Express which is the platform of the whole system. For convenience, subsequent examples and results will be demonstrated in the MATLAB.

A. Signal Conditioning

For high-frequency noises cancellation and baseline drift removal, various types of digital filtering methods prove to be effective. Besides, discrete wavelet transform [15] can also act as a denoiser to smooth the waveform. Our signal pre-processing mainly contains two steps: high-pass FilterDxN [16] for real-time baseline drift removal and low-pass moving average filter [17] to smooth the waveform.

The proposed FilterDxN was initially named after the two parameters adjusted in the design of it, namely N for the number of the averaged signal samples and D for the distance between them. Typically, the filter can be expressed as:

$$y[i] = x[i] - \frac{1}{N} \sum_{j=-(N-1)/2}^{(N-1)/2} x[i + jD] \tag{1}$$

where $x[i]$ is the input signal and $y[i]$ is the output signal. In order to avoid the phase shifting, N should be selected as an odd number. It can be perceived that we can simply adjust D and N in accordance with the performance we expect. The implementation of the filter is relatively easy, compared with the complex and time-consuming frequency and time domain conversion. For the consideration of the actual performance, we manually conducted averaging over a group of 25 samples with a distance of 15 samples between each other, thereby realizing a comb filter to reduce the baseline drift.

As the name implies, the moving average filter operates by averaging a number of consecutive samples from the input

signal to replace corresponding samples in the output signal:

$$y[i] = \frac{1}{N} \sum_{j=-(N-1)/2}^{(N-1)/2} x[i+j] \qquad (2)$$

Again we can see that N should be an odd number just for symmetrical consideration. In our system (sampling frequency of 250Hz), we chose N as 21 to realize a low-pass filter in removing high-frequency noises.

Fig. 13 displays the original PPG signal as well as the results of signal conditioning (baseline removal and noise cancellation), respectively. From the figure, it can be seen that the signal conditioning removes baseline drift and noises, resulting PPG with only very little dc component. This would be more convenient for us to utilize the information inside the amplitude in the peak detection. However, the tradeoff of this single conditioning is to have minor loss of samples at both ends due to the moving average used in both detrending and denoising.
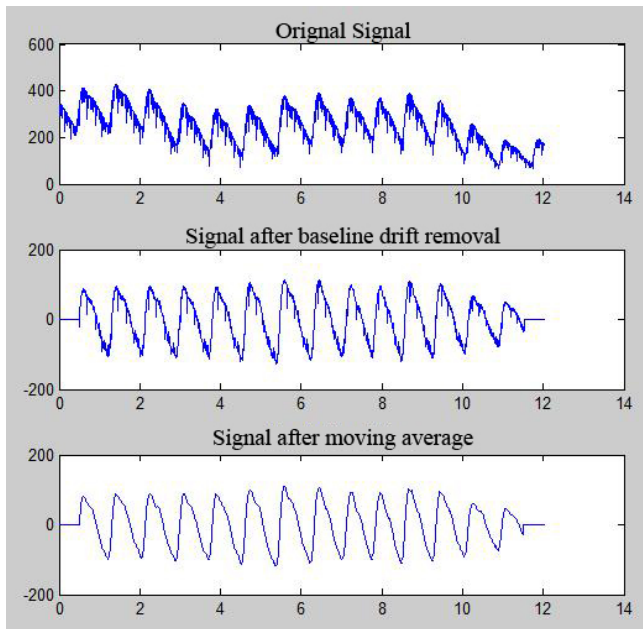

Fig. 13.   Original PPG signal and results of detrending and denoising

B. Peak Detection

Actually, the original ideal of our peak detection method comes from one adaptive threshold method for the peak detection of PPG waveform [11]. However, we have modified or even improved it by changing the adaptive threshold rule and adding some new considerations to deal with certain extreme waveform conditions. We call it the sliding and climbing (S&D) peak detection method because the peak detection procedure is quite similar to the repetitive process of sliding downhill from one peak and then climbing uphill to the next peak. The overall flow diagram of the S&D method is described in Fig. 14.

In order to better clarify the procedure of the S&D peak detection method, a typical example is graphically illustrated in Fig. 15. Other more complicated or tough conditions will be shown later to demonstrate the advancement and robustness of our peak detection method.

In the process of S&D peak detection, the value of threshold is decreased with an adaptive slope during the period when the threshold is higher than the PPG signal. Like simple envelop detector, when meeting the signal, the threshold will merely follow or track the signal until it detects a new peak. At the new peak, the slope is updated according to the amplitude of current peak and next potential one, and starts another sliding and climbing process. Former procedures are repeated till the end of the signal.

In adaptive thresholding, the current slope is modified by the amplitude of the latest peak and amplitude difference between the latest peak and next potential one. The modified slope can be expressed by (3).

$$slope_i = c_r V_i + f_r (V_i - V_p) \qquad (3)$$

where $slope_i$ is the descending slope of the ith peak, c_r and f_r are current and future factor weights, and finally V_i and V_p stand for the amplitudes of current peak and next potential one. In our system, c_r and f_r are empirically selected as -0.6 and -1.0, respectively. Flexibility of this method is to allow adjusting these two parameters to seek for a better performance in the application.

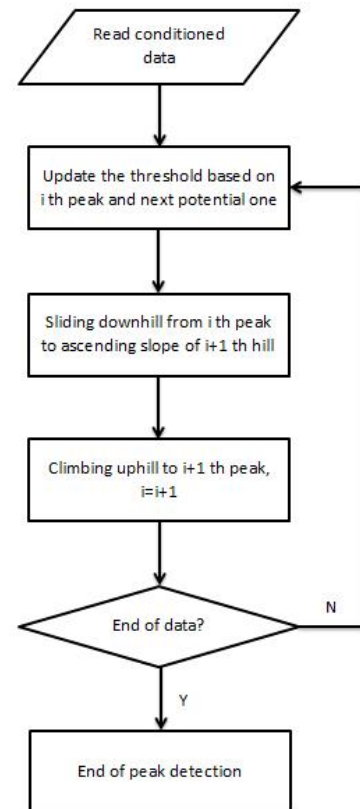After the signal pre-processing, most noises and baseline drift

Fig. 14.   Peak detection flow diagram of the S&D method

should have been eliminated. However, some rigid ripples or local maxima points usually exist to hinder the peak detection. Fig. 16(a) and Fig. 16(b) illustrate the situation and the
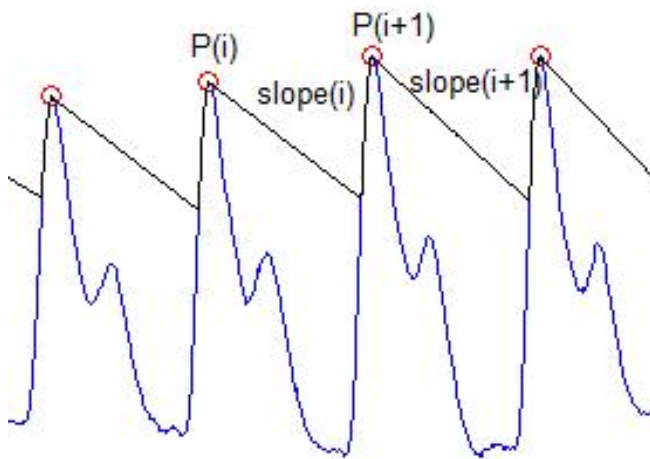
Fig. 15.　An illustration of typical procedure in S&D peak detection

associate solution to conquer it.

To overcome the ripples on ascending slope or near the peak,
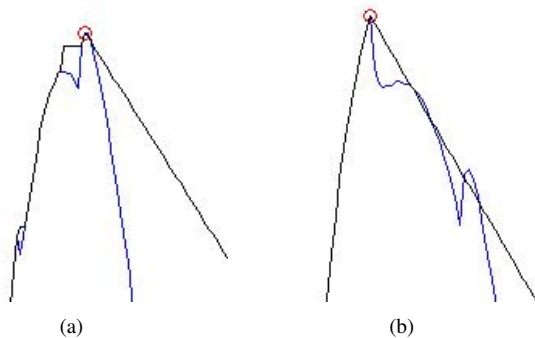

(a)　　　　　　　　　　　　(b)

Fig. 16.　(a) Ripples on the ascending slope and around the peak; (b) Ripples on the descending slope

when meeting a local maxima point, instead of regarding it as a new peak, our peak detection method will conduct a scanning action over a tiny interval exactly after the detected local maxima point. If there is no sample that has a larger value there, then the newly found point will be considered as a true peak. Otherwise, the threshold will skip the small ditch and continue to climb.

For the ripples on the descending slope, which the threshold line has a chance to meet before the ascending slope of the next hill, our S&D detection method applies a similar measure to the one used in another adaptive threshold method [11]. A criterion based on the previous average pulse interval is adopted to judge whether the threshold has arrived at the ascending slope of the next hill. If the distance between the crossing point and the latest peak is larger than 0.6 times of previous average peak interval, the threshold will stop and follow the signal. On the contrary, it will keep sliding down. This criterion also takes effect when coping with high reflected wave peak as a result of aging.

Generally, after baseline removal, there should not be any large sudden variation in amplitude between two successive waves. However, in order to test our peak detection method,

we artificially modify one period of actual signal to generate the extreme situation. To our satisfaction, the detection method successfully gets through the test, which is shown in Fig. 17.

Since the adaptive slope contains both the current and future
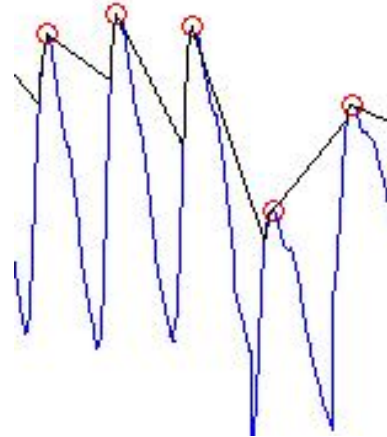

Fig. 17.　Solution of large sudden amplitude variation

information about amplitude, our detection is sensitive to the variation of amplitude, thus ensuring the validity and robustness of our peak detection method. Finally, the result of signal conditioning and peak detection for a sample PPG signal is shown in Fig. 18(a) and Fig. 18(b), respectively.
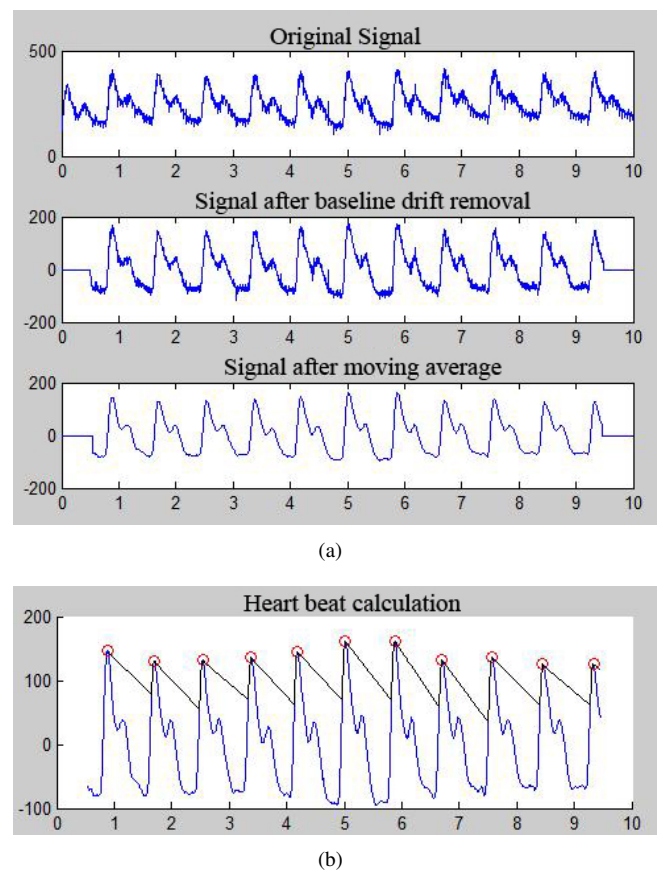

(a)

(b)

Fig. 18.　(a) Result of signal conditioning for a sample PPG signal; (b) Result of peak detection of the signal

V. Conclusions

In this work, we have successfully developed a portable heart rate detector for monitoring CVDs patients so as to address the health problem mostly related to the general public. This heart rate detector uses PPG to calculate the HRV of the patient in order to assess the abnormal symptoms such as arrhythmia, coronary artery diseases, etc. Because of the light weight PPG heart rate detector housing in a tailor made finger clip, this system is compatible with the popular Android smart phone so that the waveform of the PPG, real-time heart rate & HRV can be displayed to the user without additional hardware. Furthermore, from our design, the system can provide initial information regarding to the health status of the CVDs patients, and index for pre-diagnosis of various cardiovascular symptoms as well.

At the same time, a robust algorithm for PPG waveform processing (signal conditioning and peak detection) is designed. Without relatively complicated frequency analysis and wavelet decomposition in signal pre-processing step, this adaptive algorithm is fast enough to realize the real-time health care monitoring application with validations from experiments. Therefore, the algorithm itself should have a good application prospect.

VI. Future developments

In the future development, we would test more subjects and compare our result with the standard Holter ECG medical equipment for accuracy evaluation. On the other hand, to increase the versatility of heart rate during exercise, we shall add acceleration sensor to remove the motion artifacts. Also, we would like to extend the program in Android, so that it can transmit the PPG data to the Internet via 3/4G networks. To the final end, we can integrate all electronic devices in transmitter module into a single chip, like SOC, so that the device can be extremely small or even implantable into human for signal extraction.

References

[1] P. Wei, R. Guo, J. Zhang, and Y. Zhang, "A new wristband wearable sensor using adaptive reduction filter to reduce motion artifact," in *Proceedings of the 5th International Conference on Information Technology and Application in Biomedicine, in conjunction with The 2nd International Symposium & Summer School on Biomedical and Health Engineering*.

[2] K. I. Wong, "Design and experimentation of wearable body sensors," pp. 273–288, Rapid Prototyping Technology - Principles and Functional Requirements, Dr. M. Hoque (Ed.), Intech, 2011.

[3] W. H. Organization, "Cardiovascular diseases (cvds)," Fact sheet No. 317, Sep. 2012.

[4] F. C. Chang, C. K. Chang, C. C. Chiu, S. F. Hsu, and Y. D. Lin, "Variations of hrv analysis in different approaches," *Computers in Cardiology 2007, Vols 1 and 2*, pp. 17–20, 2007. Bja59 Times Cited:0 Cited References Count:14 Computers in Cardiology.

[5] J. Allen, "Photoplethysmography and its application in clinical physiological measurement," *Physiological Measurement*, vol. 28, no. 3, pp. R1–R39, 2007. 150JQ Times Cited:141 Cited References Count:269.

[6] R. B. Northrop, *Plethysmography*, p. 525 p. Biomedical engineering series, Boca Raton: CRC Press, 2002.

[7] J. S. Rhee, *Finger Photoplethysmographic Sensors for Vital Sign Monitoring*. PhD dissertation, Massachusetts Institute of Technology, 2000.

[8] M. Nitzan, A. Babchenko, and B. Khanokh, "Very low frequency variability in arterial blood pressure and blood volume pulse," *Med. Biol. Eng. Comput.*, vol. 37, no. 1, pp. 54–58, 1999.

[9] "www.nordicsemi.com/eng/products/2.4ghz-rf/nrf24l01," *Last accessed on Feb. 2012*.

[10] "http://www.fortus.com/products/fortus-400mc.aspx," *Last accessed on Feb. 2012*.

[11] H. S. Shin, C. Lee, and M. Lee, "Adaptive threshold method for the peak detection of photoplethysmographic waveform," *Computers in Biology and Medicine*, vol. 39, no. 12, pp. 1145–1152, 2009.

[12] W. Chen, S. Lei, L. Guo, Y. Chen, and M. Pan, "Study on conditioning and feature extraction algorithm of photoplethysmography signal for physiological parameters detection," in *Image and Signal Processing (CISP), 2011 4th International Congress on*, vol. 4, pp. 2194–2197.

[13] B. Nenova and I. Iliev, "An automated algorithm for fast pulse wave detection," *International Journal Bioantomation*, vol. 14, no. 3, pp. 203–216, 2010.

[14] S. Lu, H. Zhao, K. Ju, K. Shin, M. Lee, K. Shelley, and K. H. Chon, "Can photoplethysmography variability serve as an alternative approach to obtain heart rate variability information?," *Journal Of Clinical Monitoring And Computing*, vol. 22, no. 1, pp. 23–9, 2008.

[15] A. K. Bhoi, S. Sarkar, P. Mishra, and G. Savita, "Pre-processing of ppg signal with performance based methods," *INTERNATIONAL JOURNAL OF COMPUTER APPLICATION*, vol. 4, no. 2, pp. 251–256, 2012.

[16] I. T. Iliev, "Combined high-pass and power-line interference rejecter filter for ecg signal processing," *Proceedings of the Technical University - Sofia, Bugaria*, vol. 58, no. 2, pp. 7–13.

[17] S. S. W., *The Scientist and Engineers Guide to Digital Signal Processing*. San Diego, CA,: California Technical Publishing, 2nd ed., 1999.

Chi Kin Lao, received the Bachelor degree in Electrical and Electronics Engineering, University of Macau, Macau, 2012.

U Kin Che, received the Bachelor degree in Electrical and Electronics Engineering, University of Macau, Macau, 2012.

Wei Chen, received the Bachelor degree in Automation from Zhejiang University, China, 2012. Now he is pursuing his master degree in Electrical and Computer Engineering from University of Macau and is a student member of IEEE. His current research interests are Digital Signal/Image Processing, Intelligent Control and Computational Intelligence.

Sio Hang Pun, received the Master degree in Computer and Electrical program from the University of Porto, Portugal, 1999. He also received the Ph. D Degree in the Electrical and Electronics Engineering from the University of Macau, Macau, 2011. Since 2000, he has performed research in the areas of biomedical engineering. His research interests are Bio-electronic circuits, Intra-Body Communications, and Bio-electromagnetism. He is currently an Assistant Professor of the State Key Laboratory of Analog and Mixed-Signal VLSI, University of Macau, Macau.

Peng Un Mak received his BSc. from National Taiwan Univ., MSc. & PhD from Michigan State Univ., all in Electrical Eng. Since, 1997, he has joined University of Macau as an assistant professor in Dept. of Electrical & Computer Engineering. His current research interests are Bio-electromagnetism, Intra-Body Communication & bio-electric signals acquisition. He has authored/coauthored over 100 peer-reviewed technical publications (journal, book-chapter, conference proceedings, and etc.).

Feng Wan received the PhD degree in Electrical and Electronic Engineering from the Hong Kong University of Science and Technology, Hong Kong. He is currently an Assistant Professor in the Department of Electrical and Computer Engineering, Faculty of Science and Technology, University of Macau, Macau. His research interests include biomedical signal processing, brain-computer interfaces, neurofeedback training, computational intelligence and intelligent control.

Mang I Vai, received the Ph.D. degree in Electrical and Electronics Engineering from the University of Macau, Macau SAR, China in 2002. Since 1984, he has performed research in the areas of digital signal processing and embedded systems. He is now an Associate Professor of the Department of Electrical and Computer Engineering, Faculty of Science and Technology and the State Key Laboratory of Analog and Mixed-Signal VLSI, University of Macau.

Protection of Passive Optical Networks by Using Ring Topology and Tunable Splitters

Pavel Lafata

Abstract—**This article proposes an innovative method for protecting of passive optical networks (PONs), especially the central optical unit – optical line termination (OLT). PON networks are typically used in modern high-speed access networks, but there are also several specific applications, such as in business, army or science sector, which require a complex protection and backup system against failures and malfunctions. A standard tree or star topologies, which are usually used for PON networks, are significantly vulnerable mainly against the malfunctions and failures of OLT unit or feeder optical cable. The method proposed in this paper is focused on forming PON network with ring topology using passive optical splitters. The main idea is based on the possibility of placing both OLT units (primary and secondary) on the opposite sides of the ring, which can potentially increase the resistance of network. This method is described in the article and scenarios and calculations using symmetric or tunable asymmetric passive optical splitters are included as well.**

Keywords—**Passive Optical Networks, Passive Optical Splitters, Protection, Ring Topology, Tunable Splitters.**

I. INTRODUCTION

The passive optical networks (PONs) are usually used mostly as modern high-speed last-mile access networks. The present generation of PONs, such as XG-PON according to ITU-T G.987 [1] or 10GEPON in IEEE 802.3av [2] recommendations, offers typical shared transmission capacity up to 10 Gbps for up to 128 connected users for a distances such as 20 or 40 km [3]. Other special applications of PONs can include local backbone data networks with optimized topology and optical distribution network with optimized bus topology [4]. However, PONs can be also used for several specific applications in industry, business, office or army sectors, which usually require higher level of protection and availability using protection and backup mechanisms. These applications typically require high network availability together with the guarantee of maximum functionality of the whole network infrastructure. That is

why it is necessary to develop simple and efficient methods of protecting the critical optical units in PONs as well as of the whole optical distribution network.

One of these problems consists of protecting the optical line termination (OLT), which is a central optical unit of the whole PON. This unit provides mainly communication controlling, management and servicing functions of the whole network and it also connects the PON network into the backbone telecommunication infrastructure [3]. It is obvious that its potential failure or malfunction would surely result into a collapse of the whole PON.

A typical optical distribution network usually has a star topology with a single branching point, or a tree topology with several branching points [3], which makes the methods for OLT backup difficult. While in case of a star or a tree topology all optical fibers are concentrated into one single central point, backup (secondary) OLT can be placed only into the same place as the primary one, as illustrated in following Fig. 1. Such backup cannot be very reliable and the whole infrastructure is still vulnerable to many situations, e.g. global power failure, floods, terrorist action, breaking of feeder optical cable etc.
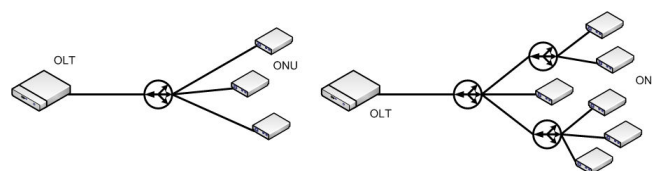

Fig. 1. Typical star and tree topology in case of PONs.

That is why the optimal topology for the critical application of PON is a ring topology [5], but presented applications require special optical network units (ONU) with optical switches and others nonstandard enhancements. However, ring topology could be also easily formed by using standard passive optical splitters with symmetric or asymmetric splitting ratios, which would enable placing the secondary OLT unit into any possible position in a ring thus making the whole infrastructure less vulnerable. It is evident that a ring topology in case of PON would probably suffer several disadvantages, so it would not be very useful for standard PON applications, such as providing network connection for ordinary households and typical end-users, but its application for well protected specific situations in local area networks could enhance the overall security of the whole infrastructure.

Another problem of a PON with ring topology is a high value of insertion loss of passive optical splitters. That is why forming an optical distribution network with ring topology using only standard symmetric passive splitters would result into a very uneconomic solution, because only a

limited number of network units could be connected in such case. However, using asymmetric passive optical splitters with splitting ratios calculated and optimized for specific scenario or tunable splitters, could significantly balance the attenuation in the whole infrastructure, thus enabling more ONUs to be connected [4].

This paper contains an initial idea of forming PON with ring topology consisting of two independent OLT units and passive optical splitters. The next part is focused on calculations of attenuation and its balancing for two scenarios of ring topology – using standard symmetric splitters, and using asymmetric splitters (or tunable splitters) with optimized but rounded splitting ratios, which can be easily manufactured and are widely available.

II. PON with Ring Topology

The ring topologies are usually used for backbone telecommunication networks (SDH, OTH, SONET), because they offer simple possibilities for efficient network protection (e.g. optical units, optical fibers). The situation in typical PONs is slightly different. Since the whole traffic and the whole network is controlled and operated from central OLT unit, its failure would certainly result in global PON malfunction [6]. As described in the text above and illustrated in Fig. 1, a star topology or a tree topology usually offers only one possible place for OLT, which makes it further vulnerable while both (primary and secondary) OLTs can be stroked at once. A possible solution is to use a ring type topology of optical distribution network. PON networks with a ring topology were already presented for the purpose of WDM-TDM long reach PON [5], but these applications are based on special optical network units (ONU) with optical switches and others nonstandard enhancements. However, the simple ring topology can be easily created by using only standard passive optical splitters. This solution is presented in Fig. 2.
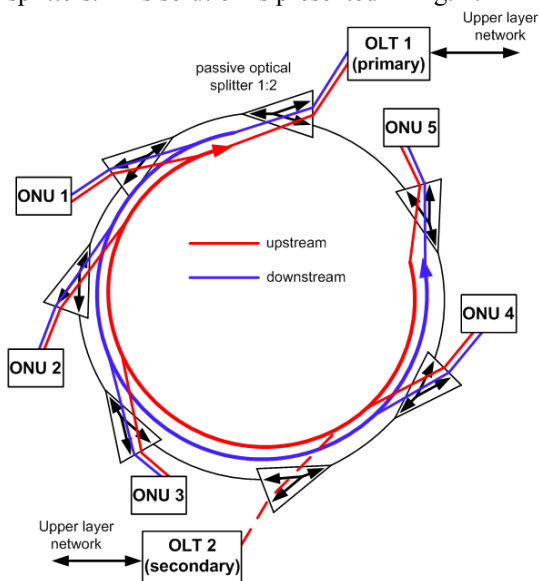

Fig. 2. Proposed ring-type PON network, initial state.

The proposed infrastructure contains two independent OLT units, which can be simply placed in any possible location within ring topology, however the symmetric situation with placing both OLT units exactly to the opposite positions of a ring (two identical halves) is optimal. This is

the main advantage of proposed solution compared to the standard tree or star topologies – the relative independence of both (or even more) OLTs locations. While in case of a tree or star topology both OLT units (primary and secondary) can be stricken with a single attack or single global failure in one location, the OLTs in case of a ring topology are mutually almost independent and their elimination could be more difficult, because they can be located anywhere within the ring infrastructure. All optical units (OLTs, ONUs) are connected via standard passive optical splitters with splitting ratios 1:2. Assuming PLC (planar) type of splitters, their directivity and return loss is high enough to prevent crosstalk and other negative disturbing between neighboring units and transmission directions. Both OLT units are connected into the upper layer networks (backbone telecommunication networks) via standard Ethernet (metallic, optical), the more detailed description is discussed in the last section of this article.

In initial state, the primary OLT (OLT 1) acts as a main OLT and is providing all standard functions in PON network. The secondary OLT (OLT 2) is in warm-state backup and is only monitoring the upstream traffic for detecting the potential failures. If the malfunction or failure of the primary OLT appeared, the secondary OLT could switch to the main role and it could take over the whole traffic. This situation is illustrated in Fig. 3.
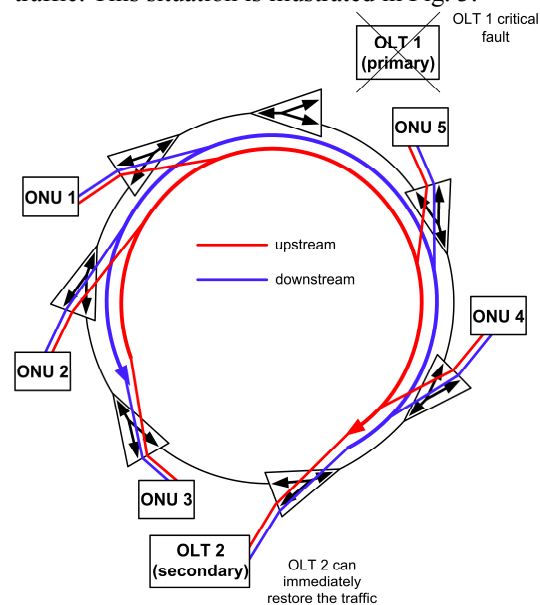

Fig. 3. If the critical fault of primary OLT occurs, the secondary OLT can restore the traffic.

By comparing Fig. 2 and 3 it is evident that both traffic directions can be easily adapted when the secondary OLT switches into the main role. It is also obvious that presented ring topology is basically a bus type topology with unused interconnection between the last ONU and the first section of a ring (OLT unit). Therefore it is necessary to perform detailed calculations and planning of attenuation and optical signal levels in all network nodes to prevent loops occurring of forthcoming optical signals. The calculations of splitting ratios and resulting attenuations for all passive splitters as well as practical example are presented in the next part of this article.

It would be therefore possible to use this proposed ring topology for designing more complex network

infrastructures, e.g. two semi-dependent PON rings with two OLTs, as presented in Fig. 4.
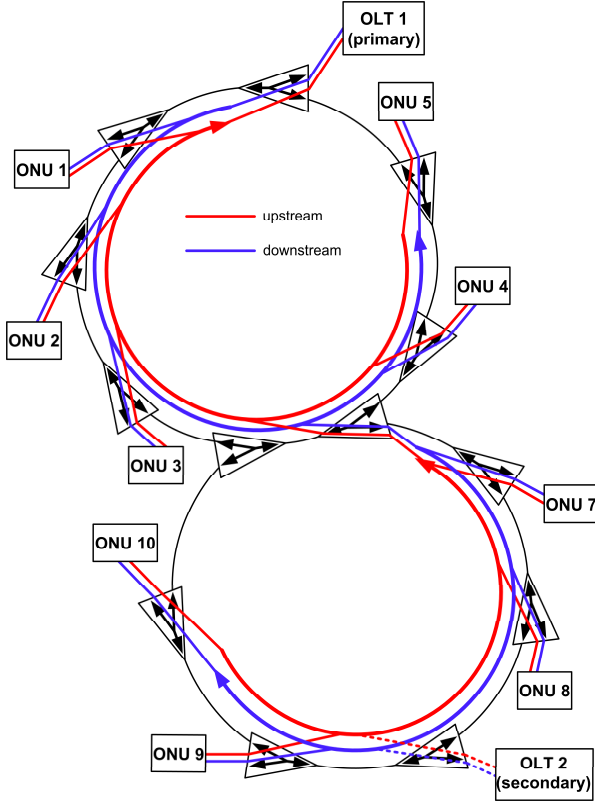

Fig. 4. Using ring topology for designing two semi-dependent protected PON networks.

In this scenario, each OLT can provide connection separately only to ONUs in each of two rings, or it would be also possible that one OLT acts as a primary unit for both rings and in case of its failure, the secondary OLT can switch to the primary role and take the data traffic over the whole infrastructure. For this reason, the splitting ratios of all passive splitters should be calculated and optimized to prevent loops occurring. If the optical level of looping optical signal is equal or lower than a minimum receivable signal on ONU side after passing throughout the whole ring, it would not influence the forthcoming traffic in downstream or upstream direction. Otherwise it would act as a disturbing signal increasing the noise level. Another possible solution would be the usage of band-stop and band-pass type filters, which would be placed at the ends of loops in both rings.

The splitting ratio of all tunable splitters should be optimized in all scenarios for enabling maximum ONUs to be connected into such infrastructure. This optimization could be performed using the algorithms presented in [4] and according to the lengths and number of optical fibers and ONUs. Practical application and example of results for a simple ring topology is presented within the next section of this article.

III. OPTIMIZATION OF PON WITH RING TOPOLOGY

Presented PON with ring topology in Fig. 2 and 3 is based on passive optical splitters with ratio 1:2 and two basic scenarios are possible – symmetric splitters (with uniform splitting ratio 50:50%), and asymmetric tunable splitters with calculated and optimized but rounded splitting ratios.

A. Symmetric and Asymmetric Passive Splitters

The splitting ratio is a key parameter of the optical splitter. The splitting process itself is implemented by passive method, using elementary Y-junctions (a single Y-junction has a splitting ratio of 1:2), which can be made using short fibers fused together or using a planar technology. Subsequently, it is possible to obtain higher desired values of splitting ratio by cascading several elementary Y-junctions. Another important parameter of the passive optical splitter is the value of its total insertion loss A_C, which consists of the loss A_D due to the process of dividing the input optical power into N outputs and it also consists of the second part represented by a residual loss A_Z [3]. The loss A_D depends on the splitting ratio 1:N (it depends on the number of outputs N), the residual loss A_Z represents the additional loss of fibers, connectors, fused joints and its irregularity, manufacturing tolerations, etc. The loss A_D due to the dividing of input optical power for the i-th branch can be expressed as:

$$A_{Di} = 10\log\left(\frac{P_{in}}{P_{out_i}}\right) \quad [dB; W, W]. \tag{1}$$

Where A_{Di} is a loss given by splitting the optical signal with an input optical power P_{in}, while the power of the optical signal on that output is P_{outi}. The summary output optical power is therefore given by summarizing all outputs:

$$P_{in} = P_{out} = \sum_i P_{out_i} \quad [W; W]. \tag{2}$$

In case of a symmetrical splitter with only one Y-junction (1:2 splitter) and a uniform splitting ratio of the input optical power to its outputs $P_{out1} = P_{out2} = 0.5 * P_{in}$, the splitting loss is $A_{D1} = A_{D2} = 3.01$ dB. The asymmetric passive optical splitter with a non-uniform variable splitting ratio on its particular outputs can be made either with the fixed splitting ratio, or as a tunable optical splitter with the controllable splitting ratio [7]. The asymmetric splitter (Y-junction in this case) provides asymmetric ratio of optical powers on its outputs, therefore it is possible to express following conditions:

$$P_{out_1} \neq P_{out_2} \quad [W; W]; A_{D_1} \neq A_{D_2} \quad [dB; dB]. \tag{3}$$

The initial condition of summary output power is still valid:

$$P_{in} = P_{out_1} + P_{out_2} \quad [W; W, W]. \tag{4}$$

If a general attenuation A_1 is connected to the first branch of Y-junction and attenuation A_2 ($A_1 \neq A_2$) to the second branch, it is possible to derive general formula for calculating desired splitting ratio in way, in which the resulting summary attenuations of both branches remain the same as:

$$\frac{P_{in}}{P_{out_1}} = 1 + 10^{\frac{A_2 - A_1}{10}} \quad [W, W; dB, dB]$$

$$\frac{P_{in}}{P_{out_2}} = \frac{1 + 10^{\frac{A_2 - A_1}{10}}}{10^{\frac{A_2 - A_1}{10}}} \quad [W, W; dB, dB] \tag{5}$$

Thanks to this equation, balanced (equal) attenuation of both branches of asymmetric splitter could be reached:

$$A_{D_1} + A_1 = A_{D_2} + A_2 \quad [dB, dB; dB, dB]. \tag{6}$$

Finally, to obtain the resulting condition of optimizing

(balancing) attenuations for specific application of asymmetric splitter, desired attenuations or levels of optical signals on its outputs are necessary. Detailed descriptions and evaluations of the formulas were already presented in [4], [8].

Basically, there are two different approaches to the practical applications of asymmetric passive optical splitters. One possibility is to use each splitter individually, with the splitting ratio being fully optimized for specific conditions, which further means to perform necessary calculations of required value of splitting ratio in the entire infrastructure first, and then to manufacture each splitter separately. The second option is the usage of tunable optical splitters.

B. Calculations and Optimizations of Splitting Ratios for PON with Ring Topology

The initial calculation is performed for standard symmetric passive optical splitters with uniform splitting ratios. Then, the following calculation is carried out for the asymmetric tunable passive splitters with specific splitting ratios, which are rounded in their percentage expressions. Common set of basic network parameters and parameters of typical optical elements are, as follows:

- Passive optical network is a GPON type with attenuation class C, the interval of granted attenuation is therefore A_{min} = 15 dB, A_{max} = 30 dB.
- The optical fiber used in the entire optical distribution network is specified according to the ITU-T G.652 recommendation as a D type fiber. Its attenuation coefficient at 1310 nm is therefore α = 0.4 dB/km.
- The ring-type PON is proposed for special applications, such as a local protected network [4], therefore the distance between two passive optical splitters is l_1 = 200 m, while the distance between the splitter and the optical network unit ONU (the length of a branch) is l_2 = 50 m. These distances were considered to be the optimal lengths for following example of a local high-speed network.
- The connection of optical network termination OLT and optical network units ONUs to an optical network is realized with a connector with the insertion loss A_k = 0.2 dB. The residual loss of modern planar passive optical splitters should not exceed 0.5 dB, therefore together with small compensation, it is possible to assume A_z = 0.55 dB. The attenuation reserve for the compensation of aging effect and temperature changes is A_r = 0.5 dB.

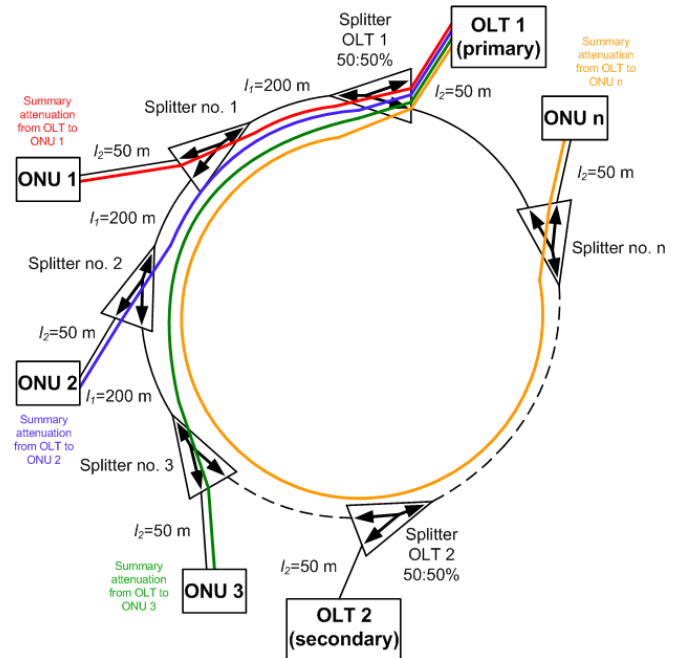Proposed ring-type PON is illustrated in the following schematic in Fig. 5.

Fig. 5. Schematic illustration of proposed PON example with ring topology.

It is evident that one of the necessary functions of splitters connecting both OLTs is to prevent optical signal looping in a ring, thus isolating the last and first section of a ring. Therefore it is necessary to calculate the attenuation of the whole ring and to calculate the level of looping optical signal, which is transmitted through the last optical splitter. Because the whole infrastructure is symmetric, which means both sides of the ring contain the equal numbers of optical splitters (ONU units), the optimum splitting ratios of the splitter connecting primary OLT (OLT 1) should be 50:50% and the same splitter should also connect the secondary OLT 2 unit. Symmetrical splitters (50:50%) in case of connecting OLT units are optimal, because in case of OLT switching, the direction of optical signal in a ring is adapted towards a new situation and for maximum flexibility of the whole infrastructure, the symmetrical splitters for connecting OLT units should be used.

1) Calculations in Case of Symmetric Splitters

First, the calculation of attenuation was performed for PON with ring topology with parameters described above, using symmetric passive optical splitters with uniform splitting ratio 50:50%. Graph in the following Fig. 6 presents the results of calculation of attenuations from OLT to all ONUs.
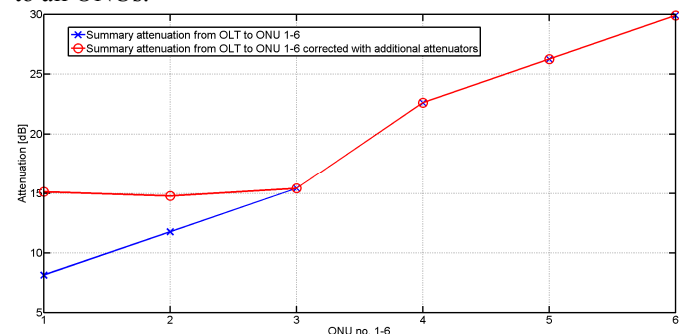

Fig. 6. Calculated attenuations from OLT to each ONU and the correction with using additional attenuators.

Based on the results, it can be concluded that with regard to maximum attenuation A_{max} for the C class of GPON it is possible to use only 6 standard passive splitters with

symmetric splitting ratio, which means only 6 optical units (ONUs) can be connected to the optical infrastructure, as illustrated in Fig. 6. Moreover, some network ring branches do not meet the minimum attenuation A_{min} specified for C class GPON. Therefore it is necessary to provide the correction by using additional attenuators for increasing their attenuation, which is also presented in Fig. 6. It is also necessary to calculate and check the overall attenuation of the whole ring infrastructure, so the optical signal passing throughout the ring and appearing on its beginning (interfering signal) is attenuated enough to not interfere with main transmission. This value of SIR (Signal to Interference Ratio) can be expressed as:

$$SIR = \frac{2(1-N_M)}{H_0 N_M H_{min}} [dB].\qquad(7)$$

Where M is the number of ONU units in a ring network, N_M represents the transmission function of the passive splitter of M-th ONU, H_0 stands for the basic transmission function of a network segment between two passive splitters and H_{min} is a minimum transmission function satisfying the condition of minimum receivable optical signal the last ONU unit in the ring topology. The value of N_M in case of all symmetrical splitters is $N_M = 0.5$. H_0 can be expressed as:

$$H_0 = 10^{-\frac{A_0}{10}} \quad [-;dB].\qquad(8)$$

Where A_0 can be calculated using attenuation coefficient α and the summary length l of each segment of proposed ring topology. The general formula for calculating minimum transmission function H_{min} of ring network for M-th ONU unit satisfying the A_{min} value can be expressed as:

$$H_{min} = \frac{1}{2} H_0^{M+1+j} \prod_{i=j}^{M} N_i \cdot (1-N_j) \prod_{k=0}^{j-1} N_k^2 .\qquad(9)$$

Where N_i, N_k stands for the cascaded transmission functions of M passive optical splitters in the ring topology towards the ONU units and fiber segments.

The value of the SIR parameter in the first scenario with symmetric passive splitters is approx. 33.32 dB, which is fully suitable for proper function of proposed PON network.

2) Optimization of Ring Topology Using Asymmetric Tunable Splitters

The next calculation considers the usage of asymmetric tunable passive splitters with a non-uniform splitting ratio, which can be calculated and optimized. Nowadays, tunable optical splitters are still not very common, while they usually require external power source and management and are more expensive than standard passive optical splitters. However, several technologies have been already proposed to produce tunable optical splitters with various types of their internal structure and parameters. Different methods of achieving non-uniform tunable splitting ratio have been utilized in [7], [9]. The splitting ratios of these tunable splitters in proposed ring topology were individually calculated for each passive optical splitter according to the equations (4), (5) and they were rounded in their percentage expression. The initial idea of a successful optimization process is achieving balanced attenuation values for all ring paths between OLT and each ONU. These values should approach, in an ideal state, the

A_{max} value of 30 dB for selected variant GPON class C. Following graph in Fig. 7 presents the results of calculated values of splitting ratios for all passive splitters.
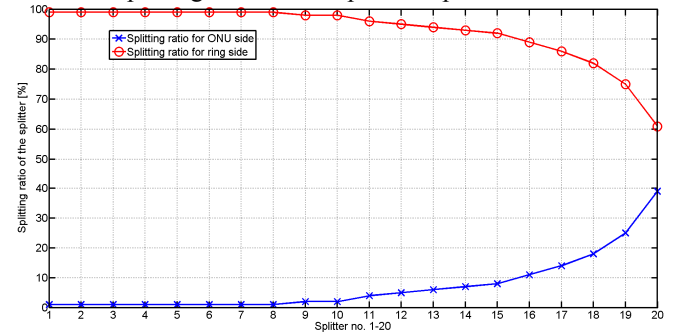

Fig. 7. Calculated splitting ratios of individually optimized splitters.

Through optimization, the balanced values of attenuation are reached in all sections of designed ring topology. Therefore, it is possible to connect 20 passive splitters (20 ONUs) to this optical infrastructure, which is significantly more than in case of symmetric splitters. The values of summary attenuation for each ring branch (paths from OLT to each ONU) as well as the attenuation of all sections of proposed ring topology are presented in next Fig. 8.
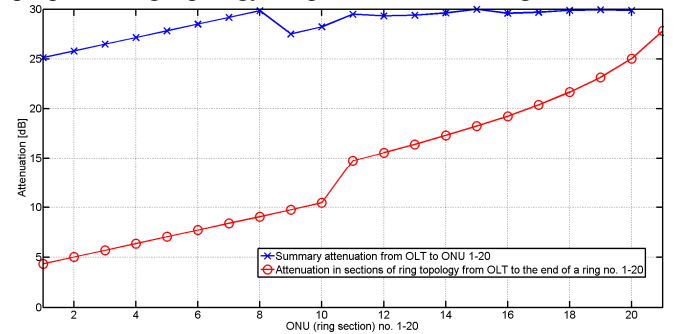

Fig. 8. Summary attenuations for all paths between OLT and ONUs and attenuations for all sections of ring topology.

In case of accurate optimization, all branches (paths) between OLT and ONUs should reach the A_{max} value of selected PON type and attenuation class. Due to the rounding of calculated splitting ratios in their percentage expressions, several branches are not perfectly and accurately optimized, although the attenuations of these branches are close enough to the A_{max} value and they meet the requirements for the minimum value of A_{min} and thus it is not necessary to use additional attenuators. It is obvious that in case of switching both OLT units (switching primary and secondary unit), it will be also necessary to retune splitting ratios of all used splitters, that is why using tunable splitters is proposed. It is also necessary to calculate the attenuation of interfering optical signal in the same way, as it was calculated in the previous simulation of symmetric splitters using formula (7). The value of SIR in this case is:

$$SIR = 31.37\, dB$$

This value is, again, fully suitable to guarantee error-free transmissions in a ring.

IV. PRACTICAL APPLICABILITY OF RESULTS

It is evident that a ring topology in case of PON would probably suffer several disadvantages, so it would not be very useful for standard PON applications, such as providing network connection for ordinary households and typical end-users, but its application for well protected specific

situations in local area networks could enhance the overall security of the whole infrastructure. Previously presented calculations of physical parameters (attenuation) in case of PON with ring topology illustrated that proposed infrastructure could be possibly used for a real application. It is evident that the proposed ring topology is applicable and could be realized even with the use of standard symmetric splitters (50:50%) for some specific situations. In the first presented scenario, only a limited number of 6 ONU units could be possibly connected into this ring topology to meet the maximum attenuation given for the specific PON type (GPON class C in this case). However, even such solution could be practically realized and applied for some specific scenario of well protected local PON network, when higher network reliability and protection against OLT unit failure is required.

To increase the number of connected ONU units, tunable asymmetric splitters are necessary to use, as it is presented in the previous section with calculation of optimized splitting ratios of tunable splitters. The previous example illustrated that this scenario could result into connecting of 20 ONU units, which is significantly higher than in previous case with symmetric splitters. The tunable splitters are not usually common components today, however, several theoretical proposals have been already presented [7], [9], [10], so these splitters will be probably available soon. It would be also possible to use asymmetric splitters with fixed splitting ratio (non tunable), however, in case of OLT units switching, the attenuation of optical signal in case of some ONU units would not meet the demands given in a specific recommendation.

Future research in this area should be focused on practical realization and testing of proposed ring topologies to verify its parameters and functions. Another function that needs to be verified is the switching mechanism of OLT units. These units are usually connected via Ethernet (metallic, optical) to the backbone telecommunication networks, therefore there are two possible scenarios:

- Switching is an internal function of OLT units,
- Switching would be performed by a network node (element) of a higher layer network.

While the first option requires a proprietary internal protocol (or rules) implemented in the OLT units, the second scenario could be used on standard OLT units without any enhancements. The time necessary for switching the OLT units could be shorter in the first scenario, because it could be triggered by OLT units themselves in case of low level of optical signal detection (OLT 2 units passively monitors the traffic and in case of low or no signal detection, it could switch to the main role). The second scenario would be possibly based on using a network element in upper layer network, which again in case of no incoming traffic from OLT 1 unit would activate the backup OLT 2 unit. Again, a proprietary protocol would be necessary or it would be also possible to use standard spanning-tree protocol, which is often applied in Ethernet networks to prevent loops occurring and which can be also configured for dynamic reconfiguration of network. That is why in case of some OLT unit failure the upper node could quickly switch the traffic via the backup one. All these situations are needed to be verified and properly tested. however, the necessary equipment was not available at the present time. Therefore these tasks are to be focused on and to be evaluated through further research.

V. CONCLUSION

This article proposes an innovative method for protection of PON networks, especially its central optical unit − OLT. This method is focused on forming of PON with ring topology using passive optical splitters and neither special enhancements nor optical switches are necessary. The main idea is based on the possibility of placing both OLT units (primary and secondary) on the opposite sides of the ring. This could increase the resistance of whole PON infrastructure against failures of a single central OLT unit, because secondary OLT operates in a warm-state backup and could restore the traffic. By using this method, more complex double-rings or multiple-rings topologies can be created and they can offer several specific benefits for network protection or management.Standard symmetric passive splitters with uniform splitting ratio offer only limited possibilities for PON with ring topology, therefore due to the optimization process and using asymmetric passive splitters, the number of connected ONUs in a ring topology could be significantly increased. However, in case of switching primary and secondary OLT units, the splitting ratios of all used splitters have to be optimized and tuned again to meet the requirements for a new situation.

REFERENCES

[1] ITU-T, "G.987.1 - 10-Gigabit-capable passive optical network (XG-PON) systems: Definitions, Abbreviations, and Acronyms," *ITU-T*, January 2010. Available http://www.itu.int/rec/T-REC-G.987-201001-I.

[2] IEEE, "IEEE Standard 802.3av-2009, Amendment 1: Physical Layer Specifications and Management Parameters for 10 Gb/s Passive Optical Networks," *IEEE 802.3av 10G-EPON Task Force*. [online], September 2009. Available http://www.ieee802.org/3/av/.

[3] C. F. Lam, *Passive Optical Networks: Principles and Practice*. Academic Press of Elsevier Inc., Burlington, USA. 2007.

[4] P. Lafata, J. Vodrážka, "Application of Passive Optical Network with Optimized Bus Topology for Local Backbone Data Network," *Microwave and Optical Technology Letters*. 2011, vol. 53, no. 10, p. 2351-2355.

[5] S. Dong-Min, J. Eui-Suk, K. Byoung-Whi, "A simple passive protection structure in a ring-type hybrid WDM/TDM-PON," *11th International Conference on Advanced Communication Technology. ICACT 2009*, February 2009, p. 447-449.

[6] C. M. Machuca, J. Chen, L. Wosinka, "PON protection architectures achieving total cost reduction," *Conference and Exhibition (ACP) of Communications and Photonics, 2010 Asia*, December 2010, p. 707-708.

[7] S. Xia, Q. J. Zeng, J. Wang, H. Zhao, H. Chi, Y. Wang, F. Liu, F., X. Zhu, "Tunable optical splitter technology," *SPIE Proceedings*, Vol. 4870-70, SPIE, July, 2002.

[8] P. Lafata, J. Vodrážka, "Návrh pasivních optických sítí s optimálními rozbočovacími poměry," *Elektrorevue*. 2010, vol. 13, no. 67, p. 67-1-67-8. Available: http://elektrorevue.cz/cz/clanky/komunikacni-technologie/0/navrh-pasivnich-optickych-siti-s-optimalnimi-rozbocovacimi-pomery/.

[9] Z. Yun, L. Wen, Ch. Long, X. Qingming, "A 1x2 Variable Optical Power Splitter Development," *Journal of Lightwave Technology*, vol. 24, no. 3, March 2006.

[10] X. Tang, J. Liao, H. Li, L. Zhang, R. Lu, Y. Liu, "Design and analysis of a novel tunable optical power splitter," *Chinese Optics Letters*, vol. 9, no. 1, January 2011.

Nasal Cavity Detection in Facial Thermal Images for Non-contact Measurement of Breathing

Dai Hanawa, Toshiki Morimoto, Shota Shimazaki and Kimio Oguchi

Abstract— **In this paper, we propose a method of improving the accuracy of detecting nasal cavity location in far infrared images for non-contact measurement of human breathing. We found that although our previous method for far infrared imaging can detect regions that include nasal cavities well, it suffers from high false alarm rates. In order to reduce this rate, we extend our method with a false alarm classification function. Object detection based on a boosted cascade of Haar-like feature classifiers is applied to find the candidates of regions that include the nasal cavities. In false alarm classification, binarization is employed to strictly segment facial area and background. Based on the results of binarization, false alarms on the background can be accurately classified. 5,100 FIR images are collected to train our nasal cavity detector; we evaluate the number of false alarms and detection failures. The results show that the proposed method can reduce false alarm events.**

Keywords— **Non-contact measurement of breathing, Facial thermal image, Nasal cavity detection, Binarization.**

I. INTRODUCTION

In recent years, considerable research has been focused on the techniques for the extraction of vital signals from the human body, including heart rate, blood pressure, body temperature and breathing. By applying these techniques, information and communication services can be created to better support human activities (especially daily life for infants and the elderly). These applications include human activity monitoring, medical treatment, daily care, emotion analysis, and human computer interaction. In order to realize such applications, a technique for monitoring human breathing is one of the important goals, because human breathing is closely related to health, activity, emotion, and so on. However, most of the current major methods for monitoring human breathing take the contact approach. Therefore, development of non-invasive, non-contact type

D. Hanawa is with the Dept. of Compt. Inf. Sci., Faculty of Sci. and Tech., Seikei University, 3-3-1, Kichijojikitamachi, Musashino, Tokyo, 180-8633, Japan (corresponding author to provide phone: +81-422-37-3732; fax: +42-37-3871; e-mail: hanawa@st.seikei.ac.jp).

T. Morimoto was with the Dept. of Compt. Inf. Sci., Faculty of Sci. and Tech., Seikei University, 3-3-1, Kichijojikitamachi, Musashino, Tokyo, 180-8633, Japan. He is now with Allied Telesis K.K., Japan.

S. Shimazaki and K. Oguchi are with the Grad. School of Sci. and Tech., Seikei University, 3-3-1, Kichijojikitamachi, Musashino, Tokyo, 180-8633, Japan. (e-mail: {dm116221@cc, oguchi@st}.seikei.ac.jp).

method is needed.

In this paper, we study nasal cavity detection in facial thermal images to capture non-contact human breathing. Far Infra-Red (FIR) imaging is receiving attention as an attractive way of realizing this function. We have been studying a machine learning algorithm to detect the nose in thermal images of the user's face [1]. We found that while our previous method can detect regions that include nasal cavities well, the false alarm rate is not insignificant. Based on the results of our previous studies, we develop a false alarm classification technique for integration with our previous method that can reduce false alarms on non-facial regions. We also evaluate the frequency of missed-nose and of false alarms by conducting simulation experiments using 5,100 far infrared (FIR) images.

The rest of this paper is organized as follows. In Section II, we briefly review previous related work. Section III presents details of our proposed method. Section IV describes the results of our experiments. Section V concludes this paper.

II. RELATED WORKS

Several studies on the monitoring of human breathing have been reported [2]-[5]. Most of them do not use the non-contact approach, so that user stress created by the placement of or the detachment of sensor devices by body motion, are unavoidable.

An automatic respiration monitoring system by using rgb imaging was proposed by Nakai et al. [6]. However, this system can monitor only users sleeping on a sensor-equipped bed. The works of K. Abbas et al. [7] and Fei et al. [8], showed that FIR imaging had promise for the monitoring of human breathing. We have also shown that human breathing can be automatically captured by FIR imaging [9]-[11]. However, in these works, including our own, the relative position between the user's face and the FIR camera must be kept stable. Therefore, the detection of breathing becomes difficult when the position of the user's face is unknown.

Studies for tracking the human nose in thermal images based on particle filters [12] or image processing [13] have been reported. These offer some fixed robustness against head motion. However, in these methods, both naked eyes of the user must be constantly captured by the FIR camera. Moreover, these methods assume that the entire face is captured by the FIR image. How to recognize whether a face exists in an FIR image or not, was not discussed. B. Kaur et al. have proposed a method for tracking region including nasal cavities on thermal image [14]. However, in this method, manual operation to determine the initial position of nose is

needed.

In our study, we try to find whether nasal cavities exist on FIR image automatically, and to extract the region including nasal cavities from FIR images under the simple condition that nasal cavities are captured by FIR camera.

III. PROPOSED METHOD

We propose a method to detect the nose in FIR images by applying a current facial image processing scheme and false alarm classification. A block diagram of proposed method is shown in Fig.1.

A rapid object detection method based on a boosted cascade of rectangular feature (called Haar-like feature) classifiers proposed by Viola and Jones [15] and improved by Lienhart and Maydt [16] is applied in our work. Face-detectors using their method have become popular because of their speed and robustness. In this research, we replace the gray-scale training images with FIR images for nose detection and replace gray-scale input image with an FIR image for detection [1]. GentleBoost is used here to learn classifiers in our method. We introduce the above method to detect the region including nasal cavities. By applying this method, we get n, $x_d(t)_k$, $y_d(t)_k$, $w_d(t)_k$, and $h_d(t)_k$ ($k=1,2,...,n$) from a trained nose-detector and input FIR image $f(x, y, t)$ captured at time t. Here, n, $x_d(t)_k$, $y_d(t)_k$, $w_d(t)_k$, and $h_d(t)_k$ denote the number of detected region, horizontal position of the left-upper corner of the detected rectangle region, its vertical position, width of the rectangle and its height, respectively. However, we confirmed that its detection results included regions other than the correct nasal region [1]. The frequency of erroneous nose detection was not negligible.

In order to reduce such errors, we introduce false alarm classification. This classification consists of a binarization process and a classification process with a threshold. We introduce these processes to isolate the human face in the FIR image. In most cases, the human face is hotter than the other areas. Therefore, we can isolate the face by using the suitable threshold described as follows:

$$g(x,y,t) = \begin{cases} 1 \ (f(x,y,t) \geq th_t) \\ 0 \ (f(x,y,t) < th_t) \end{cases} \quad (1)$$

Where, $g(x, y, t)$ and th_t are the binarized FIR image at time t and the threshold for segmentation, respectively. From $g(x, y, t)$, we calculate the sum of pixels in each detected region by (2).

$$L(p,q,r,s,g(x,y,t)) = \sum_{i=p}^{p+r-1} \sum_{j=q}^{q+s-1} g(i,j,t) \quad (2)$$

Here, (p, q) is the left-upper corner position of the rectangle on $g(x, y, t)$. r and s are its width and its height, respectively. Next, the containing ratio of the facial area in the above rectangle is calculated by (3).

$$R(p,q,r,s,f(x,y,t))$$
$$= L(p,q,r,s,g(x,y,t))/ (r \cdot s) \quad (3)$$

Finally, the detected region is classified as false alarm if $R(x_d(t)_k, y_d(t)_k, w_d(t)_k, h_d(t)_k, f(x, y, t))$ is lower than threshold th_r. Otherwise it is classified as nasal region. All detected regions $(x_d(t)_k, y_d(t)_k, w_d(t)_k, h_d(t)_k)$ in each input FIR image $f(x, y, t)$ are classified based on the above algorithm.
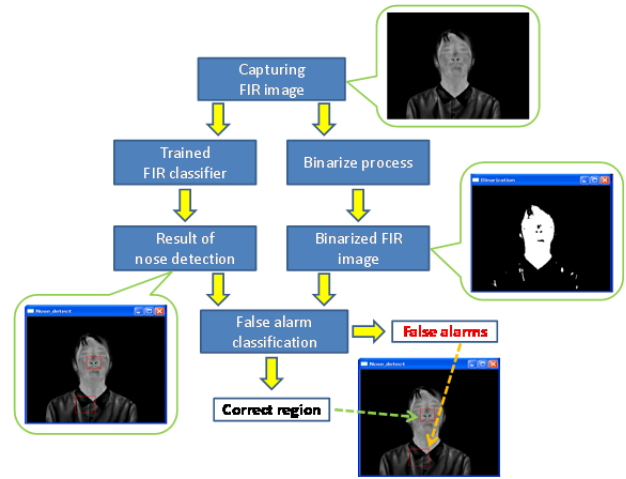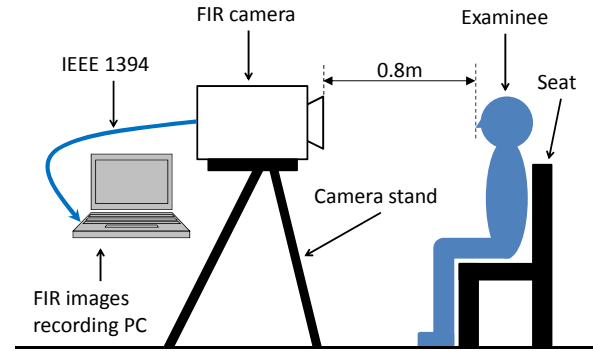

Fig.1. Block diagram of proposed method.

Fig.2. Relationship between FIR camera and subject.

IV. EXPERIMENTS

Experiments were conducted to evaluate the frequency of nasal cavity detection failure and false alarm. Moreover, the relationship between false alarm and threshold th_r was experimentally examined.

A. Recording FIR Image

Facial thermal images were captured by an FIR camera with the following specifications.

- Type: NEC/Avio, TH7102MX
- Capture wavelength: 8-14 μm
- Thermal resolution: 0.06 ˚C
- Size of sensor (active area): 320x240 pixels
- Contrast: 256 levels (8bit), Gray scale
- Frame rate: 30 fps
- Temperature range: 32.0-40.0 ˚C

Room temperature was around 26 ˚C and remained constant throughout all trials. The subject sat in front of the camera in a room (Fig. 2). Each subject was asked to breathe normally via the nose while being recorded. FIR images from nine subjects (nine males with ages from 22 to 23 years) were acquired. FIR images were recorded for one minute for each subject. 300 continuous frames (ten seconds) wherein the subject breathed stably were selected. Finally, nasal region in each frame was manually extracted for training the FIR classifier for each subject. Minimum and maximum size of

nasal region extracted from the FIR images of each subject were 23x13 pixels and 31x23, respectively. FIR images totaling 2,700 patterns were acquired as positive samples. Moreover, FIR images totaling 2,400 patterns, which included no human face, were collected as negative samples. Examples of positive data and negative data are shown in Fig. 3 and 4, respectively.

B. Training and Evaluation

The nine-fold cross-validation procedure was employed. Here, a set of 2,400 positive samples (8 subjects) and the remaining 300 samples (1 subject) were used as training and test material, respectively. Negative samples for training were fixed, so that 2,400 samples were used. Experiments were performed for one hundred and one (0, 1, …, 100%) ratios of the facial area. These processes were repeated nine times with each of nine subject's samples used once as the validation data. Threshold th_t for binarization was set at 100. This value (corresponds to about 35 ˚C) was selected from the results of preliminary experiments.

Experimental metrics were *correct-detection* ratio (denoted as R_c), *miss-detection* ratio (denoted as R_m), and false alarm ratio (denoted as R_f). Correct-detection means that one of the detection results indicated the correct nasal region. Miss-detection means that the detection results did not include a correct nasal region. On the other hand, false alarm means that one of the detection results indicated a region other than the correct nasal region. These metrics were calculated as follows.

$$R_c = N_c/N_{all} \tag{4}$$
$$R_m = N_m/N_{all} \tag{5}$$
$$R_f = N_f/N_{all} \tag{6}$$

Here, N_c, N_m, N_f, and N_{all} denote the number of the frames with correct-detection, those with miss-detection, those with false alarm and total number of frames, respectively.

C. Results

At first, results for positive samples were analyzed. Fig. 5 and 6 show the results for training samples and test samples, respectively. Here, average in R_c, that in R_m and that in R_f were calculated for all data sets. In the case that th_r=0, the results show the performance of the previous method.

Fig. 7 shows the change in the number of non-facial region detection for each threshold. Here, the number of the detected rectangle region as false alarm in each frame was totaled and its average per frame was calculated.

Fig. 8 and 9 show an example of detection by the previous method and that by proposed method using the same input image, respectively. Fig. 10 shows an example of the results yielded by the proposed method including correct-detection and false alarm.

Optimal threshold for the proposed method for each subject was examined based on the experimental results. Table I and II show detailed results for training samples and test samples, respectively. Also the optimal threshold for each subject, and corresponding R_f values, are shown in the two rightmost columns. These were selected under the condition that R_c is equal to that in the previous method so that R_f is smaller.

Next, results for negative samples were analyzed. Fig. 11 shows the results for the training samples. Here, the average R_f for all data sets is calculated. When th_r=0, the results show

the performance of the previous method. Fig. 12 shows the change in the number of non-facial regions detected for each threshold. Table III shows the detailed results for training samples. Here, optimal th_r in Table I was used for each data set.

Fig.3. Examples of positive samples.
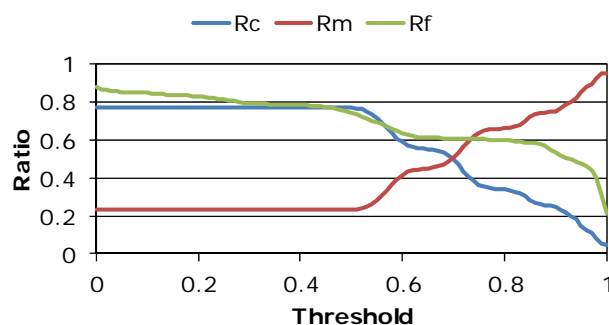

Fig.4. Examples of negative samples.

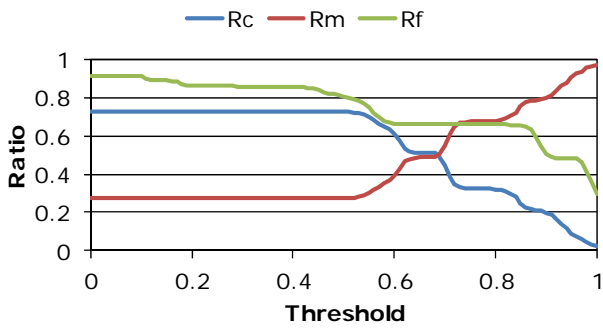Fig.5 Results for training samples (positive samples).

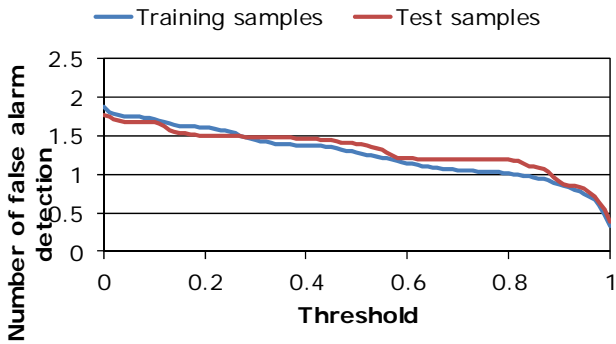Fig.6. Results for test samples (positive samples).

Fig.7. Average number of false alarms (positive samples).

TABLE I
DETAILED RESULTS FOR TRAINING DATA
(POSITIVE SAMPLES, N_{ALL}=2400)

Data set	Previous method			Proposed method	
	R_c [%]	R_m [%]	R_f [%]	R_f [%]	Th_r
Except for A	81.5	18.5	73.3	61.0	0.48
Except for B	68.0	32.0	76.2	62.7	0.50
Except for C	85.7	14.3	89.6	77.3	0.48
Except for D	60.6	39.4	91.6	74.8	0.50
Except for E	84.3	15.7	97.4	87.3	0.48
Except for F	80.9	19.1	86.1	59.4	0.53
Except for G	83.9	16.1	87.8	74.1	0.48
Except for H	65.8	34.2	98.2	94.3	0.51
Except for I	83.0	17.0	90.3	78.6	0.48
Average	77.1	22.9	87.8	77.7	-

TABLE II
DETAILED RESULTS FOR TEST DATA
(POSITIVE SAMPLES, N_{ALL}=300)

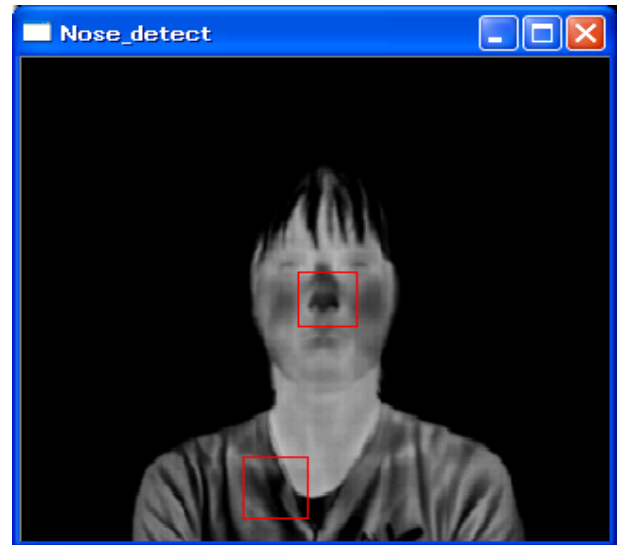| Data set	Previous method			Proposed method	
	R_c [%]	R_m [%]	R_f [%]	R_f [%]	Th_r
A	6.7	93.3	93.0	85.0	1
B	100.0	0.0	50.7	7.3	0.58
C	54.7	45.3	100.0	45.3	0.94
D	100.0	0.0	100.0	100.0	0.84
E	100.0	0.0	99.7	99.3	0.90
F	90.7	9.3	94.7	94.7	0.49
G	69.7	30.3	89.3	0.0	0.67
H	30.7	69.3	100.0	100.0	0.80
I	100.0	0.0	96.7	91.3	0.78
Average	72.5	27.5	91.6	69.2	-

Fig. 8. An example of detection by the previous method. Red rectangles at the center and at the bottom are correct-detection and false alarm, respectively.

Fig. 9. An example of detection by proposed method. Red rectangle is correct-detection. False alarm in Fig. 8 was eliminated.
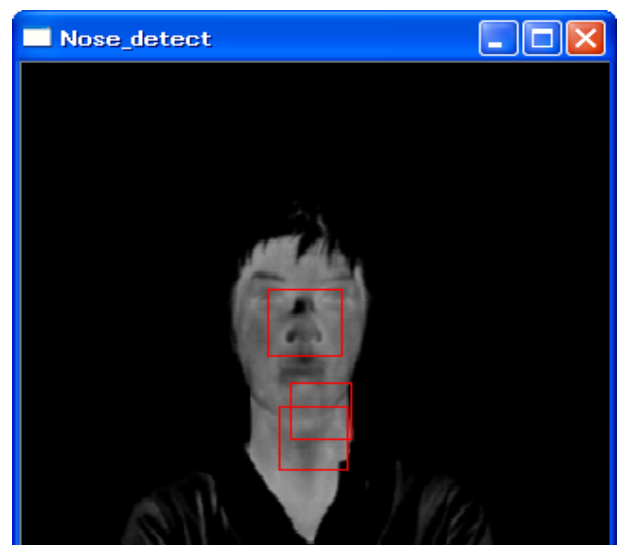

Fig. 10. An example of false alarm by proposed method. Red rectangles other than the one at the center are false alarms.
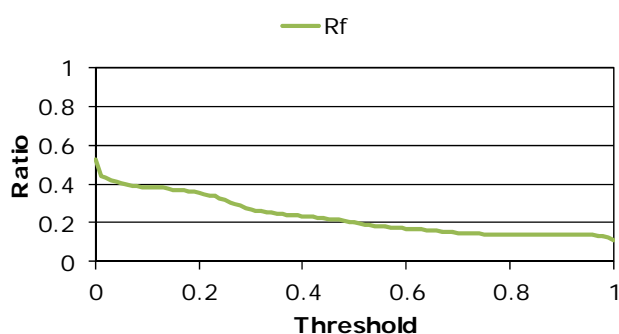
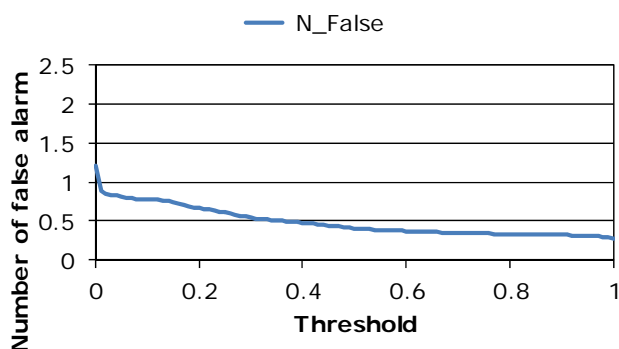Fig.11. Results for training samples (negative samples).

Fig.12. Average number of false alarms (negative samples).

TABLE III
COMPARISON OF FALSE ALARM FOR TRAINING DATA
(NEGATIVE SAMPLES, $N_{ALL}=2400$)

Data set	Previous method [%]	Proposed method [%]
Except for A	47.5	24.5
Except for B	35.7	15.0
Except for C	32.1	6.2
Except for D	53.7	23.8
Except for E	69.2	29.8
Except for F	68.0	2.5
Except for G	52.5	26.9
Except for H	56.5	25.4
Except for I	58.1	30.1
Average	52.6	20.5

D. Discussion

According to Fig. 5 and 6, the average false alarm ratio of the proposed method improved 10% around th_r=0.5 for positive data compared to the previous method, while the proposed method basically matches the correct-detection ratio of the previous method. This optimal threshold was mostly fixed for all data sets (Table I). Analysis of the detection result shows false-alarm occurring in non-facial regions were eliminated by the proposed method. These results show that proposed method can reduce the detection of non-nasal regions by using a suitable threshold. In Fig. 8, the previous method yielded one false alarm due to wrinkles on clothing. On the other hand, the proposed method was able to classify it as a false-alarm (Fig. 9). In Fig. 11 and Table III, the proposed method improved the false alarm ratio by 32% around th_r=0.5 for negative data compared to the previous method. False alarm events in negative data were classified more accurately. We confirmed that false alarms generated in areas other than the face were eliminated by the proposed method with optimal threshold.

In Fig. 7 and 12, the average number of false alarms detected around th_r=0.5 for positive samples and that for

negative samples improved by about 0.5 and 0.8, respectively. It is useful to classify all detection results as either correct-detection or false alarm. However, the proposed method can not overcome false alarms that occur in the facial area such as throat or jaw (Fig. 10). The area including these parts was classified as facial area based on their temperature, because the surface skin was uncovered. We believe that this type of false alarm can be eliminated by observation of the variation in temperature over several frames, since the nasal cavities exhibit cyclic changes in temperature. Moreover, another object detection method could be examined. For example, an object detection method based on support vector machines seems to be useful. Studies on improving the accuracy of nasal region detection are future works.

From Table II, optimal thresholds for test data varied only slightly among the subjects. Average false alarm ratio was improved by 22% by using the optimal threshold for each subject. On the other hand, optimal thresholds for training data were about 0.5 regardless of the subject. The proposed method seems to provide a fixed performance for known users. How to estimate the optimal threshold for an unknown user should be examined in order to reduce the number of false alarms. This challenge is another future work.

All in all, the above results confirm the validity of our proposed method for reducing the false alarm rate in detecting the nose.

V. CONCLUSION

We proposed to apply false alarm classification into our previous method to detect the nasal region accurately in thermal images of the user's face. The intent is to reduce the false alarm rate of our previous method. First, a method to classify false alarms was proposed; it accurately detects the region that includes the nasal region from thermal facial images. Next, the performance of our proposed method was evaluated by experiments. Our results suggested that the proposed method suffers far fewer false alarm events than our previous method even though it uses simple image processing operations. Moreover, the proposed method minimizes miss-detection if a suitable threshold is used.

However, several technical issues hinder the achievement of breathing detection with few constraints on the user. For example, our method can not eliminate false alarm events that occur in the facial area. A method that can handle arbitrary poses also should be studied. The results described in this paper clarified several technical issues when we apply the object detection method by Viola and Jones to FIR images.

In future work, we will study how to classify the nasal region more accurately from detection results. For example, we plan to study how to choose better training samples. Moreover, we plan to combine the proposed method with observation of the variation in temperature over several frames, or consider the use of another object detection method.

REFERENCES

[1] D. Hanawa, T. Morimoto, S. Terada, T. Sakai, S. Shimazaki, K. Igarashi and K. Oguchi, "Nose detection on far infrared image for non-contact measurement of breathing," in *Proc. IEEE-EMBS BHI 2012 [USB-Memory]*, Hong Kong and Shenzhen, China, Jan. 2012, pp.878-881.

[2] Y. Nishida, T. Hori, "Non-invasive and unrestrained monitoring of human respiratory system by sensorized environment," *Proc. IEEE Sensor 2002*, Orland, FL, June 2002, pp. 62.4(1)-(6).

[3] Y. Nishida, T. Mori, H. Mizoguchi and T. Sato, "Sleep apnea syndrome diagnosis based on image processing," *J. RSJ*, vol.16, no.2, Mar. 1998, pp. 274-281 (in Japanese).

[4] Y. Nishida, M. Takeda, T. Mori, H. Mizoguchi and T. Sato, "Unrestrained and non-invasive monitoring of human's respiration and posture in sleep using pressure sensors," *J. RSJ*, vol.16, no.5, July 1998, pp. 705-711 (in Japanese).

[5] K. Higashikatsuragi, Y. Nakahata, I. Matsunami and A. Kajiwara, "Non-invasive respiration monitoring sensor using UWB-IR", in *Proc. IEEE ICUWB 2008*, Hannover, German, Sept. 2008, pp.101-104.

[6] N. Nakai, M. Watanabe, Y. Miyake, K. Takeda, K. Yamashita, H. Shinmori and K. Ishihara, "Automatic respiration monitoring system by time-varying image analysis," *IEICE Trans. Inf. & Syst.*, vol.J83-D-II, no.1, Jan. 2000, pp.280-288 (in Japanese).

[7] K. Abbas, K. Heiman, T. Orlikowsky, S. Leonhardt. "Non-contact respiratory monitoring based on real-time IR-thermography, " in *IFMBE Proc. of WC2009*, 25/IV, 2009, pp.1306-1309.

[8] J. Fei and I. Pavlidis, "Analysis of breathing air flow patterns in thermal imaging," in *Proc. IEEE EMBC 2006*, New York City, NY, Aug. 2006, pp.946-952.

[9] D. Hanawa, Y. Yaginuma, Y. Enomoto, T. Koide, S. Terada and K. Oguchi, "Automation of non-intrusive nasal breathing detection by using far-infrared imaging," in *Proc. u-Healthcare 2010*,Nov. 2010.

[10] D. Hanawa, T. Koide and K. Oguchi, "A proposal of nasal breathing detection method by using far infrared imaging in a home health care system," *IEICE Trans. Inf. & Syst.*, vol.J94-D, no.1, Jan. 2011, pp.260-263, (in Japanese).

[11] T. Koide, S. Yamakawa, D. Hanawa and K. Oguchi, "Breathing detection by far infrared (FIR) imaging in a home health care system," in *Proc. IEEE ISBB 2009 [USB-Memory]*, Melbourne, Australia, Sept. 2009, pp. 206–209.

[12] Z. Zhu, J. Fei and I. Pavlidis, "Tracking human breath in infrared imaging," in *Proc. IEEE BIBE 2005*, Minnesota, USA, Oct. 2005, pp.227-231.

[13] F.Q. AL-Khalidi, R. Saatchi, D. Burke and H. Elphick, "Tracking human face features in thermal images for respiration monitoring," in *Proc. IEEE/ACS AICCSA 2010*, Hammamet, Tunisia, May 2010.

[14] B. Kaur, J. K. Nelson, T. Williams and B. O'Kane, "Adaptive region of interest (ROI) detection and tracking for respiration measurement in thermal video," *in Proc. SPIE*, Vol.8401, May 2012, pp.840117-1-84117-9

[15] P. Viola and M. Jones, "Robust real-time face detection," *Int. J. Compt. Vision*, vol.57, no.2, May 2004, pp.137-154.

[16] R. Lienhart and J. Maydt, "An extended set of Haar-like features for rapid object detection," in *Proc. ICIP 2002*, Rochester, New York City, NY, Sept. 2002, pp.900-903.

Dai Hanawa received the B.E., M.E., and Dr. Eng. degrees from Ibaraki University in 1999, 2001, and 2005, respectively.

From 2005 to 2007, he was a Research Associate of the Department of Computer and Information Sciences at the Tokyo University of Agriculture and Technology. Since 2007, he has been a Research Associate, and from 2008 he has been an Assistant Professor of the Department of Computer and Information Science at Seikei University. His research interests are in the area of human communications, especially the networked virtual environment, sensor network, vital information sensing and their applications.

Dr. Hanawa is a member of IEEE Computer, IEEE Communications, ACM, IEICE, the Virtual Reality Society of Japan and Human Interface Society. He received the first IEICE HCG Prize and IEICE MVE Prize 2009.

Toshiki Morimoto received the B.E. degree from Seikei University in 2012. From 2012, he has been with Allied Telesis K.K., Japan. His research interests include vital information sensing and its application.

Mr. Morimoto is a member of IEICE.

Shota Shimazaki received the B.E. degree from Seikei University in 2011. From 2011, he has been a Master Student of Graduate School of Science and Technology, Seikei University. His research interests include fiber-optic broadband networks.

Mr. Shimazaki is a student member of IEICE.

Kimio Oguchi received the B.E. and M.E. degrees in applied physics, and Dr. Eng. degree in electrical engineering in 1978, 1980 and 1995, respectively, from Nagoya University, Nagoya, Japan.

He joined the Yokosuka Electrical Communication Laboratory, NTT, Japan in 1980. From April, 1980 to March, 2004, he was engaged in the research and development of optical systems, in particular, fiber-optic local area networks, advanced fiber-optic digital systems, ATM-link systems, photonic transport networks, applications of advanced photonic devices, and large contents distribution systems. He was involved in the standardization activities in both ITU-T SG's 13 and 15. He now is a Professor of the Information Networking Laboratory, Graduate School and Science and Technology and Faculty of Science and Technology, Seikei University, Tokyo, Japan. His research interests include information networking issues, applications utilizing e.g. sensor networks and optical networks, and vital functions, and contents distribution networks.

Dr. Oguchi is a senior member of the IEICE, a member of IEEE Communications, IEEE Photonics, IEEE Computer, IEEE EMB Societies, OSA, ICST, Society for Running, Japanese Society for Emergency Medicine, Clinical Gait Analysis Forum of Japan, Digital Cinema Consortium of Japan, and CineGrid. He is recipient of the OECC'97 Best Paper Award, the NOC'97 Best Paper Award, the OECC'98 Best Paper Award, the Best Presentation Award at the 2001 and 2005 Annual Conference of Society for Running, 2008 ICT Accomplishment Award of the ITU Association of Japan and IEICE MVE Prize 2009.

Optimizing dictionary learning parameters for solving Audio Inpainting problem

Vaclav Mach and Roman Ozdobinski

Abstract—**Recovering missing or distorted audio signal samples has been recently improved by solving an Audio Inpainting problem. This paper aims to connect this problem with K-SVD dictionary learning to improve reconstruction error for missing signal insertion problem. Our aim is to adapt an initial dictionary to the reliable signal to be more accurate in missing samples estimation. This approach is based on sparse signals reconstruction and optimization problem. In the paper two staple algorithms, connection between them and emerging problems are described. We tried to find optimal parameters for efficient dictionary learning.**

Keywords—**Audio Inpainting, Dictionary Learning, K-SVD, Orthogonal Matching Pursuit, Signal reconstruction, Sparse Representations**

I. INTRODUCTION

Since the time audio recording and transmittion have been discovered, there is always a possibility of creation an error in the signal. In times of analogue sound carriers they were sensitive to scratching a gramophone record or tearing a magnetic tape. Digital audio carriers are more resistent to these damages mainly because of Error Correction Codes but still transmitting audio signal through e.g. IP telephony can be affected by packet loss.

Many problems connected with analogue audio recordings restoration and their digitized copies have been solved in the past by various techniques. For example distorted or missing signal recover was repaired by interpolation techniques [1], samples repetition, wavelet transform [2] or neural networks [3]. IP telephony is a common example of packet loss problem where data is lost during the transmission and they have to be recovered, e.g. by [4].

The recent research in the field of sparse signals representations has brought new approach that can be utilized for this audio restoration. Methods of solving a problem called Audio Inpainting were first mentioned in [5] as an algorithm for recovering missing samples in audio signal. This framework provides segmentwise restoration of audio signals where the position of missing samples is a-priori known. Sparse representation modeling uses Orthogonal Matching Pursuit method for solving an inverse problem. As an initial dictionary for sparse signals modeling, Gabor or DCT dictionaries are used.

More sparsity and the resulting better approximation of a missing signal can be achieved by choosing suited transform

V. Mach is with the Department of Telecommunications, Brno University of Technology, Brno, Czech Republic, Purkynova 118, 612 00 Brno, e-mail: (vaclav.mach@phd.feec.vutbr.cz).

R. Ozdobinski is with the Department of Telecommunications, Brno University of Technology, Brno, Czech Republic, Purkynova 118, 612 00 Brno, e-mail: (xozdob00@stud.feec.vutbr.cz).

function to construct the dictionary or adapting initial dictionary to the given signal. We decided to go the second way and tried to adapt an initial dictionary with the K-SVD algorithm [6]. This method is a generalization of K-means clustering process and helps the dictionary to better fit observed audio data.

In section II sparse signals modeling together with Audio Inpaing as one of sparse signals modeling application are described. The dictionary learning via K-SVD algorithm is described in section III. Section IV shows our experimental results. Software components are described in section V and optimal parameters for dictionary learning which we found out are summed up in conclusion (section VI).

II. AUDIO INPAINTING BY SPARSITY CONSTRAINTS

Sparse signal representations for inpainting problems were first used in image signal processing [7] and a few years later the Audio Inpainting algorithm was introduced in [5].

For some given signal $\boldsymbol{y} \in \mathbb{R}^N$ it is known, which samples of it are reliable and which ones are distorted or missing. Therefore, we can divide the support of the vector into the two sets $\mathcal{I}^r$ and $\mathcal{I}^m$ containing the coordinates of the reliable and missing samples, respectively. As a consequence of the partitioning we find $\mathcal{I}^r \cup \mathcal{I}^m = \{1, \ldots, N\}$ and $\mathcal{I}^r \cap \mathcal{I}^m = \emptyset$. By deleting the rows with indices in $\mathcal{I}^m$ from the $N \times N$ identity matrix we obtain the matrix $\mathbf{M}^r \in \mathbb{R}^{|\mathcal{I}^r| \times N}$ selecting the reliable samples from the signal

$$\boldsymbol{y}^r = \mathbf{M}^r \boldsymbol{y}. \tag{1}$$

Using methods based on sparsity we have to find an appropriate function system to represent this class of signals by a few prototype functions only. The design of such a collection of atoms into which we can efficiently expand our signal, will be the central concern of this contribution. Given a set of atoms $\{\boldsymbol{d}_j\}_{j=1}^M$ one can build the dictionary matrix $D \in \mathbb{R}^{N \times M}$, where the columns of the matrix are the atoms. For a given coefficient vector $\boldsymbol{c}$ we can then compute the corresponding signal as a linear combination of the dictionary atoms by the matrix multiplication

$$\boldsymbol{y} = \mathbf{D}\boldsymbol{c}. \tag{2}$$

From now on, we will assume that $\mathbf{D}$ has a full rank and that $M \geq N$ with the consequence that for a given signal $\boldsymbol{y}$ we can always find a set of coefficients such that (2) is satisfied. Such an expansion can always be computed by the pseudo-inverse of $\mathbf{D}$ denoted by $\mathbf{D}^+$, i.e. $\boldsymbol{c} = \mathbf{D}^+\boldsymbol{y}$ satisfy (2).

An expansion $\boldsymbol{c}$ is called sparse, if only few entries of the vector are different from zero. We will denote the length of the support of the coefficient vector by $\|\boldsymbol{c}\|_0$. An expansion $\boldsymbol{c}$,

which has only few entries significantly different from zero, is called compressible. It is quite clear that for a given dictionary only a certain class of signals will admit sparse expansions. In the later sections we will be concerned with audio signals and for this specific class a number of different dictionaries has been proposed, among them Gabor and DCT systems [5].

As we need these dictionaries later for performance comparison, we will define them now. For $0 \leq j < N$, we define the corresponding atom in the points $0 \leq m < N$

$$d_j[m] = \cos\left[\frac{\pi}{N}\left(n + \frac{1}{2}\right)\left(j + \frac{1}{2}\right)\right]. \qquad (3)$$

The resulting transform is purely real and will admit a certain level of sparsity for audio signals due to its harmonic structure. Gabor dictionaries can be constructed as DCT atoms with additional phase information. Due to the additional parameter, there is possibly a better fit to the signal, making the coefficients sparser. For some $0 \leq j < N$, $0 \leq n < N$ and $\varphi \in (0, 2\pi)$ we define

$$g_j[m] = \cos\left[\frac{\pi}{N}\left(n + \frac{1}{2}\right)\left(j + \frac{1}{2}\right) + \varphi\right]. \qquad (4)$$

Now we want to turn to the problem of audio inpainting, i.e. we want to reconstruct the missing samples in an audio signal. The problem we have to solve is: given the reliable samples $\boldsymbol{y}^r = \mathbf{M}^r \boldsymbol{y}$ reconstruct the full signal $\boldsymbol{y}$ under the assumption that $\boldsymbol{y}$ can be represented by a sparse set of coefficients. Incorporating this information, we formulate the following optimization problem

$$\hat{\boldsymbol{c}} = \arg\min_{\boldsymbol{c}} \|\boldsymbol{y}^r - \mathbf{M}^r \mathbf{D}\boldsymbol{c}\|_2 \text{ s.t. } \|\boldsymbol{c}\|_0 \leq k_0. \qquad (5)$$

Solving this NP-hard non-convex optimization problem is not feasible, therefore we will use orthogonal matching pursuit (OMP), a greedy algorithm, instead [8]. In the following we will describe the steps in detail in Algorithm 1 as it is not only used for the audio inpainting but also plays a major role in the K-SVD algorithm presented in Section III. This algorithm always yields a coefficient vector with $\|\boldsymbol{c}\| \leq s$ for some user determined sparsity parameter s.

Due to the length of the signals under investigation, one usually processes the data segment-wise. Therefore, the steps explained above have to be executed for every time slice and then one re-synthesizes from these individually obtained small portions. While for some pre-specified dictionaries (such as Gabor and DCT) there exist fast transforms, it would not be feasible to perform the steps described above for the dictionaries that we will construct in Section III.

III. DICTIONARY LEARNING

A. Overview

Static prespecified dictionaries like the introduced DCT or Gabor dictionaries are efficient because the transform process can be realized in a fast way. They are usually tailored to a specific group of signals. In the following we will discuss how to flexibly construct a dictionary adapted to the signal allowing for sparser representations.

Algorithm 1 Orthogonal matching pursuit

  Input: $\boldsymbol{y}$... signal segment,
        $\mathbf{D}$... dictionary,
        s... level of sparsity,
        ϵ... approximation error
  Initialization: $i = 0$,
        $\boldsymbol{c}$ = zero vector of length M
        $\Omega_0 = \emptyset$... support set
  Individual Steps:
1: Compute pseudo-inverse of dictionary $\mathbf{D}^+$
2: $R = \boldsymbol{y}$
3: **while** $\|R\|_2^2 > \epsilon$ and $i \leq s$ **do**
4:     $i = i + 1$
5:     Choose index j with maximal absolute value in $\mathbf{D}^+ R$
6:     Update support $\Omega_i = \Omega_{i-1} \cup j$
7:     Add the j-th entry of $\mathbf{D}^+_{\Omega_i} y$ to the j-th entry of $\boldsymbol{c}_k$
8:     $R = \boldsymbol{y} - \mathbf{D}_{\Omega_i}\boldsymbol{c}_k$
9: **end while**
  Output: $\boldsymbol{c}$... sparse coefficients approximating $\boldsymbol{y}$

This process has got two main stages: first one is to make a training set of signals from reliable segments of the input audio data. These portions of samples are selected from the input signal following user specifications. In the second stage, an adapted dictionary is obtained from the learned data. Designing a new adapted dictionary brings additional computational burden because each dictionary atom has to be compared with the training data.

B. Brief history of Dictionary Learning

The idea of dictionary learning was first introduced in 1996 by Olshausen. This method was called Maximum Likelihood Method [9], other method called Method of Optimal Directions (MOD) was introduced in 2000 by Engan et al. [10]. Another approach that used Maximum A-Posteriori Probability was introduced by Engan (1999) [11] and Murray (2001) [12]. Few years later Lesage et al. presented Unions of orthonormal bases [13].

C. The K-SVD algorithm

This algorithm was first presented by Aharon et al. [6]. It is inspired by the K-means algorithm [14] solving the vector quantization problem. Vector quantization is a process where training examples are assigned to their nearest neighbors, each example is represented with just one coefficient and given the coefficients, dictionary $\mathbf{D}$ atoms are constructed. There is an obvious relation between sparse representations and quantization. Vector quantization is an extreme sparse representation when only one atom is allowed in the signal decomposition and this coefficient value must be 0 or 1.

As a predecessor and the closest algorithm of K-SVD is MOD (Method of Optimal Directions) which updates the whole dictionary in each learning iteration. The advantage of K-SVD is that it updates just one vector (atom) in each iteration and at the same time coefficients corresponding to this atom are updated, therefore the convergence is accelerated.

The goal of this algorithm is to adapt a dictionary $\mathbf{D}$ to represent the input signal $\boldsymbol{y}_k$ more sparsely by using any pursuit algorithm that approximates an optimization problem

$$\hat{\boldsymbol{c}}_k = \arg\min_{\boldsymbol{c}_k}\|\boldsymbol{y}_k - \mathbf{D}\boldsymbol{c}_k\|_2^2 \text{ s.t. } \|\boldsymbol{c}_k\|_0 \leq S_0. \qquad (6)$$

In this case we use OMP algorithm, which is described in Section II.

The K-SVD algorithm is described below (2), details can be found in [8][6].

Algorithm 2 K-SVD

Initialization: $\mathbf{D}^{(0)} \in \mathbb{R}^{n \times K}$,

$\qquad\qquad J = 1$,

$\qquad\qquad S_{\max}\dots$ max. sparsity of vectors $\boldsymbol{c}_i$

Repeat until convergence (stopping rule):

Sparse coding

1: Solve using any pursuit algorithm

$\qquad \min_{\boldsymbol{c}_k}\{\|\boldsymbol{y}_k - \mathbf{D}\boldsymbol{c}_k\|_2^2\}$ s.t. $\|\boldsymbol{c}_k\|_0 \leq S_{\max}$

Dictionary update

$\qquad$ For each atom $k = 1, 2, \dots, K$ in $\mathbf{D}^{J-1}$ update by:

2: Set the group of indices using updated atom

$\qquad \omega_k = \{i | 1 \leq i \leq N, \boldsymbol{c}_T^k(i) \neq 0\}$

3: Compute the error matrix $\mathbf{E}_k$ by

$\qquad \mathbf{E}_k = \mathbf{Y} - \sum_{j \neq k} \boldsymbol{d}_j \boldsymbol{c}_T^j$

4: Restrict $\mathbf{E}_k$ choosing only columns corresponding to ω_k to obtain $\mathbf{E}_k^R$

5: Apply SVD decomposition $\mathbf{E}_k^R = \mathbf{U}\Delta\mathbf{V}^T$

6: Update dictionary atom $\tilde{\boldsymbol{d}}_k$ (first column of $\mathbf{U}$)

7: Update coefficient vector $\boldsymbol{c}_R^k$ (first column of $\mathbf{V}$ multiplied by $\Delta(1,1)$)

8: Set $J = J + 1$

Every time the dictionary $\mathbf{D}$ is modified, it has to be checked whether it is ℓ_2-normalized.

There is no guarantee that the K-SVD algorithm can reach a global or even a local minimum. The purpose of this paper is to find basic approximated parameters for the convergence of audio signals dictionary learning using K-SVD algorithm. However, there is no possibility to check the convergence inside the algorithm, the only chance is to do it externally by comparing the results with another experiment.

IV. EXPERIMENTAL RESULTS

A. Optimizing K-SVD parameters

Audio inpainting presented in [5] was performed only with static dictionaries. That was the motivation for using the K-SVD algorithm to adapt the dictionary on the observed signal and therefore improve the reconstruction of missing signals. Software utilized for our experiments is specified in Section V. Audio Inpainting Toolbox also contains testing wave files with speech (sampling frequency $f_s = 8\,\text{kHz}, 16\,\text{kHz}$) and music ($f_s = 16\,\text{kHz}$). We have done several tests to obtain optimal parameters for dictionary learning and with these parameters we tried to compete our approach with static dictionaries. These tests were performed on one channel audio
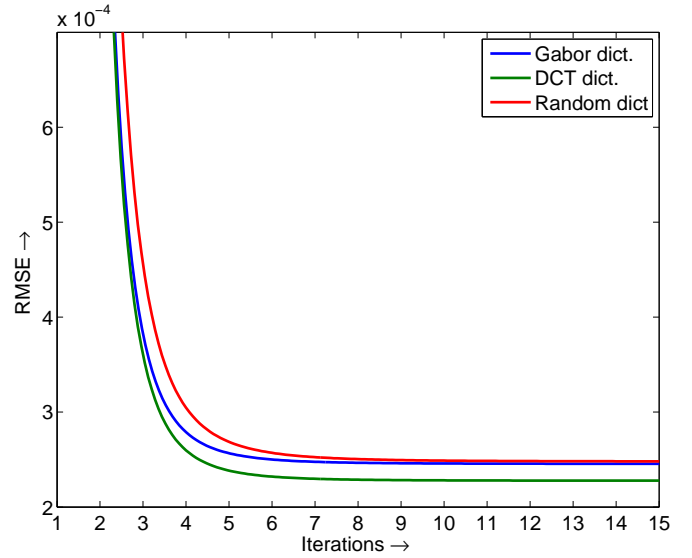

Fig. 1.   RMSE according to number of iterations using different initial dictionaries.

file *music07_16kHz.wav* with sampling frequency $f_s = 16\,\text{kHz}$ and length of 5 seconds.

After each iteration of dictionary learning via K-SVD algorithm, Root Mean Square Error (RMSE) is computed by

$$\text{RMSE} = \sqrt{\frac{\|\mathbf{Y} - \mathbf{D}_{\text{opt}}\mathbf{C}\|_F^2}{N \times M}}. \qquad (7)$$

After a few iterations RMSE settles at some value and remains unchanged. You can see in fig. 1 that four iterations are enough to reach satisfying RMSE value and after about 10 iterations RMSE is stabilized at its minimum. Because the lowest RMSE

Other experiment was focused on minimizing RMSE according to space between segments obtained from reliable samples to get the training data. If you have a short audio file and you do not have enough training segments of the signal, it has to be decided between smaller segment shift for more training data and larger segment shift for less training data. However, decreasing the segment shift is nothing but artificial enlarging the amount of training data and the samples are repeated in training segments. We got results presented in fig. 2. Using the audio file mentioned above of length $80\,000$ samples, we have the segment length of 256 samples, redundancy factor 3, therefore dictionary $\mathbf{D}$ has got a size of 256×768. With these parameters we can set up a shift of segments from interval $(1; 100)$. You can see that by increasing the segment shift value we get smaller RMSE during the dictionary learning process.

One of parameters of the dictionary learning explored further is the maximum number of nonzero coefficients $S_{\max}$. For $S_{\max} \in \{1, 2, 3, 4, 5\}$ dictionary learning experiments was made with focus on lowest RMSE depending on different $S_{\max}$ and therefore reaching the minimal error. In figure 3 it is obvious that after six iterations the minimal RMSE is reached by $S_{\max} = 3$ and remains minimal with very little change.
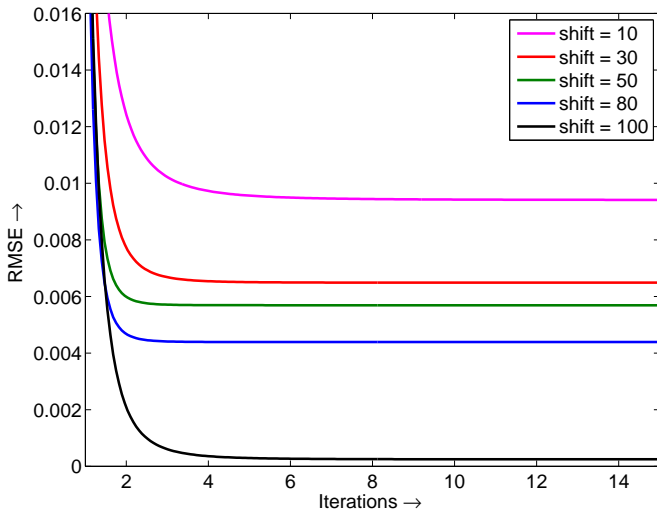
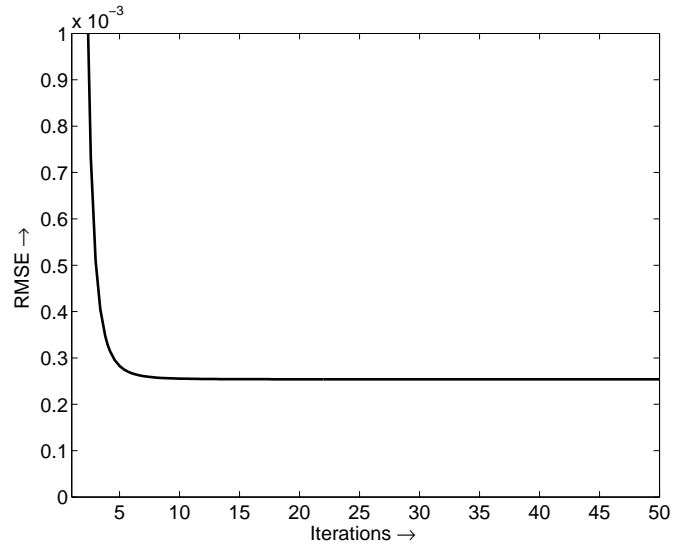Fig. 2.   RMSE according to shift of the original signal segmentation for training data.
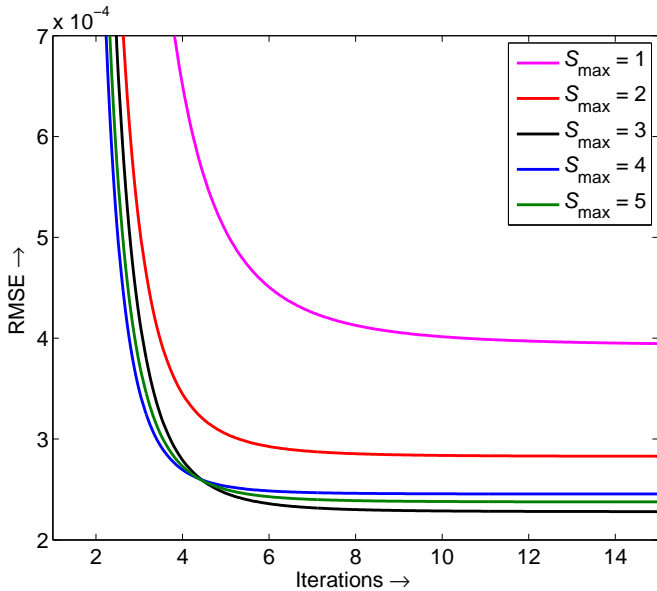

Fig. 3.   RMSE according to max. number of non-zero coefficients during the dictionary learning.

Fig. 4.   RMSE according to number of iterations.

TABLE I
K-SVD PARAMETERS

Segment length N	256 samples
Initial dictionary $\mathbf{D}$	Random
Number of iterations	50
Max. number of non-zero coefs. $S_{\max}$	3
Segment shift	100 samples

Fitting Toolbox was utilized to make a trendline (approximation by quadratic function).

B. Dictionary comparison on real signals inpainting

Now we will show the comparison of audio inpainting results of different sound files and utilizing various dictionaries. Both static (DCT and Gabor) and trained versions of these dictionaries were used to compare reconstruction results. The redundancy of all the dictionaries is 3. The parameters of the K-SVD dictionary learning algorithm are summarized in table I. The initial dictionary for K-SVD learning was filled with random values because during our experiments we got the most satisfying dictionary learning process. In each of audio files a gap (sequence of samples with zero value) is made with the size from 1 to 240 samples and evaluation of the signal reconstruction process is computed as Signal-to-Noise Ratio (SNR) only for missing samples by

$$\text{SNR}(\boldsymbol{y}, \hat{\boldsymbol{y}}) = 10 \log \frac{\|\boldsymbol{y}(\boldsymbol{I}^{\text{m}})\|_2^2}{\|\boldsymbol{y}(\boldsymbol{I}^{\text{m}}) - \hat{\boldsymbol{y}}(\boldsymbol{I}^{\text{m}})\|_2^2}. \quad (8)$$

Our first experiments were made with male (*male04_16kHz.wav*) and female voice (*female04_16kHz.wav*) speaking English. The hole was generated starting at $6\,000^{\text{th}}$ sample. In figure 5 you can see female voice reconstruction results. The best SNR values were obtained using Gabor dictionary and as you can see the trained dictionary (supposed to better approximate the input signal) is in some cases worse than static dictionaries.

Figure 6 shows the reconstruction results of male speech and you can see that results of different dictionaries are almost

Choosing the number of iterations has to be set up deliberately, since the number can be small and RMSE will remain high (the dictionary is not adapted as much as it can be) or the number can be too high and after reaching the minimum RMSE the algorithm can waste the time with new iterations or worse the RMSE can go up. That is why another experiment observing RMSE was performed with best parameters obtained above. Figure 4 shows that satisfying RMSE can be obtained with three or four iterations. This test was done for number of iterations from interval $(1; 200)$. For different signals number of iterations for settling, the RMSE can be various and during our experiments we used number of iterations of 50.

After settling the RMSE value on its minimum values were oscilating, therefore for all of the plots above, Matlab Curve
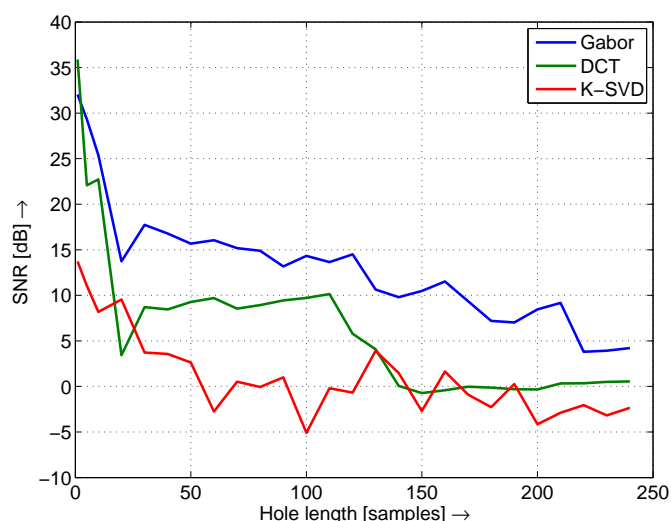
Fig. 5. Female speech missing signal reconstruction.
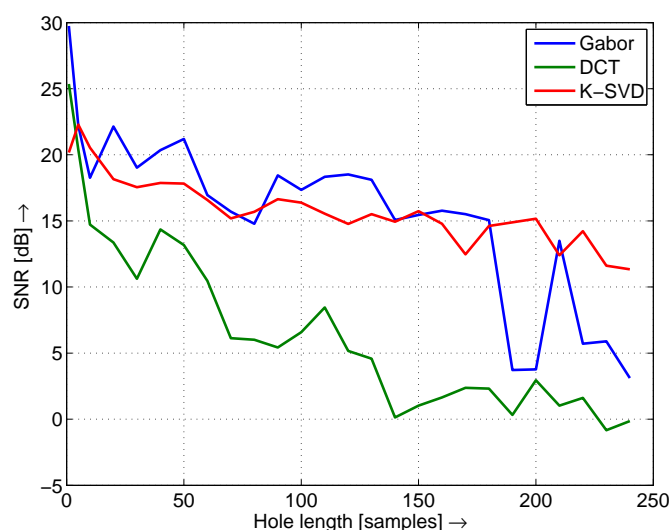

Fig. 7. A woman singing missing signal reconstruction.
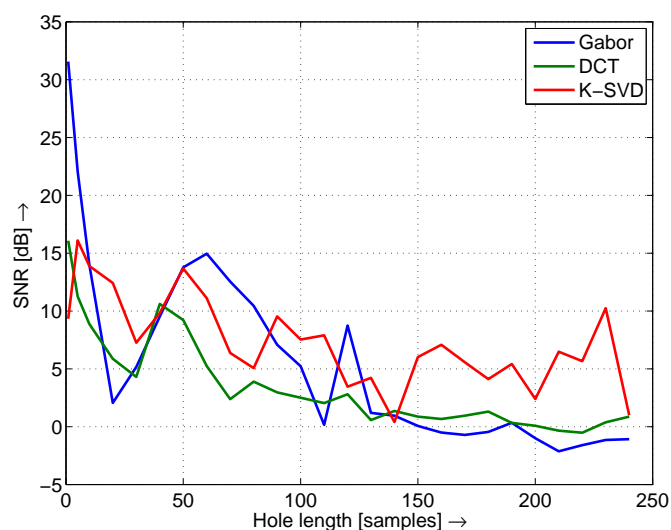

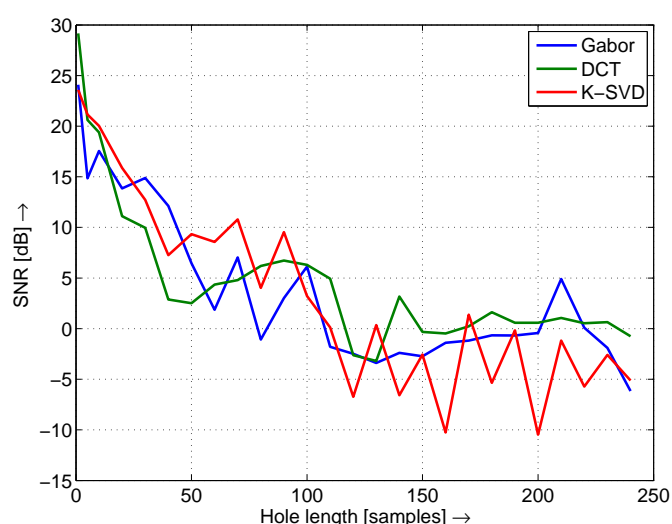Fig. 6. Male speech missing signal reconstruction.

Fig. 8. Drums playing missing signal reconstruction.

the same, but starting 160 samples hole length the trained dictionary overcomes static dictionaries.

Other experiments were done for audio files containing music samples. The gap was generated with $33\,000^{\text{th}}$ sample starting. First music file (*music06_16kHz.wav*) contains woman voice singing and the reconstruction error is shown in figure 7. Here, Gabor and trained dictionary are overcoming the DCT dictionary and K-SVD trained dictionary looks like to be more stable in larger gaps.

A sample of drums playing is recorded in (*music07_16kHz.wav*) file. In figure 8 you can see that all the dictionaries produce more or less the same reconstruction results in the sense of SNR.

Last experiment was performed with guitar playing music sample (*music11_16kHz.wav*). Figure 9 shows that for gap length from 40 to 110 K-SVD trained dictionary strongly overcomes static dictionaries of about $10\,\text{dB}$. Static dictionaries reconstruction results are almost the same.

V. Software

For Audio Inpainting process we used the Audio Inpaiting Toolbox (http://small-project.eu/keyresults/audio-inpainting) and the dictionary learning was done by SMALLbox v. 1.9 (http://small-project.eu/software-data/smallbox/).

These toolboxes are freely downloadable from the given links. Source m-files for reproducing our experiments were created on functions from Audio Inpainting Toolbox and can be downloaded from [15].

Files are created and may be run by using MATLAB. It has to be noted that results obtained by using random dictionary could differ because every time you run *randn()* function in MATLAB, you get a new matrix.

VI. Conclusion

In this paper, we presented a connection of two techniques to improve the reconstruction of missing audio signal infor-
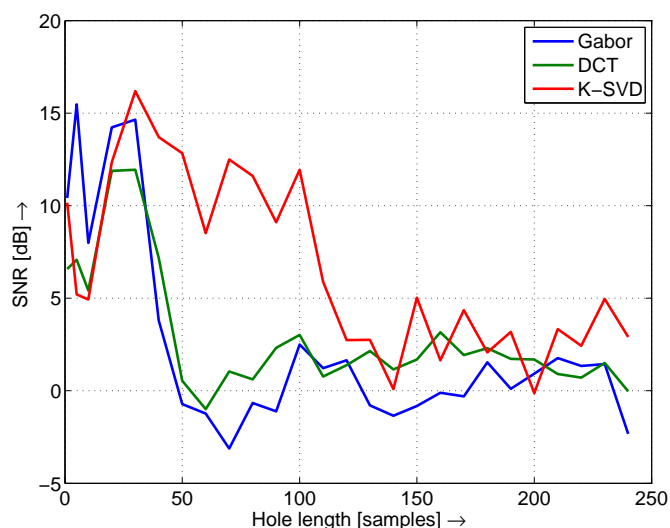
Fig. 9.   A guitar playing missing signal reconstruction.

mation. Solving the Audio Inpainting problem was done by Orthogonal Matching Pursuit algorithm and adapting of the dictionary was processed by the K-SVD algorithm. Both of them are described in the text. The adapted dictionary was compared with static DCT and Gabor dictionaries.

Our aim was to find optimal parameters for dictionary learning via K-SVD and compare these results with static dictionaries. Construction of the building blocks of the dictionary is signal dependent and there are no general rules for setting up the parameters. In most cases the trained dictionary overcomes static dictionaries but it has to be taken into account the higher computational load. However, there are cases, where the reconstruction error of trained dictionary was the worse among these three dictionaries. Using real signals we have done several tests which are presented in the paper.

Future work will be focused on construction of the dictionary atoms and moving this problem to time-frequency plane. Knowledge presented in the paper will be utilized for solving real problem of old traditional music recordings which have signal gaps surrounded in high noise level.

References

[1] W. Etter, "Restoration of a discrete-time signal segment by interpolation based on the left-sided and right-sided autoregressive parameters," *IEEE Transactions on Signal Processing*, vol. 44, no. 5, pp. 1124 –1135, may 1996.

[2] P. Rajmic and J. Klimek, "Removing crackle from an LP record via wavelet analysis," in *Proceedings of the 7th international conference on digital audio effects DAFx04*, 2004, pp. 100–103. [Online]. Available: http://dafx04.na.infn.it/WebProc/Proc/P_038.pdf

[3] G. Cocchi and A. Uncini, "Subbands audio signal recovering using neural nonlinear prediction," in *IEEE International Conference on Acoustics, Speech, and Signal Processing (ICASSP '01)*, vol. 2, 2001, pp. 1289 –1292 vol.2.

[4] C. Rodbro, M. Murthi, S. Andersen, and S. Jensen, "Hidden markov model-based packet loss concealment for voice over ip," *IEEE Transactions on Audio, Speech, and Language Processing*, vol. 14, no. 5, pp. 1609 –1623, sept. 2006.

[5] A. Adler, V. Emiya, M. Jafari, M. Elad, R. Gribonval, and M. Plumbley, "Audio inpainting," *IEEE Transactions on Audio, Speech, and Language Processing*, vol. 20, no. 3, pp. 922 –932, March 2012.

[6] M. Aharon, M. Elad, and A. M. Bruckstein, "K-SVD: An algorithm for designing of overcomplete dictionaries for sparse representations," *IEEE Transactions on Signal Processing*, vol. 54, pp. 4311–4322, 2006.

[7] M. Elad, J. Starck, P. Querre, and D. Donoho, "Simultaneous cartoon and texture image inpainting using morphological component analysis (mca)," *Applied and Computational Harmonic Analysis*, vol. 19, no. 3, pp. 340–358, 2005.

[8] M. Elad, *Sparse and Redundant Representations: From Theory to Applications in Signal and Image Processing*.   Springer, 2010.

[9] B. Olshausen and D. Field, "Natural image statistics and efficient coding," in *Computation in Neural Systems*, vol. 7, January 1996, pp. 333–339.

[10] K. Engan, S. O. Aase, and J. H. Husy, "Multi-frame compression: theory and design," *Signal Processing*, vol. 80, no. 10, pp. 2121 – 2140, 2000. [Online]. Available: http://www.sciencedirect.com/science/article/pii/S0165168400000724

[11] K. Engan, B. D. Rao, and K. Kreutz-Delgado, "Frame design using FOCUSS with method of optimal directions (MOD)," in *Proc. NORSIG 1999, Tronheim, Norway*, June 1999, pp. 65–69.

[12] J. F. Murray and K. Kreutz-Delgado, "An improved focuss-based learning algorithm for solving sparse linear inverse problems," in *Conference Record of the 35rd Asilomar Conference on Signals, Systems and Computers*, November 2001.

[13] S. Lesage, R. Gribonval, F. Bimbot, and L. Benaroya, "Learning unions of orthonormal bases with thresholded singular value decomposition," in *IEEE International Conference on Acoustics, Speech, and Signal Processing, 2005. Proceedings. (ICASSP '05).*, vol. 5, march 2005, pp. v/293 – v/296 Vol. 5.

[14] A. Gersho and A. Gray, *Vector Quantization and Signal Compression*, ser. The Kluwer International Series in Engineering and Computer Science.   Springer-Verlag GmbH, 1992. [Online]. Available: http://books.google.cz/books?id=DwcDm6xgItUC

[15] V. Mach and R. Ozdobinski. (2012) Source codes for audio inpainting with dictionary learning. [Online]. Available: http://www.stud.feec.vutbr.cz/~xmachv00/paper2012/

Vaclav Mach received the B.Sc at the Department of Telecommunications at the Faculty of Electrical Engineering and Communication at Brno University of Technology in 2009. He received Ing. (M.Sc) at the same department in 2011. Now he is a Ph.D student at the same faculty.

The area of his professional interests is utilizing sparse representations in audio signal processing, old recordings restoration and acoustics. He is a student member of Audio Engineering Society.

Roman Ozdobinski received the B.Sc at the Department of Telecommunications at the Faculty of Electrical Engineering and Communication at Brno University of Technology in 2012. Currently he is a master student at the same department. His interests has been concentrated in audio signal processing, mainly sparse representations.

13 >